MOLECULAR DETERMINANTS OF THE β4 nAChR SUBUNIT IN CHANNEL FUNCTION AND NICOTINE-MEDIATED BEHAVIOR

Inaugural-Dissertation

to obtain the academic degree

Doctor rerum naturalium (Dr. rer. nat.)

submitted to the Department of Biology, Chemistry and Pharmacy

of Freie Universität Berlin

by

Marta Anna Ślimak

from Wrocław

March 2012

This work was carried out in the period from October 2007 until February 2012 under the supervision of Dr. Inés Ibañez-Tallon and Prof. Dr. Constance Scharff at the Max-Delbrück-Center for Molecular Medicine (MDC) in Berlin.

1st Reviewer: Dr. Inés Ibañez-Tallon

2nd Reviewer: Prof. Dr. Constance Scharff

Date of defense: 25.06.2012

Scientific Acknowledgments

This thesis would not have been possible without the essential and gracious support of many individuals.

First and foremost, I would like to thank my supervisor, Dr. Inés Ibañez-Tallon for her help, patience and guidance during the time of my work in her group. I am also thankful for the excellent example she has provided as a successful woman in neuroscience.

I would like to thank my fellow lab members, both current and past: Dr. Silke Frahm-Barske, Beatriz Antolin-Fontes, Branka Kampfrath, Dr. Sebastian Auer, Dr. Jessica Ables, Dr. Martin Laqua, Dr. Julio Santos-Torres, Susanne Wojtke, Dr. Annika Stürzebecher and Daniela Kurzhals for creating an inspiring academic and social environment, which I truly enjoyed.

Furthermore, I would like to express my gratitude to Dr. Julio Santos-Torres for carrying out the electrophysiological recordings in primary hippocampal neurons and to Dr. Silke Frahm-Barske for help with the stereotactic injections into medial habenula. Your excellent support help made this thesis possible. I would like to thank to Dr. Jean-Fred Fontaine for comparative analysis of the nicotinic receptor subunit sequences.

I would like to thank Prof. Dr. Constance Scharff from the Freie Universität Berlin for being so kind to become my FU supervisor and Prof. Dr. Gary R. Lewin from Max-Delbrück-Center for Molecular Medicine for fruitful discussions in the shared group lab meetings.

I would express my gratitude towards the coordinators of the International Program "MoNeuro" for an excellent cooperation over the last 4 years.

Personal acknowledgements

Moim Rodzicom składam serdeczne wyrazy wdzięczności za okazane mi wsparcie podczas mojej niezwykle długiej edukacji oraz za pomoc w rozpoczęciu nowego życia za granicą.

Questa tesi è dedicata specialmente a te. Ti ringrazio per il tuo amore, l'interesse, il supporto e la forza che mi hai dato, soprattutto durante l'ultimo periodo di stesura della tesi. Non ci sono parole per esprimere quanto sono grata di essere parte della tua vita e quanto importante sei tu nella mia.

Table of contents

1. Introduction

1.1 Neuronal circuits underlying reward and pain, and their contribution to addictive behaviors

The complexity of the mammalian brain is established by the existence of at least several hundreds of distinct classes of neurons and glia, arranged into complex circuits that control specific aspects of cognition and behavior. The cellular and molecular interactions within a neural circuit are extremely precise, yet flexible, enabling an organism to collect, relay and process the information from its surroundings and produce a long lasting and complex behavior. A comprehensive understanding of the development and maintenance of functional circuits requires investigations of the specific properties of individual neurons as well as of their connectivity. Although relatively general principles of connectivity and physiology have been established for certain brain areas as cortex, cerebellum and others, current knowledge about the intricate patterns modulating neuronal circuits is still limited. Yet, the identification of these patterns is crucial to understand the function of the brain both in health and disease.

The neuronal circuits involved in reward, pain and addiction have been shown to be strongly interconnected. Reward can be defined as a complex biological mechanism mediating behavior motivated by pleasurable events. Evolutionarily conserved reward pathways are designed to direct behavior towards goals that are beneficial to the organism or species survival[1]. However, a loss of flexibility and loss of the ability to make free decisions, i.e., extreme control of behavior, as described in addiction, may be seen as one of the distinguishing features between pleasure/reward and addiction, inducing a compulsive behavior of substance seeking and intake. This goes along with a loss of control of limiting intake and the emergence of a negative emotional state when access to the substance is prevented[1-2]. On the other hand, all substances with particularly strong addictive properties (named ‘drugs of abuse’), like opiates[3], nicotine[4] or alcohol[5] have been shown to have analgesic properties. Evidence of pleasure-related anesthesia has been also reported by various studies on both human and animal subjects. It has been shown that pain is decreased by pleasant odors, images, food and sexual behavior. Recent

molecular-imaging and animal studies have demonstrated the important role of the opioidergic and dopaminergic systems in modulating both pain and pleasure[6]. Emerging evidence from the pain, reward and addiction research fields points to extensive similarities in the anatomical substrates of painful and pleasant sensations.

The reward circuit

A key component of the reward circuit is the dopamine mesolimbic system, which comprises the ventral tegmental area (VTA), nucleus accumbens (NAcc), amygdala and prefrontal cortex. Reward-inducing stimuli activate the VTA, which in turn releases dopamine in the NAcc and into the forebrain. The NAcc is associated with acquiring and eliciting conditioned behaviors and involved in the increased sensitivity to drugs as addiction progresses[7]. The nucleus accumbens (NAcc) consists mainly of medium-spiny projection neurons (MSNs), which are GABA neurons[8]. The prefrontal cortex, more specifically the anterior cingulate and orbitofrontal cortices, is important for the integration of information, which contributes to whether a behavior will be elicited. It appears to be the area in which motivation originates and the salience of stimuli is determined[9]. The basolateral amygdala projects into the NAcc and is thought to be important for motivation[9]. Further evidence points out to a role for the hippocampus in drug addiction because of its importance in learning and memory. Much of this evidence has been gained from investigations manipulating cells in the hippocampus, which influence dopamine levels in NAcc, and firing rates of VTA dopaminergic cells[10].

Motivation/reward components in addiction forming

Nearly all addictive drugs, directly or indirectly, act on the brain reward system. Acute administration of almost all drugs of abuse leads to decreased brain stimulation reward thresholds (i.e., increased reward[11]) and when they are administered chronically an increase in reward threshold is usually observed during withdrawal (i.e., decreased reward). The acute rewarding properties of psychostimulant drugs have been known to depend on activation of the mesolimbic dopamine system, but activation of this system is not necessarily

critical for the acute reinforcing effects of other drugs of abuse[12-14]. Nicotinic receptors, mainly implicated in the reinforcing actions of nicotine, are localized in the brain mesocorticolimbic dopamine system[15-18]. However, nicotine may alter the function of both the mesocorticolimbic dopamine system and the opioid peptide systems in the same neural circuitry associated with other drugs of abuse[15]. Additionally, neurotoxin-selective lesions of the mesocorticolimbic dopamine system block the reinforcing effects of cocaine and -amphetamine[19]. In contrast, neurochemically specific lesions of dopamine in the nucleus accumbens with 6-hydroxydopamine failed to block heroin or ethanol self-administration[20]. The mesolimbic dopamine system is activated by acute administration of opioids, ethanol, nicotine, and Δ9-THC[21].

The pain circuit and its connection to pleasure and addiction

Pain is an evolutionary conserved pathway to protect the body from harm, producing an unpleasant sensory and emotional experience and causing reflexive retraction from the painful stimulus. Pain circuitry involves nociceptors (first-order neurons) at the dorsal root ganglion (DRG), which project to second-order neurons in the spinal cord and medulla, which then carries the sensory information (in the form of electrical impulse) to the thalamus, where it synapses with third-order neurons that transmit the impulse to the cortex. Second-order neurons send their sensory inputs to the thalamus via two ascending pathways: the dorsal column medial-lemniscal system and the anterolateral system (includes the spinothalamic, spinoreticular, and spinotectal fibers). The former transmits impulse involving position sense, touch, and pressure. The latter pathway is involved in pain transmission[22]. A functional overlap between the pain and the reward pathways has been identified. For example, NAcc, which is known to be an important component of the mesolimbic dopaminergic reward system (implicated in addiction forming), also plays a role in pain modulation. However, although microinjection of opioids directly into the NAcc has been shown to induce antinociception[23-25] and microinjection of the opioid antagonist naloxone into the NAcc has been shown to attenuate the antinociceptive effect of systemically administered morphine[23,26], the physiological mechanisms underlying the role of the NAcc in nociception are poorly understood. It has been recently demonstrated that nucleus accumbens opioidergic mechanisms

participate in a novel ascending nociceptive control circuit[27]; that is, intraaccumbens microinjection of naloxone blocks the antinociceptive effect of pharmacological interventions made at the level of the spinal cord [28].

1.2 The habenulo-interpenduncular (Hb-IPN) circuit as an emerging relay pathway for pain and addiction

Recent evidence indicates that the habenula is a major crossroad for addiction and pain pathways because of its anatomical location and connectivity, as well as, because of its uniquely high enrichment in nicotinic acetylcholine receptors (nAChRs), opioid receptors tachykinin receptors and their ligands (Substance P) and other molecules, receptors and ion channels relevant for pain and sensitivity to drugs of abuse. Besides these emerging roles, the habenular complex has been implicated in broad range of behaviors, including olfaction, pain, stress, anxiety, sleep, decision making, as well as cognitive and motor dysfunctions[29-31]. The habenulo-interpenduncular tract consists of the habenular nuclei, also known as habenular complex. This is one of the most ancient brain structures and is already present in lower vertebrates such as zebrafish[29]. The habenular complex in the mammalian brain is located in the posterior-dorsal-medial end of the thalamus, adjacent to the third ventricle. It comprises bilateral nuclei on each side of the habenular commissure, medial (MHb) and lateral (LHb) habenula, each of them remarkably distinct in its connectivity. The medial habenula (MHb) receives afferent inputs from the septum and NAcc, predominantly via the stria medullaris and projects through the fasciculus retroflexus to the interpenduncular nucleus (IPN), which further sends outputs to the median and dorsal raphe nuclei. In contrast, the major source of innervation to the lateral habenula seems to emerge from the endopenduncular nucleus (EP), a part of the pallidal complex, as well as form the lateral hypothalamus. The LHb sends its efferent projections to the ventral tegmental area (VTA) and substantia nigra pars compacta (SNpc) [30,32]. The internal connection between medial and lateral habenula is asymmetric: only the medial habenula sends outputs to the lateral habenula[33].

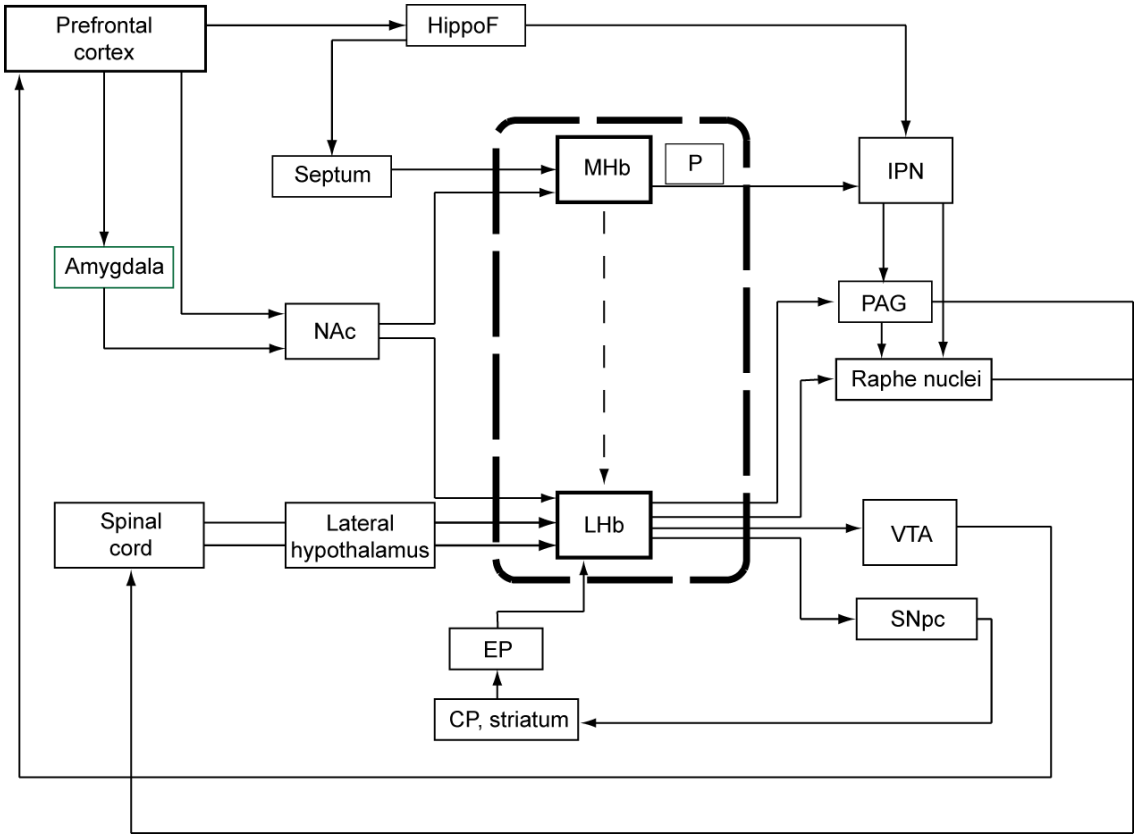

Figure 1. The connectivity of the habenular complex [modified from [30]].

HippoF hippocampal formation; *MHb* medial habenula;, *LHb* lateral habenula; *P* pineal; *IPN* interpenduncular nucleus, *PAG* periaqueductal grey; *VTA* ventral tegmental area, *SNpc* substantia nigra pars compacta; *CP* caudate put amen, *EP* endopenduncular nucleus, *NAcc* nucleus accumbens.

Habenula and pain

The role of the habenular complex in the perception of pain has been suggested based on its neuronal connections with brain areas known to process pain. Pain inputs to the habenula are sent directly from spinal cord[34] or are transmitted indirectly via the lateral hypothalamus, a structure known to be involved in pain processing and modulation[35], which itself receives projections from the spinal cord [36]. Further indirect pain modulatory projections to the habenular nuclei seem to stem from frontal cortex[37] and nucleus accumbens[38], well known to be involved in nociception. Moreover, it has been suggested that periaqueductal grey, habenula and nucleus accumbens may form a unidirectional loop to play their roles in this process [39]. It has been shown, that intrahabenular injections of naloxone, a μ-opioid receptor antagonist, inhibit analgesia produced by morphine injected into the periaqueductal grey (PAG). Furthermore, when

naloxone was injected into nucleus accumbens, the analgesic effects of intrahabenular morphine injections were no longer observed[40]. This finding suggests, that habenula acts as a relay station in descending pain modulation from the NAcc to the PAG. The PAG has been described to play a role in modulating the descending pain pathways[41-42]. Habenula's efferent projections to dopaminergic (VTA, SNpc) and serotonergic (dorsal and medial raphe nuclei) brain areas additionally support their contribution to pain modulation [43-45].

Habenula and its role in addiction

The medial habenula is one of the few discrete sites of expression of α3β4(α5) nAChRs in the brain and recently has been linked to nicotine consumption and nicotine self-administraton[46-47]. Despite the habenula being a converging point between pain, reward and addiction circuits, its contribution in detail for the addiction forming has not yet been extensively elucidated.

1.3 Nicotinic acetylcholine receptors (nAChRs)

Nicotinic acetylcholine receptors (nAChRs) belong to the ligand-gated ion channel superfamily, which includes glycine, $GABA_A$ and 5-HT_3 receptors. They are cation selective, ligand-gated channels, activated by the endogenous neurotransmitter, acetylcholine, as well as other agonists including the plant alkaloid nicotine, present in tobacco. Nine different α (α_1 – α_7 and α_9 – α_{10}) and four β (β_1 – β_4) nAChR subunits have been cloned in mammals. These exist as pentamers, arranged around a central pore, composed of at least two pore-forming α and two or three structural β subunits [48-49]. Exceptions from this rule are α_7, and α_9, (note a8 is only in chicken so I would not mention) which were shown to be able to form functional α-monomeric channels. However, it has been recently shown, that α_7 can also form functional heteromers with β_2 and β_3 nAChR subunits *in vitro*[50-52]. Nicotinic acetylcholine receptors can form multiple subunits combinations, each with different expression patterns and pharmacological properties.

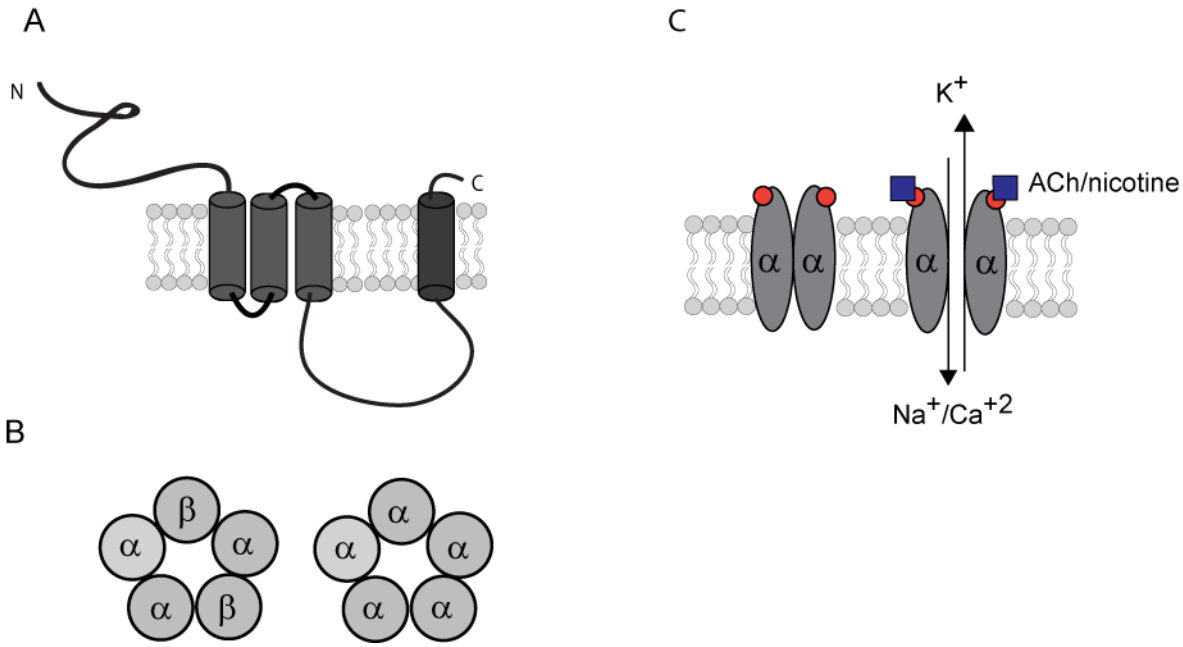

Figure 2. The structure of neuronal nicotine acetylcholine receptors

(A) Each nAChR subunit consists of four transmembrane domains. (B) They form pentamers in the membrane, composed of alternating α and β subunits (heteromeric) or only α subunits (homomeric) (B). Agonist binding (acetylcholine or nicotine) occurs on the α- α subunit interface and triggers conformational changes that allow opening of the cation-selective pore.

A single nAChR subunit contains four membrane-spanning domains (named M1-M4) with a long extracellular N-terminal domain, a large intracellular loop between domains 3 and 4 and a small extracellular C-terminal domain. The N-terminal domain contains key elements for ligand recognition and binding. The transmembrane domains anchor the channel in the plasma membrane and possibly contribute to the regulation of channel kinetics. The long intracellular loop is enriched in phosphorylation sites and may play a role in the regulation of nAChR trafficking, mediation of cytoskeletal interactions, receptor assembly and functional desensitization[53]. These structural domains are very well conserved among various subunits and have a very high sequence similarity between different species.

nAChRs are widely distributed in the central nervous system and play a critical role in regulating neuronal excitability. They can be found in somato-dendritic, axonal, presynaptic, or postsynaptic locations. Presynaptically located nAChRs contribute to the release of the other neurotransmitters to the synaptic cleft, while postsynaptic and somatic nAChRs mediate fast excitatory transmission. nAChRs play a critical role in learning and memory processes, participate in the synaptic

plasticity by modulating the activity-dependent circuits [54-55]. Decline, disruption, or alterations of nAChR mediated effects have been connected to various dysfunctions, such as schizophrenia, epilepsy, autism and Alzheimer's disease [54,56-61].

1.4 Role of nAChRs in nicotine addiction

Nicotine addiction

Nicotinic acetylcholine receptors were identified as key players in nicotine dependence, as they bind and are activated by nicotine, the major addictive component of tobacco[62].Tobacco use has been shown to have both relaxing and stimulating effects on human brain. In humans, acute nicotine administration, e.g. smoking of a cigarette, produces increased alertness, sharpness, relaxation and enhanced cognition [63]. Nicotine addiction can be defined as a series of events leading to switch from voluntary to compulsory use of nicotine, despite its negative consequences as a leading cause for premature death in developed countries. This series of reinforcing stimuli leads to the repetitive use of tobacco, which usually leads to nicotine dependence within a short period. Persisting tobacco smoking is a risk factor for heart attack, stroke, chronic obstructive pulmonary disease (COPD), as well as lung and larynx cancer. However, although over 70% of smokers express the desire to quit, only 5% of them are successful. It is believed that this happens due to the withdrawal symptoms that emerge within hours upon cessation of nicotine. Withdrawal symptoms include somatic symptoms like bradycardia, gastrointestinal disturbances and weight gain due to increased appetite, next to the affective symptoms like anxiety, irritability, depressed mood, lack of concentration, mild cognitive deficits and nicotine craving [64]. The avoidance of withdrawal symptoms, as well as the positive subjective effects of nicotine motivates to nicotine use [65-69]. Given that drug abuse is a major public health problem calling new therapeutic strategies, animal models have been developed in order to study behavioral and neurobiological basis of addiction.

Mouse models and genetic tools for the dissection of neurocircuits

A number of approaches have been developed to gain more insight into the complexity of neuronal circuits, including approaches to investigate the cellular and molecular specialisation of single cells within a neural circuit, as well as to understand how the combined work of the circuit results in a particular behaviour. These methods include the use of conditional knock outs and transgenic mice as well as of viral vectors encoding different effectors or reporters that can be used to monitor or perturb cellular processes in identified neuronal populations and dissect circuit function. For example, BAC transgenic mice [70-71]accurately overexpress genes of interest in the endogenous expression sites, allowing dissecting their contribution to the circuit. This method utilises bacterial artificial chromosomes (BACs), which can incorporate large genomic intervals (up to 300 kb) from other species that are preserved and duplicated along with the BACs. The ability to include a large piece of genomic DNA is of a great advantage, as important regulatory elements of mammalian genes can be located kilobases up- or downstream of the gene coding sequences, as well as it allows the gene to use its own promoter/enhancer system. Alternatively, the cre/loxP technology allows to alter gene expression, in a selected cell population and hence study, for instance the effect of a gene deletion in a specific class of neurons[72]. Utilization of the cre/loxP intersectional system *in vivo* requires either two mouse lines: one expressing the Cre-recombinase and the other the conditional floxed allele, or one mouse line either carrying Cre or loxP transgenes and a viral vector containing a flox cassette or the Cre recombinase respectively. The loxP conditional mouse line is generated using ES cell technology. Typically, the target gene is altered, by homologous recombination in ES cells, such that genomic regions critical for protein activity are flanked by loxP sites (“floxed” gene). Mice derived from these ES cells should ultimately contain floxed alleles in all cells. These mice should be phenotypically normal because the loxP sites were inserted into introns where they theoretically do not affect gene function. The second line of transgenic mice is generated by standard oocyte injection techniques. These mice express Cre under the control of a transgenic promoter. Mating of the two mouse lines should result in Cre-mediated gene disruption only in those cells in which the promoter is active[73-74].Mouse neurocircuitry studies have also benefited from optogenetics,

a method combininggenetic engineering with fiber optics. With this technique, flashes of light activate a neuron that has been genetically modified to express a light-sensing protein. That neuron then stimulates the next neuron in the circuit, allowing for exact identification of which neurons communicate with each other. This technique has been refined greatly over the past years, now allowing for direct recordings in freely moving transgenic animals[75-76]. Optogenetic techniques provided recently an important insight into neural circuits relevant to autism, schizophrenia, drug abuse, anxiety, and depression[76-80]. Another technique for mapping neural circuits utilizes neurotropic viruses as tracers of the neural connections. Several types of viruses, like the most used pseudorabies possess the ability to infect and replicate in neurons following central or peripheral administration and then propagate, either antero- or retrogradely (depending on the pseudotype of the virus), in synaptically connected nerve cells[81-84]. With the recent development of tract-tracing methodology based upon the use of neurotropic viruses it is now possible to directly visualize neurons that are linked together in a circuit. Additionally, different neuroimaging techniques have been developed to investigate the activity of neural networks *in vivo*. The use of functional neuroimaging to investigate the structure or function of the brain is common, either as simply a way for better assessing brain injury with high resolution pictures, or by examining the relative activations of different brain areas. Such technologies may include fMRI (functional magnetic resonance imaging), PET (positron emission tomography) and CAT (computed axial tomography). Functional neuroimaging uses specific brain imaging technologies to take scans from the brain, usually when a person is doing a particular task, in an attempt to understand how the activation of particular brain areas is related to the task. In functional neuroimaging, especially fMRI, which measures hemodynamic activity that is closely linked to neural activity, PET, and electroencephalography (EEG) is used[85-86]. Despite the increasing sophistication of the experimental methods and enormous advancement in methodology, our knowledge about the neuronal circuits underlying complex behaviour is still insufficient. However, a remarkably detailed insight has been gained recently into the circuits of pain, reward and, stemming from these two, drug dependence.

Behavioral assays for nicotine addiction and withdrawal in mouse models

No single current mouse behavioral model can capture the broad human experience of human smoking or nicotine addiction, but separate mouse models generated over the years quite accurately mimic the full spectrum of the behavioral and neurobiological changes of this complex addiction[87]. One of the behavioral models to study the reinforcing properties of nicotine in rodents is nicotine self-administration. In the IV self-administration paradigm animals are trained to self-administer nicotine in an operant chamber, where by pressing the lever they receive intravenous bolus of nicotine. Alternatively, mice in their home cage are presented with two water containers supplemented with or absent of nicotine (oral self-administration).

Conditioned place preference (CPP) is another behavioral model used to assess the rewarding effects of nicotine in rodents. This experimental paradigm uses an apparatus consisting of a box divided in three distant compartments, interconnected with the door. Each compartment differs in the wall pattern (color, texture) and floor grid (mesh shape or size). In this paradigm, intraperitoneal injection of nicotine is repeatedly paired with one chamber of the CPP apparatus, whereas saline injection is paired with the other. After consistent repetitive pairings during 3-5 consecutive days, a rodent is given access to both chambers. If the animal spends more time in the nicotine-paired chamber this is considered as indicative that the animal has experienced nicotine as rewarding. Similarly, when the animal avoids the drug-paired chamber, this result is taken as a measure of nicotine aversion. This behavioral model is assumed valid, as cigarette smoking also produces rewarding effects (mild euphoria and relaxation). In addition to the rewarding properties of nicotine, this system measures also the ability to form contextual associations between the effects of nicotine and the environmental cues, very similar to the habitual smoking in humans[88-89].

Nicotine withdrawal may be successfully assayed in rodents by chronic nicotine administration, followed by injection of nicotinic antagonist. In this paradigm mice first undergo long-term nicotine exposure, either by drinking water supplemented with nicotine or by continuous release of nicotine from subcutaneously implanted osmotic pumps for several days. Afterwards the mice receive an injection of mecamylamine (nAChR antagonist) and the withdrawal symptoms (grooming,

scratching, chewing, shaking, cage scratching, head nodding, and jumping) are counted[88].

Molecular biology of nicotine addiction

Nicotinic receptors differ significantly in their sensitivity to nicotine and expression pattern, therefore it seems that various aspects of nicotine dependence (e.g. craving, withdrawal, tolerance, sensitivity) may be due to the distinct properties of the different nAChR subunit combinations[90]. Several approaches have been already undertaken to elucidate this issue. One of them has been the generation of mouse knock-outs models, as well as knock-ins or BAC transgenic mice, deleting or overexpressing nAChR subunits. The majority of the nicotinic receptors expressed in the brain are α4β2 nAChRs, accounting for 80% of the high affinity nicotine-binding sites[91]. The studies of β2 knock-out mice[92-93] and of knock-in mice with a gain-of-function mutation of α4[94] have revealed, that the α4β2 subunit combination has a major contribution to nicotine self-administration. The nAChR α4 subunit is almost invariably co-expressed with α3 and the resulting α3β4* nAChR combination is present only in very few brain areas e.g. the medial habenula (MHb) and interpeduncular nucleus (IPN), and in autonomic ganglia[95]. The auxiliary α5 subunit, unable to bind nicotine due to the absence of a ligand binding site, assembles in certain number of cases with the α3β4 combination, but it can be as well incorporated into α4β2 receptor complexes. α3β4* nAChRs have lower affinity for nicotine than α4β2 receptors and are not saturated by the nicotine levels found in smokers, suggesting that α3β4* nAChRs could play an important role in tobacco addiction, since they retain their sensitivity to fluctuating nicotine levels in smokers[96]. β4 and α5 knockout mice show similar phenotypes, including decreased signs of nicotine withdrawal symptoms[97-99], hypolocomotion and lack of nicotine-induced seizures[100-101]. The role of α3 subunit in terms of nicotine consumption has been difficult to determine since knock-out mice die at early postnatal age due to severe abnormalities of the bladder[102].

1.5 Transgenic α3β4α5 cluster (Tabac) mice as a model system to study nicotine consumption

The present studies were prompted by the study of Frahm and colleagues showing that BAC transgenic mice with targeted overexpression of β4 subunit (Tabac mice) exhibit strong aversion to nicotine[46]. Tabac mice were generated by insertion of a BAC transgene containing the *Chrnb4-Chrna3-Chrna5* gene cluster with the intergenic and 5' flanking regions encompassing the *cis*-regulatory elements that coordinate co-transcriptional control of the genes in the cluster[103-106]. The genes in the cluster were modified so that the *Chrnb4* gene, encoding for the β4 subunit of the nAChR was kept intact. *Chrna3* was modified by insertion of an EGFP cassette followed by polyadenylation signals at its ATG translation initiator codon[107]. This modification drives expression of EGFP instead of *Chrna3* (referred to as *Chrna3/*eGFP). *Chrna5* sequence is truncated in this BAC (exon 1 is absent), therefore the expression of α5 is not elevated in these mice. As a result, Tabac mice express elevated levels of the β4 protein in endogenous sites in the brain (namely medial habenula and interpenduncular nucleus) shown by both EGFP fluorescence and audioradiographic ligand binding assays. Electrophysiological recordings performed in α3β4* neurons in medial habenula showed an increased response to nicotine in these cells. When assayed with nicotine, Tabac mice display strong aversion to nicotine-containing solution.

1.6 Genetic variants in the CHRNB4/A3/A5 gene cluster associated to predisposition to develop nicotine dependence

Genetic epidemiological studies have reported, that the heritability compound of nicotine dependence (ND) can be as high as 40 to 75% [108-112]. Candidate gene association studies [113-139], and genome-wide association scans (GWASs)[140-144] have searched for, and, at varying levels of significance, identified, common variants associated with measures of response to tobacco, tobacco consumption, nicotine dependence, nicotine metabolism, or smoking cessation. Among them, genetic variants in the *CHRNB4-CHRNA3-CHRNA5* gene cluster were identified as risk factors for nicotine dependence and lung

cancer[113,134,139,144-145]. These single nucleotide polymorphisms (SNPs) can be defined as DNA sequence variations occurring when a single nucleotide in the genome differs between paired chromosomes in an individual. They include non-coding variants across the gene cluster, as well as amino acid substitutions (full list: http://www.ncbi.nlm.nih.gov/snp/), leading to generation of missense variants or frame shifts. Given that *cis*-regulatory elements within the cluster coordinate transcription of these genes for assembly of functional α3β4-containing (α3β4*) and (α3β4α5*) nAChRs[105-106] the fact that a large number of SNPs map to non-coding segments of the cluster suggests that altered regulation of these genes can contribute to the pathophysiology of tobacco use. However, the precise relationship between ND and variants on the CHRNA5–CHRNA3–CHRNB4 gene cluster still needs to be elucidated. The most strongly associated single nucleotide polymorphism (SNP) in several genome-wide association studies (GWAS) of nicotine dependence[115,134,144,146] and correlated traits is rs16969968 in CHRNA5. The CHRNA5 rs16969968 is a nonsynonymous SNP that corresponds to an amino acid change of aspartic acid to asparagine at codon 398 in the α5 nicotinic receptor protein[137,147] and was shown to be associated with ND [115,134,144,147-148]. Evidence that the amino acid change is functionally relevant is supported by the fact that in vitro, α4β2α5 nicotinic receptors with the aspartic acid variant (D398) exhibited a greater maximal response to a nicotinic agonist than did α4β2α5 nicotinic receptors with the asparagine amino acid substitution (N398). Because the allele that codes for asparagine is associated with increased risk for developing nicotine dependence and nicotinic receptors containing the α5 subunit with this amino acid (N398) exhibit reduced function in vitro, reduced function of α4β2α5 nicotinic receptors may lead to an elevated risk for developing nicotine dependence. The observation that decreased nAChR function is associated with increased risk for nicotine dependence is consistent with the observation that individuals who are extensive metabolizers of nicotine (reduced receptor activation per cigarette) are at increased risk for nicotine dependence[115]. This finding is of particular interest because α5 contributes to the α4β2α5 nicotinic receptor, which is involved in nicotine-stimulated dopamine release in the striatum, a brain region involved in the reward pathway and crucial to the development of substance dependence[149-150]. Additionally, a group of highly correlated variants, including the SNP rs588765 near CHRNA5, were

shown to increase CHRNA5 mRNA expression and increase the risk of nicotine dependence independently of rs16969968[138,151]. Therefore, it appears that risk for nicotine dependence seems to stem from at least two separate mechanisms: the variability in the mRNA levels of these genes and functional changes due to non-synonymous amino acid variants[152]. It has been reported, that two rare missense variants in CHRNB4, rs12914008 (T91I) and rs61737499 (T375I) lead to decreased receptor function and are associated with lower risk for nicotine dependence in African Americans and European Americans[50,153]. rs12914008 in CHRNB4 has been also linked to the point prevalence abstinence in response to nicotine cessation therapy[154].

Despite broad and strong human data on the CHRNA3/B4/A5 gene cluster polymorphisms, there is very little experimental evidence on how these polymorphisms modify the channel function and how this corresponds to changes in the response to nicotine.

1.7 Aims of this work

The central aim of this work is the elucidation of the contribution and molecular determinants of the β4 nicotinic receptor subunit to the regulation of nicotine intake and pain in mice. We conceived this work based on our finding that mice overexpressing the β4 subunit in the midbrain medial habenular nucleus show strong aversion to nicotine[46]. This discovery together with the fact that, in humans, single nucleotide polymorphisms (SNPs) located in this gene locus, associate to differences in the predisposition to smoking, provided us with a valuable frame to establish a model system in which to test β4 variants and their contribution to habenular function *in vivo*. As described in the following detailed aims, this work starts with the *in vitro* electrophysiological characterization of β4 mutants, chimeras and SNP variants, extends to the construction and tests of lentiviral constructs for neuronal transduction in culture and in living mice, and leads to the last part which involves the behavioral analyses of the mice microinjected in the habenula with different β4 variants.

Aim 1: Elucidate the molecular determinants that confer to the β4 nAChR subunit its ability to increase nicotine-elicited currents when overexpressed

This aim includes the electrophysiological characterization of β4 in combination with different alpha subunits by *in vitro* two-electrode voltage clamp recordings in *Xenopus* oocytes. Subsequently, chimeras of β4 and the highly homologous b2 subunit were generated and characterized to identify the unique element in β4 nAChR subunit responsible for its rate-limiting property.

Aim 2: Investigate the balance between α5 and β4 subunits

Given that, in the habenula, β4 mostly combines with α3 subunits with or without α5 to form α3β4 and α3β4α5 pentamers, the next aim was to address whether the inclusion of α5 or α5D398N, which is the most common variant associated to smoking, would compete for β4 sites and modulate nicotine-evoked currents.

Aim3: Generation and electrophysiological analyses of rare missense SNP variants of the β4 subunit

Genome-wide association studies (GWAS) have identified 67 rare missense SNP variants in the coding sequence of CHRNB4. Given that two of these variants predispose to a reduced risk of nicotine dependence, we wanted to assess whether these two variants and another non-characterized variants would produce differences in nicotine-evoked currents. For this aimed we characterized 16 CHRNB4 SNPs with a heterozygocity index>0,001 in the human population.

Aim 4: Construction of lentiviral vectors for transduction and analysis of neuronal cultures and for neuronal gene delivery in the mouse.

Next, we aimed to generate lentiviral particles carrying functionally different β4 SNPs and use them for infection and subsequent patch-clamp recordings in rat hippocampal neurons. These vectors were also created for use *in vivo* in the mouse.

Aim 5: In vivo analyses of β4 SNPs in mice injected into the medial habenula

The habenula has been shown to be a critical relay station for nicotine intake[46-47] and pain processing[30-31] as well as being one of the unique areas of expression of α3β4 nAChRs in the brain. We aimed at assessing the contribution of β4 rare missense variants to nicotine consumption and nociceptive behavior by stereotactic microinjection of lentivirus encoding different β4 variants in the habenula of living mice followed by behavioral analyses. These include behavioral tests of nicotine intake, anxiety and measurements of pain perception in basal conditions, after inflammation and after neuropathic injury.

2. Materials and Methods

2.1 Chemicals

Name	Company
Acridin ointment	WDT eG, Garbsen, Germany
Agarose, ultra-pure	Invitrogen GmbH, Karlsruhe, Germany
Antibiotic-Antimycotic	Invitrogen GmbH (Gibco), Karlsruhe, Germany
Ammonium chloride	Carl Roth GmbH & Co. KG, Karlsruhe, Germany
Ampicillin sodium salt	Sigma-Aldrich Chemie GmbH, Schnelldorf, Germany
B27-Supplement	Invitrogen GmbH (Gibco), Karlsruhe, Germany
Betaisodona	Mundipharma, Limburg/Lahn, Germany
Bovine serum albumin (BSA)	Sigma-Aldrich Chemie GmbH, Schnelldorf, Germany
Bromphenolblue	Carl Roth GmbH & Co. KG, Karlsruhe, Germany
Calcium chloride dihydrate	Merck KgaA, Darmstadt, Germany
Chloroform	Carl Roth GmbH & Co. KG, Karlsruhe, Germany
Collagenase Type I	Sigma-Aldrich Chemie GmbH, Schnelldorf, Germany
Dimethyl sulfoxide (DMSO)	Merck KgaA, Darmstadt, Germany
dNTP-Mix	Sigma-Aldrich Chemie GmbH, Schnelldorf, Germany
EDTA disodium-dihydrate	Carl Roth GmbH & Co. KG, Karlsruhe, Germany
Ethanol	Carl Roth GmbH & Co. KG, Karlsruhe, Germany
Ethidium bromide	Carl Roth GmbH & Co. KG, Karlsruhe, Germany
FBS (fetal bovine serum)	Invitrogen GmbH (Gibco), Karlsruhe, Germany
D-(+)-glucose	Sigma-Aldrich Chemie GmbH, Schnelldorf, Germany
D-MEM	Invitrogen GmbH (Gibco), Karlsruhe, Germany
DNAse I	Sigma-Aldrich Chemie GmbH, Schnelldorf, Germany
Glacial acetic acid	Carl Roth GmbH & Co. KG, Karlsruhe, Germany
GlutaMAX™	Invitrogen GmbH (Gibco), Karlsruhe, Germany
Glycine	Carl Roth GmbH & Co. KG, Karlsruhe, Germany
Glycerol	Carl Roth GmbH & Co. KG, Karlsruhe, Germany
HBSS (10x)	Invitrogen GmbH (Gibco), Karlsruhe, Germany
HEPES	Carl Roth GmbH & Co. KG, Karlsruhe, Germany

Immu-Mount™	Thermo Scientific, Pittsburgh, PA, USA
Isopropanol	Carl Roth GmbH & Co. KG, Karlsruhe, Germany
Ketamin 10 %	WDT eG, Garbsen, Germany
Lipofectamine™ 2000	Invitrogen GmbH, Karlsruhe, Germany
ß-mercaptoethanol	Sigma-Aldrich Chemie GmbH, Schnelldorf, Germany
Methanol	Carl Roth GmbH & Co. KG, Karlsruhe, Germany
$MgCl_2$ (50 mM)	Invitrogen GmbH, Karlsruhe, Germany
Mineral oil	Carl Roth GmbH & Co. KG, Karlsruhe, Germany
Neurobasal medium	Invitrogen GmbH (Gibco), Karlsruhe, Germany
Nicotine-tartrate	Sigma-Aldrich Chemie GmbH, Schnelldorf, Germany
O.C.T.™ Tissue Tek	Sakura Finetek, Zoeterwoude, Netherlands
Oligonucleotides	BioTeZ Berlin Buch GmbH, Berlin, Germany
Opti-MEM®	Invitrogen GmbH (Gibco), Karlsruhe, Germany
Paraformaldehyde	Sigma-Aldrich Chemie GmbH, Schnelldorf, Germany
PBS (10x)	Invitrogen GmbH (Gibco), Karlsruhe, Germany
PCR Rxn buffer (10x)	Invitrogen GmbH, Karlsruhe, Germany
Penicillin/streptomycin	Invitrogen GmbH (Gibco), Karlsruhe, Germany
Peptone	Carl Roth GmbH & Co. KG, Karlsruhe, Germany
Poly-D/L-ornithine hydrobromide	Sigma-Aldrich Chemie GmbH, Schnelldorf, Germany
Poly-L-lysine 0.01 %	Sigma-Aldrich Chemie GmbH, Schnelldorf, Germany
Protease inhibitor tablets complete mini	Roche Pharma AG, Grenzach-Wyhlen, Germany
Regephitel®	Alcon Pharma GmbH, Freiburg, Germany
Rompun® (2% Xylazin)	Bayer Vital GmbH, Leverkusen, Germany
Sodium chloride	Carl Roth GmbH & Co. KG, Karlsruhe, Germany
Sodium hydrogen sulfate	Sigma-Aldrich Chemie GmbH, Schnelldorf, Germany
Sodium hydroxide	Sigma-Aldrich Chemie GmbH, Schnelldorf, Germany
Sucrose	Sigma-Aldrich Chemie GmbH, Schnelldorf, Germany
TEA	Sigma-Aldrich Chemie GmbH, Schnelldorf, Germany
Tricaine	Sigma-Aldrich Chemie GmbH, Schnelldorf, Germany
TRIS	Carl Roth GmbH & Co. KG, Karlsruhe, Germany
Triton X-100	Sigma-Aldrich Chemie GmbH, Schnelldorf, Germany
Trypsin-EDTA (0.25 %)	Invitrogen GmbH (Gibco), Karlsruhe,

	Germany
Trypsin inhibitor Type I-S (soybean)	Sigma-Aldrich Chemie GmbH, Schnelldorf, Germany
Tween 20	Serva Electrophoresis GmbH, Heidelberg, Germany
Xylene cyanol	Carl Roth GmbH & Co. KG, Karlsruhe, Germany
Yeast extract	Carl Roth GmbH & Co. KG, Karlsruhe, Germany

Table 1. List of chemicals used in this work

2.2 Buffers and solutions

All buffers and solutions described below were prepared using either double-distilled water provided by the MDC water purification system or MQ (Millipore) water produced with a Barnstead E-pure water purification system. Nicotine tartrate salt solutions for nicotine drinking experiments were prepared with tap water.

General buffers and solutions

Name	Composition
1 kb DNA ladder	1 kb plus DNA ladder (Invitrogen), 10 mM Tris-HCl, 50 mM NaCl, 1x DNA loading buffer
4% PFA	4% paraformaldehyde in 1 x PBS with 0.2 M $Na_2H_2PO_4$ pH 7.4
50x TAE	242 g/l Tris base, 5.71 % (v/v) Glacial acetic acid, 0.05 M EDTA, pH 8.0
6x loading dye	0.2 % Xylene cyanol, 0.2 % Bromphenolblue, 30 % Glycerol
Blocking solution for immunostaining	1 x PBS with 10 % goat serum
Cryosection buffer	0.1 M phosphate buffer with 25% glycerol and 25 % ethylene glycol, pH 7.4
Hippocampus culture dissection buffer	1x HBSS with 25 mM Glucose and 15 mM HEPES
Hippocampus culture digestion buffer	1 mg trypsin in 10ml 1xPBS with 20 mM glucose, 15 mM HEPES and 1 mM EDTA
Hippocampus culture digestion inhibition buffer	15 mg trypsin inhibitor type I-S in 12 ml Neurobasal medium
LB agar	LB-medium + 15 % (w/v) agarose
Lysis buffer (in vitro transcription)	20mM Tris-HCl pH=7.5, 1% SDS, 100mM NaCl, 10mM EDTA
PBS (10x)	80 g/l NaCl, 2 g/l KH2PO4, 2 g/l KCl, 21.6 g/l Na2HPO4•7H2O
PEI (polyethylenimine)	1mg PEI MAX per 1ml MQ water
TE buffer	10 mM Tris pH 8.0, 1 mM EDTA

Table 2. List of general-use buffers used in this work

Solutions for electrophysiology surface expression in *X.laevis* oocytes

Name	Expression system	Composition
OR-2 buffer	Xenopus oocytes	82.5 mM NaCl, 2,5 mM KCl, 1 mM $MgCl_2$, 1 mM $CaCl_2$, 1 mM $NaHPO_4$ and 5mM HEPES at pH 7.8
Calcium-free Ringer buffer	Xenopus oocytes	82,5 mM NaCl, 2 mM KCl, 1 mM $MgCl_2$, 10 mM HEPES at pH 7.4
Oocyte digestion solution	Xenopus oocytes	82,5 mM NaCl, 2 mM KCl, 1 mM $MgCl_2$, 10 mM HEPES at pH 7.4, 2mg/ml Collagenase type I
Ringer buffer	Xenopus oocytes	82.5 mM NaCl, 2 mM KCl, 1 mM $MgCl_2$, 1 mM $CaCl_2$, 10mM HEPES at pH 7.4
External (bath) solution	Rat hippocampal neurons	105 mM NaCl, 3 mM KCl, 10 mM HEPES, 5mM glucose, 2mM $CaCl_2$, 1mM $MgCl_2$, 100µM $CdCl_2$
Internal (pipette) solution	Rat hippocampal neurons	90 mM K-gluconate, 5 mM EGTA, 5 mM HEPES, 5 mM glucose, 0.5 mM $CaCl_2$ and 4 mM $MgCl_2$

Table 3. List of the buffers used for electrophysiology

Solutions for surface expression in *Xenopus laevis* oocytes

ND96+ Ca^{+2}	Xenopus oocytes	96mM NaCl, 2mM KCl, 1.8mM $CaCl_2$,1mM $MgCl_2$, 5mM HEPES at pH= 7.6
ND96+ Ca^{+2} + 1% BSA	Xenopus oocytes	96mM NaCl, 2mM KCl, 1.8mM $CaCl_2$,1mM $MgCl_2$, 5mM HEPES at pH= 7.6, 1% BSA w/v

Table 4. Solutions used for the surface expression experiment

Culture media

Name	Composition
LB medium	10 % Tryptone, 5 % Yeast extract, 10 % NaCl, adjusted to pH 7.0
Mammalian cell culture medium	10 % FBS in D-MEM with GlutaMAX™
Rat hippocampus culture start medium	Neurobasal medium with 1x B27-supplement,1x Antibiotic/Antimycotic, GlutaMAX (0.5mM), glutamate (0.01 mM), 1% FBS and ß- mercaptoethanol (0.025mM)
Rat hippocampus culture medium	Neurobasal medium with 1x B27-supplement,1x Antibiotic/Antimycotic, GlutaMAX (0.5mM) and ß- mercaptoethanol (0.025 mM)

Table 5. Figure List of culture media

Solutions for behavioural experiments

Name	Composition
Nicotine drinking solution	12.5, 25, 50 and 100µg/ml of nicotine tartrate salt in 100 ml tap water
5% formalin	2.7 ml of 37% formalin in 17,3 ml of 0.9% NaCl (for 20 ml)

Table 6. List of culture media

2.3 Molecular biology reagents

Bacteria strains

Name	Genotype
E.coli TOP10	F-*mcr*A Δ(*mrr-hsd*RMS-*mcr*BC) φ80*lac*ZΔM15 Δ*lac*X74 *rec*A1 *ara*D139 Δ(*ara*leu) 7697 *gal*U *gal*K *rps*L (StrR) *end*A1 *nup*G
E.coli DH5α	F-φ80*lac*ZΔM15Δ(*lac*ZYA-*arg*F)U169 *rec*A1 *end*A1 *hsd*R17(rk^-, mk^+) *pho*A *sup*E44*thi*-1 *gyr*A96 *rel*A1 *ton*A
E.coli Hb101	F- *sup*E44, *hsd*S20(r_B^-,m_B^-), *rec*A13, *ara*-14, *pro*A2, *lac*Y1, *gal*K2, *rps*L20, *xyl*-5, *mtl*-1, *leu*B6, *thi*-1

Table 7. Bacteria strains used in this work

Cell lines

Name	Source	Affiliation/Address
HEK 293T	System Biosciences (SBI)	Mountain View, CA, USA

Table 8. Cell lines used in this work

Plasmids

Name	Source	Affiliation/Address
pCS2+	Addgene Inc.	Cambridge, MA, USA
pFUGW	Addgene Inc.	Cambridge, MA, USA
Lentiviral packaging plasmids pLP1, pLP2, pLP-VSV-G	ViraPower™ Lentiviral expression system; Invitrogen GmbH (Gibco)	Karlsruhe, Germany

Table 9. Plasmids used in this work

Oligonucleotides used for cloning

Name	Sequence 5‘- 3‘	Purpose
AgeI-koz-β4-F	CTGACCGGTGCCGCCACCATGAGGGGTACGCCCCTGCTCCTCGTCTCT	pCS2A- β4-HA forward primer with kozak sequence (blue)
XbaI-HA-β4-R	CTGTCTAGACTAAGGTCCTCCCAGGCTGGCATAGTCAGGCACGTCATAAGGATAGAGGCCCTTGGAGGGTGCGTGGATCTGGAAGAGGGGTGGATCCTACGTGGTTTCTTCTGCC	pCS2A- β4-HA reverse primer with HA tag (blue)
SOE-β4-F	GGATTCATGAGGGGTACGCCCCTGCT	SOE cloning
SOE-β4-R	TGTAGAAGAGTGGCTTGCGCTTGATG	SOE cloning
SOE-β2-F	CCACTCTTCTACACTATCAACCTCAT	SOE cloning
SOE-β2-R	CTCGAGTCACTTGGAGCTGGGAGCTG	SOE cloning
SOE2-β2-F	CAGGATCCATGGCCGGGCACTCCAACTCAA	SOE cloning
SOE2-β2-R	GGGTGAACGGTGGTGCACATTGAGCACACA	SOE cloning
SOE2-β4-F	CACCACCGTTCACCCAGCACTCACACCATG	SOE cloning
SOE2-β4-R	GGCTCGAGCTCGTCGTCCTTGTAGTCGGTA	SOE cloning
Primer A	GCACCGGTATGGCCGGGCACTCCAACTCAATGGCGCTGTTCA	SOE cloning
Primer B	CCTGCGGCTGACCCACCATCCAACCTCTATGGGAATTCCATGTACTGTACTGTACCTGCTTTTGTC	SOE cloning
Primer C	GACAAAGCAGGTACAGTACAGTACATGGAATTCCCATAGAGGTTGGATGGTGGGTCAGCCGCAGG	SOE cloning
Primer D	AT GCGGCCGC TCACTTGGAGCTGGGAGCTGAGTGGTCAGGGTGG	SOE cloning
inloop_β4_F	AGCGTGTGTGTGCTCAATGTGCACCACCGTTCACCCAGCACT	SOE cloning
inloop_β4_R	GACAAAGATCCAGAGGAACAGGCGGTCGACGACCATTGCGAC	SOE cloning
A_gmβa2_F	CGACCGGTATGGCCCGGTGCTCCAACTCTATGGCGCTGCT	SOE cloning
B_gmins19	TTCCCGGAGGCCACAGCTGCATGGGCCCATGGACCTCAGCCGGGCATCCCTGGGGAGGCCTGCCGTGTGGGAGCTGACTGCAGACTTCATTGATGCAGGATTGACAAAGCAGGTACA	SOE cloning
C_gmins19_R	TGTACCTGCTTTGTCAATCCTGCATCAATGAAGTCTGCAGTCAGCTCCCACACGGCAGGCCTCCCCAGGGATGCCCGGCTGAGGTCCATGGGCCCATGCAGCTGTGGCCTCCGGGAA	SOE cloning
D_gmβ2_R	GCTTCTAGATCACTTGGAGCTGGGAGCTGAGTGGTCAGG	SOE cloning
IRES2_R	GAATGCTCGTCAAGAAGACAG	sequencing
Ub_F2	GTCCGCTAAATTCTGGC	sequencing
WPRE_R2	GCCATACGGGAAGCAATAG	sequencing

Table 10. Oligonucleotides used in this work

Oligonucleotides for site-directed mutagenesis of the murine β4 nAChR subunit

Primer name	Sequence 5‘- 3‘
β4R21C_F	CTTCAGCCTGGGGACTGCTGCCTGGCCAACGCAGAGGAGA
β4R21C_R	TCTCCTCTGCGTTGGCCAGGCAGCAGTCCCCAGGCTGAAG
β4R38C_F	CTGAACAAAACCTGCTACAACAACCTGATC
β4R38C_R	GATCAGGTTGTTGTAGCAGGTTTTGTTCAG
β4N40S_F	AACAAAACCCGCTACAGCAACCTGATCCGC
β4N40S _R	GCGGATCAGGTTGCTGTAGCGGGTTTTGTT
β4I65F_F	TCCTCCCAGCTCTTCTCCATCCGCCTGGAG
β4I65F_R	CTCCAGGCGGATGGAGAAGAGCTGGGAGGA
β4A90I_F	ACTGACTACCGCCTGATCTGGAACAGCTCCTGCTAT
β4A90I_R	ATAGCAGGAGCTGTTCCAGATCAGGCGGTAGTCAGT
β4R108H_F	ATTCCTGCAAAGCACGTCTGGTTGCCTGAC
β4R108H_R	GTCAGGCAACCAGACGTGCTTTGCAGGAAT
β4R135Q_F	AACGTGATCGTGCAGTCCAACGGCAGCATC
β4R135Q_R	GATGCTGCCGTTGGACTGCACGATCACGTT
β4V310I_F	ACCTTTTCCATCATCACCACTGTGTGTGTC
β4V310I_R	GACACACACAGTGGTGATGATGGAAAAGGT
β4R321S_F	CTCAATGTGCACCACAGTTCACCCAGCACT
β4R321S_R	AGTGCTGGGTGAACTGTGGTGCACATTGAG
β4R348C_F	CCCACCTTCCTCTTCATGAAGTGCCCTGGTCTGGAAGTCA
β4R348C_R	TGACTTCCAGACCAGGGCACTTCATGAAGAGGAAGGTGGG
β4T374I_F	GAAGCTACGTCCGCCTCTGCCTTAGGCCCC
β4T374I_R	GGGGCCTAAGGCAGAGGCGGACGTAGCTTC
β4S380A_F	GCCTTAGGCCCCGCCAGCCCATCCAACCT
β4S380A_R	GAGGTTGGATGGGCTGGCGGGGCCTAAGGC
β4N394T_F	AATTCCATGTACTTTGTGACCCCTGTCCCTGCCACTCCTA
β4N394T_R	TAGGAGTGGCAGGGACAGGGGTCACAAAGTACATGGAATT
β4A348V_F	TTAGAGGGCGTCGTGTTCATCGCACAGCAT
β4A348V_R	ATGCTGTGCGATGAACACGACGCCCTCTAA
β4D447Y_F	GATGATCGATATCAGAGTGTCATCGAGGAC
β4D447Y_R	GTCCTCGATGACACTCTGATATCGATCATC
β4F465Y_F	GTCGACCGCCTGTACCTGTGGGTGTTCGTG
β4F465Y_R	CACGAACACCCACAGGTACAGGCGGTCGAC

Table 11. List of the primers used for site-directed mutagenesis of β4 nAChR

Oligonucleotides for site-directed mutagenesis of the murine α5 nAChR subunit

Primer name	Sequence 5‘- 3‘
α5D397N_F	GAGGCCGCGCTCAATTGCATTCGCTACATC
α5D397N_R	GATGTAGCGAATGCAATTGAGCGCGGCCTC
α5R400C_F	GCGCTCGATTGCATTTGCTACATCACGAGA
α5R400C _R	TCTCGTGATGTAGCAAATGCAATCGAGCGC
α5R404T _F	ATTCGCTACATCACGACACACGTAGTGAAA
α5R404T _R	TTTCACTACGTGTGTCGTGATGTAGCGAAT

Table 12. List of primers used for site-directed mutagenesis of α5 nAChR

Oligonucleotides for site-directed mutagenesis of the murine α3 nAChR subunit

Primer name	Sequence 5‘- 3‘
α3A461T_F	AAAGCACAGAATGTAACCAAAGAGATTCAA
α3A461T_R	TTGAATCTCTTTGGTTACATTCTGTGCTTT

Table 13. List of primers used for site-directed mutagenesis of α3 nAChR

Enzymes

Name	Source
Collagenase type I	Sigma-Aldrich Chemie GmbH, Schnelldorf, Germany
DNAse (Type I)	Sigma-Aldrich Chemie GmbH, Schnelldorf, Germany
Restriction enzymes	New England Biolabs GmbH, Frankfurt, Germany
Shrimp alkaline phosphatase (SAP)	USB Europe GmBH, Staufen, Germany
T4 DNA ligase	New England Biolabs GmbH, Frankfurt, Germany
T4 DNA ligase (LigaFast Rapid Ligation System)	Promega GmBH, Mannheim, Germany
Trypsin from bovine pancreas	Sigma-Aldrich Chemie GmbH, Schnelldorf, Germany

Table 14. Enzymes used in this work

Kits

Name	Supplier
EndoFree® plasmid maxi kit	Qiagen GmbH, Hilden, Germany
mMessenger mMachine® SP6 kit	Applied Biosystems (Ambion), Austin, TX, USA
QIAfilter™ plasmid maxi kit	Qiagen GmbH, Hilden, Germany
QIAprep® spin miniprep kit	Qiagen GmbH, Hilden, Germany
QIAquick® gel extraction kit	Qiagen GmbH, Hilden, Germany
QuikChange Site-Directed Mutagenesis Kit	Stratagene, La Jolla, CA, USA
QuikChange Site-Directed Mutagenesis Kit XL	Stratagene, La Jolla, CA, USA
SuperSignal ELISA Pico Chemiluminescent Substrate	Thermo Scientific, Karlsruhe, Germany

Table 15. List of the kits used in this work

Antibodies and gel markers

Name	Purpose	Supplier
Anti-GFP, polyclonal, rabbit	IS	Invitrogen GmbH (Molecular Probes), Karlsruhe, Germany
Alexa Fluor® 488 goat anti-rabbit IgG	IS	Invitrogen GmbH (Molecular Probes), Karlsruhe, Germany
Anti-β4, polyclonal rabbit	SE	Obtained from C.Gotti, Institute of Neuroscience, Milan, Italy
Goat anti-rabbit-HRP	SE	Jackson ImmunoResearch Europe Ltd., Suffolk, UK
1 kb plus DNA ladder	Agarose gels	Invitrogen GmbH (Molecular probes), Karlsruhe, Germany
RiboRuler™ high range RNA ladder	Agarose gels	Fermentas GmbH, St.Leon-Rot, Germany

Table 16. Antibodies and markers (IS: immunostaining, SE: surface expression)

2.4 Hard- and software

Molecular-/Microbiology:

MJ Research PTC-200Thermo Cycler	MJ Research, Waltham, MA, USA
FlexCycler	Analytik Jena AG, Jena, Germany
PerfectBlue mini-/midigel system	Peqlab Biotechnologie GmbH, Erlangen, Germany
Gel Jet Imager	Intas Science Imaging Instruments GmbH, Göttingen, Germany
BioPhotometer	Eppendorf AG, Hamburg, Germany
J6-MI centrifuge	Beckmann Coulter, Krefeld, Germany
Heareus Megafuge 400	DJB Labcare Ltd, Birminghamshire, UK
Microcentrifuge 5415D	Eppendorf AG, Hamburg, Germany

Microscopy:

Keyence Biozero BZ8100E	Keyence, Neu-Isenburg, Germany

Cell culture:

Incubator CB 150	Binder GmbH, Tuttlingen, Germany
Beckman Optima L-90K ultracentrifuge + SW32 Ti rotor	Beckman Coulter GmbH, Krefeld, Germany

Heraeus Multifuge 1S-R	Thermo Fisher Scientific Inc., Karlsruhe, Germany
BD FACSCalibur™ • 488nm argon laser, 635 nm diode laser • FL1 – Green emission (filter: 530/30) • FL2 – Red/Orange emission (filter: 585/42) • FL3 – Red emission (filter: 650 LP) • FL4 – Far Red emission (filter: APC – 661 nm) • software: CellQuest Pro	BD Biosciences, San Jose, CA, USA
Neubauer counting chamber	Paul Marienfeld GmbH & Co. KG, Lauda-Königshofen, Germany
Tissue culture plates 12 well Tissue culture plates 24 well	Becton Dickinson, Franklin Lakes, NJ, USA
Tissue culture flasks 75 cm^2/150 cm^2	TPP AG, Trasadingen, Switzerland
Cellstar serological pipettes 5/10/25ml	Greiner Bio-One International AG, Frickenhausen, Germany
MultiGuard™ Barrier Tips 2/20/200/1000µl	Sorenson BioScience Inc., Salt Lake City, UT, USA
Stericup vacuum filtration units, 150ml	Millipore GmbH, Schwalbach, Germany
Ultraclear centrifuge tubes 25x89 mm/16x102 mm	Beckman Coulter GmbH, Krefeld, Germany
Superfrost glass slides	Menzel GmbH & Co. KG, Braunschweig, Germany
Glass coverslips, 13mm	Karl Hecht KG, Sandheim, Germany

Electrophysiology:

GeneClamp 500B amplifier	Oocyte recordings	Axon Instruments Inc., Foster City, CA, USA
Bath Perfusion System valve controller (ALA-VM8)	Oocyte recordings	Ala Scientific Instruments, Farmingdale, NY, USA
PLI-100 pico injector	Oocyte recordings	Harvard Apparatus, Holliston, MA, USA
pCLAMP9 software	Oocyte recordings	Axon Instruments Inc., Foster City, CA, USA
EPC-9, EPC-10 patch-clamp amplifier	RHC recordings	Heka Electronic, Lambrecht, Germany
Micromanipulator SM-5, mini25	RHC recordings	Luigs & Neumann Feinmechanik + Elektrotechnik GmbH, Ratingen, Germany
Axioskop 2 FS plus microscope	RHC recordings	Carl Zeiss AG, Oberkochen, Germany
Analog Stimulus Isolator 2200	RHC recordings	A-M Systems Inc., Sequim, WA, USA
WinTida , Patchmaster, Fitmaster	RHC recordings	Heka Electronic, Lambrecht, Germany
Flaming/Brown micropipette puller P-97	RHC recordings	Sutter Instrument company, Novato, CA, USA

Patch pipettes (Borosilicate glass)	RHC recordings	World Precision Instruments, Sarasota, FL, USA
Luminometer TD-20/20	oocyte surface expression	Promega GmBH, Mannheim, Germany

Stereotaxic injections:

Benchmark digital stereotaxic instrument with fine drive and Cunningham mouse and neonatal rat adaptor	Leica Microsystems GmbH (myNeuroLab), Wetzlar, Germany
MO-10 oil hydraulic micromanipulator	Narashige Scientific Laboratory, Tokyo, Japan
Micromotor drill	Leica Microsystems GmbH (myNeuroLab), Wetzlar, Germany
PCR micropipets 1-5 µl	Drummond scientific company, Broomall, PA, USA
Microelectrode puller FP-830	Narashige Scientific Laboratory, Tokyo, Japan
Sterican® needles	Braun Melsungen AG, Melsungen, Germany
Marlin® polyglycolic acid sutures	Catgut GmbH, Markneukirchen, Germany
Reglo digital tubing pump	Ismatec Laboratoriumstechnik GmbH, Wertheim-Mondfeld, Germany
Sliding microtome SM2000R	Leica Microsystems GmbH, Wetzlar, Germany

Table 17. Hardware and software used in this work

2.5 Statistical analyses

All statistical analyses in this work were performed using Microsoft Excel 2007 and SPSS (Statistical Package for the Social Sciences). All quantified data is presented as mean ± S.E.M. Where appropriate, two-sided t-test with unequal variance was used. P values < 0.05 were considered statistically significant (* ≤ 0.05, ** ≤ 0.01, *** ≤ 0.001).

2.6 Molecular biology protocols

Vectors

Vectors encoding for FLAG-tagged β2, β4, α3, α4, α5 and α7 in pCS2+ backbone were a generous gift from Dr. Jerry Stitzel (University of Colorado, Boulder, CO, USA). pCS2 vector contains a strong enhancer/promoter CMV,

both SP6 and T3 promoters for the DNA-dependent RNA polymerases and SV40 polyadenylation site, which makes it suitable for *in vitro* transcription and for subsequent electrophysiological experiments. pCS2A plasmid was derived from pCS2+ vector by introducing the AgeI site restriction site by site-directed mutagenesis. This step has been taken to facilitate the subsequent re-cloning of the nicotinic receptor into the pFU vectors without changing the restriction sites. Chimeric β2/β4 subunits were generated by splice by overlapping extensions method and subsequently cloned into pCS2A vector. The pCS2A-β4-HA vector was generated by PCR amplification of the β4 subunit from pCS2 vector with primers carrying the long variant of HA (hemagglutinine) tag in the reverse primer and cloned into the pCS2A backbone. The α5-FLAG insert was re-cloned form pCS2+ into pCS2A vector due to mutations in the pCS2+ backbone not allowing for successful *in vitro* transcription. Lentiviral construct carrying the fusion of PDGF-R-TM and EGFP (pFU-PE) was generated by Dr. Sebastian Auer. pFU-PE carries the PDGF-receptor transmembrane domain, followed by EGFP (Enhanced Green Fluorescent Protein). pFU-β4-IE and pFU-α3-IC express the mouse β4 or α3 subunit followed by internal ribosomal entry site (IRES) and EGFP or mCherry reporter gene, respectively. This strategy allows for bicistronic expression of the gene of interest and the selectable marker controlled by one promoter, but without the potential drawback of fusing these two genes together as this may alter the function of the gene of interest. Point mutations corresponding to the 16 human single nucleotide polymorphisms in the β4 subunit were introduced by site-directed mutagenesis in pCS2A-β4-HA and in pFU-β4-IE with Quikchange or Quikchange XL site directed mutagenesis kit (Applied Biosystems, Germany), respectively. Point mutations in the pCS2A-α3-FLAG and pCS2A-α5-FLAG was introduced by Quikchange Site-Directed Mutagenesis Kit (Applied Biosystems, Germany). All primers used for the mutagenesis are listed in the **Tables11**, **12** and **13**. Sequences and vector maps of the generated constructs were created with Vector NTI 10.3 (Invitrogen) or Gentle (Magnus Manske, University of Cologne) and are attached in the appendix.

Primer design

All primers used in this study were generated using either Vector NTI 10.3 (Invitrogen, Germany) or GENtle (Magnus Manske, Universität Köln) software. Primers used for cloning were designed in accordance to the standard guideline for primer. Unless otherwise stated, the melting temperature of a primer pair was similar (~60-75 °C), the GC content did not exceed 40-60 % and no secondary structures like hairpins and cross-pairing were allowed. Primers used for cloning were flanked by restriction sites used for subsequent insertion of the amplified sequences into vector backbones. Oligonucleotides used for site-directed mutagenesis PCR were designed according to manufacturer's recommendations.

Primer synthesis and dilution

All primers in this work were synthesized by BioTeZ Berlin-Buch GmbH (Berlin, Germany). Primers were delivered as gel-purified (in case of RealTime PCR oligonucleotides: HPLC-purified) lyophilized film. Upon delivery, primers were diluted with Nuclease-Free Water (Ambion, Austin, TX, USA) to the final concentration of 10µM.

PCR reaction

The polymerase chain reaction (PCR) is an *in vitro* method for the amplification of the DNA[155]. All PCR reactions were carried out in a FlexCycler (Analytik Jena, Germany) or in MJ Research PTC-200Thermo Cycler (MJ Research).

Taq polymerase chain reaction (PCR)

PCR using Taq polymerase has been used to verify the presence of the inserts in the plasmids either self-generated or obtained from external sources. It has been also successfully used to screen the bacterial colonies for the presence of the desire insert (colony PCR). Taq polymerase has a high error rate due to the absence of 3' to 5' exonuclease proofreading activity therefore has not been used for cloning purposes. The reaction composition has been always assembled on ice. For colony PCR, the DNA template was substituted by a part

of a bacterial colony inserted directly to the PCR tube using a small pipette tip. The cycling conditions are detailed in **Tab. 19**.

Table 18. Standard PCR mix composition for Taq polymerase PCR

Amount	Substance
5 µl	10 x PCR buffer
3 µl	$MgCl_2$ (50 mM)
2 µl	dNTP mix (80 mM)
1 µl	DNA template (50 ng)
1 µl	Primer F (10 µM)
1 µl	Primer R (10 µM)
0.1 µl	Taq Polymerase
37 µl	MQ water
50 µl	

Table 19. Standard PCR program for Taq polymerase

Temperature	Duration	Cycles
94 °C	3 min	1x
94 °C	30 s	25 x
x °C*	30 s	
72 °C	x min**	
72 °C	5-10 min	1x
15 °C	∞	1x

* depending on the primer melting temperatures (50-65 °C)

** depending on the fragment length (e.g. ~1 min for 1 kb)

Phusion polymerase chain reaction (PCR)

In order to amplify the desired insert for further cloning, the PCR using the Phusion polymerase (New England Biolabs) has been performed. Phusion is the most accurate termostable polymerase with the fidelity rate about 50 fold higher than the standard Taq polymerases. The Phusion reaction has been assembled on ice using the compounds listed in the **Table 20**. The PCR program parameters are shown I the **Table 21**.

Table 20. Standard PCR mix composition for Phusion polymerase PCR

Amount	Substance
5 µl	10 x PCR buffer
3 µl	$MgCl_2$ (50 mM)
2 µl	dNTP mix (80 mM)
1 µl	DNA template (50 ng)
1 µl	Primer F (10 µM)

1 µl	Primer R (10 µM)
0.1 µl	Taq Polymerase
37 µl	MQ water
50 µl	

Table 21. Standard PCR program for Phusion polymerase PCR

Temperature	Duration	Cycles
94 °C	3 min	1x
94 °C	30 s	25 x
x °C*	30 s	
72 °C	x min**	
72 °C	5-10 min	1x
15 °C	∞	1x

* depending on the primer melting temperatures (50-65 °C)

** depending on the fragment length (e.g. ~1 min for 1 kb)

PCR-based splicing by overlapping extensions (SOE) method

The chimeric β2/β4 subunits have been generated using the gene splicing by overlapping extension method, first described by[156], that allowed for the exchange of large fragments (over 20 bp) between β2 and β4 nAChR subunits (**Fig. 6** in *Results*). First, the fragments to be recombined between the subunits were generated in separate PCR reactions. The primers for these reactions were designed so that they contained at least 18 bp at their 3' ends that were fully complementary to the other subunit and at least 18 bp on their 5’ that were complementary with the start/end of the desired construct. Thus, primer design defined the exact borders of the exchanged fragment. The amplified DNA fragments were then controlled on the 1% agarose gel to assure the correct size and integrity of the PCR product. Subsequently, these PCR products were mixed and acted as a DNA template for the final PCR amplification with the primers designed at the start and at the end of the final construct.

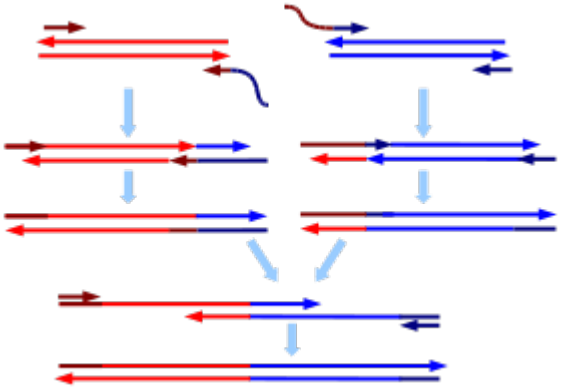

Figure 3. Splice by overlapping extension (SOE) cloning method

QuickChange Site-Directed Mutagenesis

The QuikChange site-directed mutagenesis kit was used to insert or delete single or multiple base pairs, as well as for introduction of point mutations in the specific sites of the DNA template up to 5 kb by PCR. For longer templates (>12 kb) the XL version of the kit was used. Manufacturer's instructions were followed for the assembly of the reaction and the PCR conditions. The reaction composition is shown in the **Table 22**.The PCR conditions are shown in **Table 23**. The number of cycles was dependent on the nature of mutation. Accordingly to the manual, 12 cycles were used to generate the point mutation and 16 cycles to introduce more than one base pare change. Subsequently, PCR product was incubated for 1h at 37°C with 10U *DpnI* enzyme to digest the parental DNA template. The mutated DNA was then transformed into the XL1-Blue or XL1-Gold supercompetent cells.

Table 22. Site-directed mutagenesis reaction composition

Component	Volume
5 x Reaction Buffer	5 µl
dsDNA template (50 ng)	1 µl
Primer F (10 µM)	1 µl
Primer R (10 µM)	1 µl
MQ water	X µl
dNTP mix	1 µl
Quick Solution (DMSO)*	3µl
	up to 50 µl
+ 1µl PfuTurbo DNA polymerase (2,5U/µl)	51 µl

***** Only for QuikChange XL

Table 23. PCR program for site-directed mutagenesis

Temperature	Duration	Cycles
95°C	30s	1x
95°C	30 s	25 x
55°C*	1 min	
68 °C	x min*	
25 °C	∞	

* 1min/kb of plasmid length

DNA and RNA gel electrophoresis

Electrophoresis is an analytical technique used to separate DNA or RNA that differ in size and reactivity. When nucleic acids are subjected to an electric field, they migrate toward the anode (positive terminal) according to their consistent negative charge given by their phosphate backbone. Fragments of linear nucleic acid migrate through agarose gels with a mobility that is inversely proportional to the logarithm of their molecular weight. DNA samples (PCR products, digested DNA form enzymatic reactions) or RNA samples from *in vitro* transcription were analyzed on 0,8-1% agarose gels. For a standard 1% agarose gel, 1g of agarose was dissolved in 100ml of 1XTAE buffer by heating the flask in the microwave oven. Gel was then supplemented with 0,001% ethidium bromide, poured into the horizontal gel chamber (PerfectBlue™, Peqlab, Germany) until fully polymerized. Gel samples were diluted with 6x DNA loading dye and loaded along with 1 kb plus DNA ladder (Invitrogen, Germany). Voltage of 100-120 V was applied for 1 h to separate the DNA fragments. For RNA electrophoresis, samples alongside with RiboRuler™ high range RNA ladder (Fermentas, Germany)were diluted in 5xRNA Loading Buffer (Fermentas, Germany), boiled for 10 min at 70°C .Gels were finally analysed using the Gel Jet Imager (Intas, Germany) transilluminator.

DNA purification from agarose gels

Selected DNA fragments were cut out of the agarose gel under UV light using a scalpel and processed with the QIAquick® Gel Extraction Kit (Qiagen, Germany)

according to the manufacturer's recommendations. DNA was eluted from the purification column with 30 μl MQ water.

Direct sub-cloning protocol

The direct-subcloning protocol was used to integrate the amplified PCR products into the pCS2A vector backbones. This protocol allows for immediate ligation of the amplified PCR product with the vector backbone upon enzymatic digestion, without using the non-enzymatic methods (e.g. TOPO cloning).

Restriction digest

Restriction endonucleases belong to the class of bacterial enzymes; evolutionary they were designed as a part of the host-viral pathogens defense mechanism. These enzymes cut DNA sequence at the specific recognition sites (restriction sites) by hydrolyzing the sugar-phosphate backbone, leaving a phosphate group at the 5' end and a free hydroxyl group at the 3' end of the cleavage site. Isolated PCR-resulting DNAs, as well as the vector backbones were enzymatically double-digested with 10 U of specific restriction endonucleases each (NEB, Germany), supplemented with appropriate buffer in the final volume of 50 or 20μl, respectively. All enzymatic digestions in this work created cohesive ('sticky') ends. Samples were then incubated for over 2hat 37°C.

Dephosphorylation of vector DNA

Upon digestion, plasmid vector DNA was subjected to dephosphorylation procedure to reduce its re-circularization in ligation reactions and to promote integration of the desired DNA inserts. In this step, the 5' phosphate ends left by the restriction endonucleases were removed from digested vectors by shrimp alkaline phosphatase (SAP). As a rule, 1 μl of SAP was added to a restriction digest mix and incubated for additional1h at 37°C. To inactivate the enzyme, the digestion mixture was heated up for 15 min at 75°C.

DNA Ligation

Ligation is a covalent joining of two separate DNA sequences by creating a phosphodiester bond between the 3' hydroxyl group of one nucleotide and the 5' phosphate group of another. This enzymatic procedure is mediated by the T4 ligases. Ligations of the DNA fragments in this work were performed either with 2 μl of T4 DNA ligase (NEB, Germany) and 1x ligation buffer at 16 °C o/n or with 5μl of T4 ligase (Promega, Germany) in 2X LigaFast Rapid Ligation Buffer at RT for 15 min. Reactions were performed in a total volume of 20 μl for overnight or 10μl for LigaFast ligations with3 to 6 fold molar ratios of inserts to vectors.

Preparation and transformation of chemically competent *E.coli* cells

The chemical method for the transformation of bacteria was developed based on the observation that bacteria that had been pretreated with ice-cold solutions of $CaCl_2$ took up bacteriophage DNA when briefly heated to 42◦C [157]. The same procedure was used several years later to transform bacteria with plasmid DNA and remain the basic procedure of molecular biology ever since. This method yields transformation efficiencies ranging from 10^6 to 10^9 transformants/μg of superhelical plasmid DNA in average.

$CaCl_2$ preparation of chemically competent *E. Coli* cells

Self-made $CaCl_2$ competent *E. coli* cells of DH5α and Hb101 strains have been used for regular transformations with ligated plasmids. To prepare the cells, 5ml of LB medium without antibiotics was inoculated with a bud of the bacterial glycerol stock of a respective strain and incubated overnight at 37°C with vigorous shaking. The following day, 100 ml of fresh LB medium was inoculated with 1 ml of overnight culture of *E.coli* cells and grown in the same conditions until the culture reached an OD_{600} = 0.35. All subsequent procedures were performed at 4°C. The culture was then split in two 50 ml Falcon tubes, cooled down on ice for 5 min and the cells were then harvested by centrifugation (2700 g; 10 min; 4 °C). Bacterial pellet was resuspended in 40 ml 0.1 M $MgCl_2$, spun down by centrifugation (2.700 g; 10 min; 4 °C) and again resuspended in 20 ml of 50 mM $CaCl_2$. Cells were then incubated on ice for 30 min and subjected to centrifugation (2700 g; 10 min; 4 °C), followed by resuspension in 2 ml of 50 mM

$CaCl_2$ + 15 % (v/v) glycerol. After 1h incubation on ice, the competent cells were aliquoted of 50 µl per 1.5 ml tube and immediately frozen in liquid nitrogen. To test the competence of the cells, one tube was removed from liquid nitrogen and transformed with 100ng of supercoiled plasmid. If the colony yield after o/n incubation at 37°C was as expected for this transformation protocol, cells were considered competent. The competent cells were stored at -80 °C.

Transformation of chemically competent *E.coli* cells

Ligation samples were transformed into bacteria by heat shock protocol. First, one 50µl aliquot of the cells was thawn on ice. Shortly after the tube content became liquid, 10 µl of the ligation were mixed with the chemically competent cells and incubated on ice for 20 min. Mixes were then heat shocked at 42 °C for 60 s and immediately placed on ice for 2 min. Subsequently, 500 µl LB medium were added to the tube and the cells were incubated at 37 °C for 1h with vigorous shaking at 225 rpm. After the incubation time, cells were streaked on Agar plates containing 100 µg/ml ampicillin and incubated overnight in a 37 °C incubator (Heraeus, Germany).

Glycerol stock preparation

E.coli strains can be stored for many years at -80°C in the medium containing 15% glycerol. Therefore, for the long-term storage of bacteria transformed previously with the plasmid of interest glycerol stocks were prepared. In order to prepare the stock 0.7 ml of overnight bacterial culture was mixed with 0.7 ml of autoclaved 40 % glycerol, shortly vortexed, and immediately frozen in liquid nitrogen. The glycerol stocks were then transferred to -80°C and kept there until further use. To resuscitate the culture for a subsequent plasmid preparation, a small bud of the frozen glycerol stock was immersed in the 5 ml LB medium with 5µl of 100mg/ml ampicillin using a pipette tip. The cells were then cultured at 37°C o/n and subjected to plasmid extraction or inoculation of the large-scale DNA extraction culture.

Plasmid DNA extraction

Minipreparation

Plasmid DNA from small-scale bacterial cultures was used to screen the clones for the presence of correctly inserted DNA fragments. For the DNA isolation, 2ml of LB medium, supplemented with 5µl of 100mg/ml ampicillin was inoculated with a single bacterial colony and incubated overnight at 37 °C with constant shaking. Cells were harvested the following day by centrifugation of 1ml of the bacterial culture at 13000 rpm for 1min and the medium was completely removed. The remaining portion of the culture was stored at 4°C for later inoculation of the culture for the large-scale plasmid DNA extraction. Following small-scale plasmid DNA preparation was performed using the QIAprep® spin Miniprep Kit (Qiagen, Germany) following the manual's recommendations. DNA concentration was measured with the BioPhotometer (Eppendorf, Germany). DNA samples were stored at -20 °C.

Maxipreparation

Large-scale DNA preparation was used to obtain the high-purity DNA of the pCS+ or pCS2A clones of nicotinic receptors for subsequent downstream reactions like *in vitro* transcription or further mutagenesis, as well as for the production of lentiviruses. 400ml LB medium, supplemented with 400µl of 100mg/ml ampicillin was inoculated with 200µl of the remaining portion left form the minipreparation of from the glycerol stock. The extraction of the plasmid DNA was carried out using the QIAfilter™ EndoFree plasmid maxi kit for the plasmids for lentivirus production or QIAfilter™ plasmid maxi kit for all other vectors according to manufacturer's instructions. DNA concentration was then measured with the BioPhotometer (Eppendorf, Germany). DNA for the lentivirus preparation was then diluted with TE buffer to the concentration of 1µg/µl and aliquoted of 130µl each for a single-use. DNA samples were stored at -20 °C.

Sequencing of the plasmids

All DNA obtained from maxipreparations was sequenced prior to any further use. DNA sequencing was performed by Stratec Molecular GmBH (Berlin, Germany) on 3130 Genetic Analyzer (Applied Biosystems), using the BigDye Terminator

v1.1 Cycle Sequencing Kit. Sequencing results were obtained as a FASTA file and analyzed for correctness using GENtle (Magnus Manske, Universität Köln) software. In case of uncertain readout, chromatograms of the sequencing were analyzed using the Chromas 1.45 program (Griffith University, Australia).

In vitro transcription

cRNA can be synthesized *in vitro* using phage DNA-depended RNA polymerases (the most common were obtained from SP6, T7 and T3 bacteriophages). The pCS2+ and pCS2A vectors were designed to encode for SP6 and T3 promoters in opposite directions, therefore to allow for performing the *in vitro* transcriptions of inserts previously cloned in either to generate sense or antisense RNA molecules. Only sense transcripts were used in this work. The DNA template linearization downstream of the insert prior to the *in vitro* reaction is necessary as it defines the length of the transcripts. DNA-dependent RNA polymerases are very processive, therefore circular templates will lead to very long, heterogeneous RNA transcripts.

DNA template linearization

To obtain the RNA used for a subsequent injection into *X.laevis* oocytes approx. 50 µg of plasmid DNA encoding for desired subunit in pCS2+ or pCS2Avector was linearized in a total volume of 300 µl with 100 U of AscI enzyme at 37 °C for more than 4 h. Afterwards, 300 µl of lysis buffer supplemented with 5µl of 20µg/µl proteinase K was added to the mix and incubated at 37 °C for another 30 min. The linearized DNA was then separated from the digestion mixture by 1:1 phenol/chloroform extraction and precipitated with 100% ethanol in the presence of 10M NH_4Ac. After 2h incubation at -20°C, the DNA was pelleted by centrifugation at 13600rpm at 4°C using a table-top centrifuge. The pellet was then washed with 70 % ethanol and air-dried. The linearized DNA was resuspended in 50µl nuclease-free water and its concentration measured. Finally, 2µl of the obtained DNA were run on 1% agarose gel to check for the integrity and complete linearization.

***In vitro* transcription reaction**

The following procedure was performed using the mMessage mMachine® SP6 kit (Applied Biosystems (Ambion), USA). In order to obtain RNA in this process 3 µg of linearized plasmid DNA was used as a template. The *in vitro* transcription reaction was assembled according to manufacturer's recommendations and incubated at 37°C for 3h. The reaction was terminated wit 115µl of nuclease-free water and 15µl of NH4Ac. RNA was the extracted out of the reaction mix by phenol/chloroform purification and precipitated with equal volume of -20°C isopropanol. Resulting RNA pellet was then resuspended in 50 µl of nuclease-free water (Ambion). RNA quality was assessed by agarose gel electrophoresis. The RNA quantity was measured using the BioPhotometer (Eppendorf, Germany). Obtained RNA was used for injections to oocytes for two-electrode voltage clamp experiments and surface expression assays.

Spectrophotometric quantification of nucleic acids concentration

Spectrophotometers are used to determine the concentration of nucleic acids in solution based on their ability to absorb ultraviolet light with an absorption peak at 260 nm wavelength. The more light absorbed in the sample, the higher is the DNA or RNA concentration in it (based on Lambert-Beer law). Measurements of DNA concentrations were performed in nuclease-free water, whereas RNA was measured in 10mM Tris-HCl (pH=7,4) using the BioPhotometer (Eppendorf, Germany).

2.7 Cell culture

All cell culture procedures have been performed under the flow hood using sterile procedures.

Cell culture of HEK293T cells

Adherent human embryonic kidney cells stably expressing the SV40 large T-antigen (HEK293T) cells were cultured in Dulbecco's modified Eagle medium (DMEM + GlutaMAX™), supplemented with 10% Fetal Bovine Serum (FBS) (Invitrogen, Germany). Cells were grown in the humidified Binder CB150 incubator at 37 °C and 5% CO_2 .Cells were passaged every 3^{rd}-4^{th}day (min. 80-90% confluence) by washing then with 5 ml 1 x PBS and subsequent digestion

with 1-3 ml 0.25 % Trypsin-EDTA for 2 min. Next, the enzymatic reaction was terminated by adding7 ml DMEM + GlutaMAX™ with 10% FBS. Finally, 0.5-1 ml of the obtained cells was seeded in a new culture flask.

Preparation of cryostocks of HEK293T for long term storage

Cryostocks of the HEK293Twere used to allow the storage of the cells over the long period of time. Only the cells passaged less them 3 times (low-passage cells) have been used. After harvesting the 80-90% confluent cells, cultured in the 150cm^3 flask, they were spun down by centrifugation at 1000 rpm for 2 min. Supernatant was discarded and the remaining pellet was resuspended in 3 ml ice-cold cell culture freezing medium (DMEM + GlutaMAX™, 10% FBS, 10 % DMSO). The cells were subsequently aliquoted into 2 ml cryotubes (1ml each) and cooled at the rate of -1 °C/min in a Cryo 1°C freezing container (Nalgene, Thermo Fisher Scientific, Denmark). After 24h cells were transferred to liquid nitrogen for long-term storage.

Thawing of HEK293T cryostocks for culturing

Cryostocks of HEK293T were taken out of the liquid nitrogen tank and rapidly defrozen in a 37 °C water bath. Once the cells-containing solution became liquid, it has been transferred to the 15 ml Falcon tube and supplemented with 9 ml pre-warmed medium DMEM + GlutaMAX™ with 10 % FBS. Cells were then centrifuged at 1000 rpm for 2 min and the entire volume of supernatant was discarded. The cells were finally resuspended in 30 ml culture medium in the 150 cm^3 cell culture flask and cultured at 37 °C and 5% CO_2.To completely remove all traces of cytotoxic DMSO from the culture, the medium has been changed once again after 24h. The cells were passaged at least twice before they were used for the lentivirus preparation.

2.8 Lentivirus-based gene delivery to neurons

HIV-1 lentiviral vectors (LV) have been extensively used as gene delivery tools because of their ability to infect dividing and non-dividing cells (e.g. neurons) with stable integration of the gene of interest into the host genome, without

inducing immunogenic responses, unlike adenoviral vectors (Ad). Furthermore, generation and purification of lentiviral particles is relatively easy and they are able to incorporate larger inserts (~8 kb), compared to adeno-associated virus (AAV, ~3-4 kb). For the generation of pseudo-lentiviral particles as vectors, the accessory genes of HIV-1, which encode crucial virulence factors and are essential for HIV pathogenicity have been eliminated[158]. Furthermore, cis-acting elements in the native HIV-1 genome (non-coding sequence elements required for vector RNA synthesis, packaging, reverse transcription, and integration) have been separated from the trans-elements (encoding structural, enzymatic, and accessory proteins), by subcloning to different plasmids. Division of these components to four different plasmids in the third generation of LV vectors minimizes the likelihood of generating replication competent lentivirus (RCL's), as this would require at least three recombination events. As an additional measure of safety, replication defective, self-inactivating (SIN) vectors have been generated, which use a CMV promoter with a deletion in the promoter/enhancer region in the 3' LTR, that is transposed onto the 5' LTR following the transduction of a target cell and thus prevents expression of full-length vector RNA in infected cells. Also the efficiency of LV production has been enhanced by insertion of WPRE (woodchuck hepatitis virus posttranscriptional regulatory element) at the 3'end of the insert which increases the transgene expression more than fivefold by stabilizing the mRNA. In contrast to wildtype HIV-1, most pseudo-lentiviral particles today use the vesicular stomatitis virus G protein (VSV-G) as envelope instead of the parental HIV-1 envelope. The VSV-G envelope introduces three novel features to lentivirus vector particles: (I) it broadens the vector tropism to diverse tissue and cell types of various species *in vitro* and *in vivo*, (II) it stabilizes the vector particles during centrifugation, thereby allowing vector concentration by ultracentrifugation and (III) it changes lentiviral vector entry to an endocytic pathway, which reduces the requirements for viral accessory proteins for full infectivity[159].

Lentivirus production

Recombinant lentiviral vectors were prepared using transient transfection in HEK293T cells. $4.5x10^6$ HEK293T cells were seeded on 24x 10cm dishes, which had been pre-coated for 30 min with poly-l-lysine (0.0005 % in 1 x PBS). The

next day, the lentiviral transfer vector plus the packaging vectors pLP1,pLP2 and the envelope vector pLP-VSV-G (Invitrogen, Germany) were co-transfected with calcium-phosphate transfection into the HEK293TN cells. The transfection mix was prepared with solutions pre-warmed to 37°C as follows: 7 µg lentiviral vector, 4 µg pLP1, 2 µg pLP2 and 2 µg pLP-VSV-G were added to 435 µl MQ and while vortexing, 500 µl 2xBBS and 50 µl 2.5 M $CaCl_2$ were added. Finally, after one minute incubation time at RT, 1ml of transfection mix was added dropwise to each dish and distributed by shaking gently. After 16 hours, the medium was replaced by 9 ml OptiMEM®(Invitrogen (Gibco), Germany) per dish without FBS. The virus containing medium was harvested 24-30 h after medium change, cleared by centrifugation at 3000 rpm for 10 min at 4°C and filtered through 0.45 µm Stericup® vacuum filtration units (Millipore, Germany).

Lentivirus concentration

Ultracentrifugation of harvested lentivirus was applied in order to increase final titers ~100-400 fold. The filtered supernatant was transferred to 35 ml ultraclear centrifuge tubes (Beckman Coulter, Germany), which had been placed in ultracentrifugation buckets. The centrifugation was carried out in a Beckman Optima L-90K ultracentrifuge using a SW32 Ti rotor at 50,000g for 3 h with a purification layer of 1-3 ml 20% sucrose (w/v) in 1x PBS added to the bottom of the tubes. Subsequently, the virus was resuspended in 50-500 µl1x PBS by slowly shaking on ice for 1h. In order to eliminate possibly remaining virus aggregates, the solution was centrifuged at 10,000 rpm for 10-20 s and the supernatant was transferred to a fresh tube. The virus solution was aliquoted in amounts of 5-50 µl in cryotubes with conical inserts and screw-caps, and stored at -70°C. For *in vivo* applications, the virus solution was further purified by a consecutive second ultracentrifugation step of the pooled resuspended virus samples in 17 ml centrifugation buckets for 18 h at 20,000g with the virus placed on top of a 5ml 20% sucrose cushion layer and afterwards resuspended and stored as before.

Lentivirus titration

The titer of concentrated lentiviral stocks was determined by transducing HEK293T cells with limiting virus dilutions.2 µl virus resuspension were added to 198 µl of 1x PBS to generate a 1:100 dilution, of which 100 µl was used to establish a dilution row (resulting dilutions were 1/200, 1/400, 1/800, 1/1600, 1/3200, 1/7200 and 1/14400). Then, 50 µl of each viral dilution was added to 1x 10^5 HEK293T cells per well of a 24-well plate immediately after seeding the cells. Cells were incubated at 37°C with 5% CO_2 for 72h before the medium was removed and cells were washed with PBS (0.5ml), and trypsinized. After transferring the cells to 1.5ml tubes, they were quickly pelleted by centrifugation (1000 rpm, 2 min), resuspended in 500 µl 1 x PBS and transferred to FACS tubes. Finally, the GFP positive cells were quantified by FACS analysis and the transducing units per ml, representing the number of infectious lentiviral particles, were calculated according to the following formula:

$$\mathbf{TU/\mu l = (P \times N / 100 \times V) \times 1/DF}$$

P: % GFP^+ cells, N: number of cells at time of transduction (1 x 10^5), V: volume of dilution added to each well (50 µl) and DF: dilution factor. Only dilutions yielding 1-20 % of GFP-positive cells in a linear range were considered for titer calculations, as below 1 % FACS analysis may not be accurate and above 20 % the chance for multiple infections increases. On average, titers of non-concentrated lentivirus productions were in the range of 5x 10^6transducing units (TU)/ml and concentrated virus titers were 5x 10^8–2x10^9 TU/ml.

FACS analysis

HEK293T cells were analyzed on a FACSCalibur™ system equipped with a 488 nm Argon laser and a 635 nm diode laser according to the instructions of the manufacturer. Briefly, HEK293T cells were trypsinized, washed once with medium and subsequently with 1xPBS. If virus producing cells were used, a 10 min fixation period with 4 % PFA for 10 min was added. After adjusting the settings with a control sample, EGFP fluorescence was detected (FL1 filter:

530/30)in transfected or transduced cells and the percentage of EGFP positive cells as well as the mean fluorescence intensity (MFI) were measured.

Primary neuronal cultures

Rat hippocampus culture

Cultures of dissociated rat hippocampal neurons were prepared from E19 (=embryonic day 19) rat embryos. Pregnant Wistar-Han rats (Charles River, Germany) were first anesthetized with chloroform and the sacrificed by cervical dislocation. After disinfection of the abdominal area with 70 % ethanol, the skin and uterus walls have been cut to expose the embryos. Embryos were then removed from the uterus and placed in ice-cold dissection buffer. Subsequently, they were decapitated, scalp and skull had been removed and the brains were transferred to a fresh dissection buffer kept on ice. The hemispheres were isolated by cutting dorsal to ventral between midbrain and cortex and after removing the meninges, the hippocampi were cut out. Hippocampi were then sliced and digested in the digestion buffer containing trypsin for 8 min at 37 °C. The reaction was stopped by replacing the digestion buffer with digestion inhibition solution for 3 min. Subsequently, digested hippocampi were triturated in 2 ml culture medium by passing them 10-15 times through the 1 ml and 200 µl pipette tips. They were then left standing for 3 minutes to allow non-digested tissue fragments to sink to the bottom of the tube. The upper 1.5 ml of the cell suspension were transferred to a new tube with 8 ml of the culture start medium. The number of dissociated neurons was determined by counting them in the improved Neubauer hematocytometer (0.1 cm3 in each square), calculating the mean and multiplying it with dilution factor and 10^4 to obtain cell number per ml. The cells were seeded in 1 ml of hippocampus culture start medium with a density of 2.5 x 10^5 cells per well on 13 mm glass coverslips, pre-coated overnight with poly-D-/L-ornithine in MQ (50 µg/well) that was removed and after drying replaced by DMEM + 10 % FBS. Both the positively charged ornithine and serum proteins provide a basis for neurons to bind to the glass surface. The culture plate was incubated at 37 °C and 5 % CO_2 and one third of the medium (300 µl) was replaced with hippocampus culture medium twice a week, starting at DIV 5.

2.9 Electrophysiology

Animals

Xenopus laevis frogs used in this work were obtained from *Xenopus Express* (Haute-Loire, France). Animals were kept in the 120l tanks filled with tap water, exchanged every 3rd day. The temperature of the water has been maintained at 18°C by the Aqua Medic Titan 250 coolers (Aqua Medic, USA). The frogs were kept in 12 h in dark/light cycle and fed every 2nd day with Nasco Frog Brittle for Adult *Xenopus* (Nasco, United States).

Extraction of oocytes from *X.laevis* females

Female, wild-captured, adult *Xenopus laevis* frog was placed in the opaque container containing 0.35 % Tricain (Ethyl 3-aminobenzoate methane sulfate salt; Sigma-Aldrich, Germany) in tap water (pH=7,4) for 5-10 min until no movement was present. The anesthetized animal was then placed on the shallow tray filled with ice. After covering the frog's head, heart and limbs with additional portion of ice, the animal was left for 5 min to allow for the body temperature to decrease, thus minimize the bleeding. Ventral skin of the frog was cleaned with a clean cotton swab, but no disinfectants were used as they may cause irritation and subsequent skin infection. The 10mm incision with sterile scalpel was then made through the skin and the underlying muscle layer at the level of the ovaries to expose them. Next, using forceps and small scissors several portions of the ovary have been cut out and placed in the Petri dish containing the OR-2 buffer (82.5 mM NaCl, 2,5 mM KCl, 1 mM $MgCl_2$, 1 mM $CaCl_2$, 1 mM $NaHPO_4$ and 5mM HEPES at pH 7.8). Then the pieces of the ovary were separated in the small portions and incubated in calcium-free Ringer buffer (82,5 mM NaCl, 2 mM KCl, 1 mM $MgCl_2$ and 10 mM HEPES at pH 7.4) supplemented with 2 mg/ml Collagenase Type I (Sigma-Aldrich, Germany) for 2 h at RT with constant shaking. Next, oocytes were washed 4 times 10 minutes each in OR-2 buffer, followed by single washing in OR-2/L-15 1:1 medium supplemented with 1 % penicillin/streptomycin (Invitrogen, Germany) for 15 minutes. After the last washing, oocytes were transferred to the Petri dish filled with OR-2/L-15 1:1 + 1%Pen/Strep medium and allowed to recover at 18 °C overnight. The incisions of the frog were closed using the absorbable Marlin

sutures (D/S16, 5/0; Catgut, Germany) for the muscle layer and non-absorbable Marilon sutures (D/S16, 5/0; Catgut, Germany) for the skin. Following surgery, the frog was placed back in the small container filled with chlorine-free tap water for recovery and post-surgical monitoring. Upon return to normal behavior (indicated by movement when approached), the animal was brought back to its housing tank. Each frog used in this work underwent not more than 2 surgeries on each ovary. Frogs no longer usable for surgical procedures were sacrificed by overdose of the anesthetic (that is by placing them in the Tricain solution for over 30 minutes) and disposed according to the local regulations for cadaver disposal.

Electrophysiological recordings of nAChRs in *X. laevis* oocytes

The oocyte expression vectors pCS2+ or pCS2A encoding for one of the nAChR mouse subunits were used to synthesize the corresponding cRNAs *in vitro*. *X. laevis* oocytes, upon extraction, were incubated in calcium-free Ringer buffer (82,5 mM NaCl, 2 mM KCl, 1 mM $MgCl_2$ and 10 mM HEPES at pH 7.4) containing 2 mg/ml collagenase Type I(Sigma-Aldrich, Germany) for 2 h at RT with constant shaking. Oocytes were then washed in OR-2 buffer (82.5 mM NaCl, 2,5 mM KCl, 1 mM $MgCl_2$, 1 mM $CaCl_2$, 1 mM $NaHPO_4$ and 5mM HEPES at pH 7.8) and allowed to recover in OR-2/L-15 1:1 medium supplemented with 1 % penicillin/streptomycin (Invitrogen, Germany) at 18°C overnight. Each oocyte was injected with 20 nl of a cRNA mix, composed of desired α and β subunit combination using a PLI-100 pico injector (Harvard Apparatus, USA). Macroscopic currents were recorded between 2 and 5 days after injection with a GeneClamp 500B amplifier (Axon Instruments, USA) using a two-electrode voltage clamp with active ground configuration. Borosilicate glass electrodes (0.5-2 MΩ) were filled with 3M KCl. The extracellular recording solution contained (in mM): 82.5NaCl, 2KCl, 1 $CaCl_2$, 1 $MgCl_2$ and 10HEPES at pH 7.4. Nicotine-tartrate (Sigma-Aldrich, Germany) was prepared in extracellular solution at concentrations of 10 nM to 100 mM. Solutions were gravity fed with a flow rate of ~5 ml/min using a Bath Perfusion System valve controller (ALA-VM8, Ala Scientific Instruments, USA). Currents were analyzed using pCLAMP9 software (Axon instruments, USA) with 10Hz sampling rate. Membrane potential was clamped to -70mV and only oocytes with leak currents $<$100 nA were used for

measurements. Data was analyzed using the Clampex and Clampfit software (Axon Instruments, USA).

Surface expression assay in *X.laevis* oocytes

Surface expression of the β4 subunit and its SNP variants was determined by the modified method of [160]. All steps of the assay have been performed in the 24-well cell culture plate (BD Falcon, USA). To achieve the optimal efficiency of all the procedures, not more than 10 oocytes were used per well. Between the washing steps the wells were not used twice, as the antibodies may adhere to the rough bottom of the cell culture plate and therefore may not be effectively washed out, increasing the background signal. Thirty *Xenopus laevis* oocytes have been injected with 90 ng RNA of each subunit using the PLI-100 pico injector (Harvard Apparatus, USA) and left in the OR-2/L-15 1:1 medium supplemented with 1 % penicillin/streptomycin (Invitrogen, Germany) at 18 °C overnight to allow for the complete expression on the injected subunit on the surface of the oocytes. The following day, oocytes were transferred from the storage medium and placed for 30 min with constant shaking in 1 ml of the ND96+Ca^{+2}medium supplemented with 1% BSA at 4°C to block unspecific binding. Next, oocytes have been incubated for 60 min at 4°C with anti-β4 rabbit polyclonal primary antibody (C.Gotti, Milan, Italy) diluted 1:400 in the total volume of 0,5 ml of ND96+Ca^{+2}+1% BSA. Subsequently, oocytes were washed 4 times with 2 ml of ND96+Ca^{+2} + 1% BSA buffer over the course of 30 min at RT and incubated for 30 min with HRP-coupled goat anti-rabbit IgG (Jackson ImmunoResearch, USA) at 4°C. The washing steps were then repeated and followed by 2 additional washings with ND96+Ca^{+2} w/o BSA. Individual oocytes were then placed in 50µl of the SuperSignal ELISA Pico solution (Pierce, Germany) and incubated at RT for 1min. The chemiluminesce has been quantified in a Turner TD-20/20 luminometer (Turner Design, Sunnyvale, CA, USA). The standard error of 5-20% was considered as acceptable due to unequal expression level of the subunits on the oocyte membrane.

Recordings of nicotine-evoked currents in rat hippocampal neurons

Rat hippocampal neurons were cultured on 13 mm glass coverslips in the Rat Hippocampal Culture Medium. After 9 days in culture, neurons were infected with lentiviruses carrying the α3 and one of the variants of β4 nAChR subunit. 3-4 days after lentivirus infection, nicotine-elicited currents were analyzed by whole-cell patch-clamp recordings. Patch electrodes were made from borosilicate glass (1B150F-4, World Precision Instruments, Inc.) with a microelectrode puller (P-97, Sutter Instrument CO). The internal pipette solution contained (mM): 130 KCl, 2 MgCl2, 0.5 CaCl2, 5 EGTA, 10 HEPES, pH 7.3, osmolarity 280 (resistance 5-7 MΩ). Typical series resistance was 15-30 MΩ. 30 μM nicotine was locally applied (50 ms, 18-10 psi) with a pressure device (PR-10, ALA Scientific Instruments) connected to a focal perfusion system (VM4, ALA Scientific Instruments) controlled with a trigger interface (TIB 14S, HEKA). The pipette was moved within 15-20 μm of the recorded cell with a motorized micromanipulator (LN mini 25, control system SM-5, Luigs & Neumann) for drug application and retracted after the end of the puff to minimize desensitization. Currents were recorded with a HEKA amplifier (EPC 10) using PatchMaster software (V2.20, HEKA), and analyzed with FitMaster software (V2.3, HEKA). Membrane potential was hold at -70 mV.

2.10 Stereotactic injections

Animals

All experimental procedures have been carried out in accordance to the rules established by the local governing body (Landesamt für Gesundheit und Soziales, Berlin). Male CLBL/6 mice used for the experiments were either purchased at Charles River (Sulzfeld, Germany) or were obtained from the in-house breeding colony and were all age-matched. Mice were housed in the 12h light dark cycle at the maintained temperature 22-23°C and fed *ad libitum*.

Stereotactic injections

7-12 weeks old male C57/Bl6 mouse was initially anesthetized with i.p. injection of a ketamine/xylazine mix (130 mg/kg and 10 mg/kg, respectively) and

transferred to the home cage until the pedal reflex was absent. Mouse was then placed on the soft surface for further procedures. To prevent desiccation during the time of the injection, the Regephitel® ointment was gently distributed over the eyes of the animal. Prior to the surgical procedures, the shaved area was swabbed with bethadoine solution and the fur was removed from the level of the eyes towards the neck using a pair of small scissors. Next, a small incision was made form between the eyes to between the ears and the periosteum was removed with the sterile scalpel. Subsequently, the animal was positioned on the Benchmark stereotactic frame with a Cunningham mouse adaptor (Leica Microsystems GmbH (myNeuroLab), Germany) using the incisor bar and the atraumatic ear bars to achieve the flat skull position. Next, the reference marks for brain coordinates, bregma and lambda were identified. The flat skull position has been confirmed by checking the D/V coordinates to be equal, otherwise the incision bar or the ear bars was adjusted and the procedure was repeated. Afterwards the same procedure was performed to set the D/V coordinates of the medial/lateral (M/L) axis on both hemispheres. From Bregma the injection places were identified and marked on the skull with a pen using the approximate coordinates for the medial habenula (A/P=-2,7, M/L= +/- 0,5). Using a micromotor drill with a 0.35 mm diameter burr small holes were drilled in the in the skull at the marked points these points and the dura mater was carefully opened with a sterile needle. Under the laminar flow hood the glass capillaries with a ~10-12 mm fine tip (Drummond, USA) were filled with 2 µl of lentivirus, followed by 2.5 µl of mineral oil using a self-prepared suction system. Upon careful insertion of a metal plunger serving as a driving force for the liquid in the capillary, the cannula has been secured to the arm of the stereotactic apparatus. The tip of the capillary was then placed adjacently to the drilled hole and this position was set as D/V=0. Virus-filled capillary was the positioned over the exact MHb location (A/P, M/L coordinated) and smoothly lowered to the desired D/V=X position. Using the MO-10 oil hydraulic micromanipulator (Narishige, Japan) with a flow rate of ~0.1 µl/min 1 µl of virus was injected into the medial habenula on one hemisphere over the time of 10 min. After the injection, the capillary was retained in the place of injection for another 10 min, allowing for the virus to distribute in the brain tissue and avoiding retrograde flow. Subsequently the cannula was slowly retracted and carefully positioned in the mirrored location

in the other hemisphere and then the procedure was repeated. Afterwards the mouse was removed from the frame and placed on the soft surface. The incision was closed either with absorbable Marlin® sutures (Catgut, Germany) or with the histoacryl tissue adhesive (3M, Germany). The acridine ointment was distributed evenly over the suture to prevent infection. A mouse was then placed in the animal cage warmed up by the infrared lap and left for recovery for 2h. For the period of 1 week following the surgery mice were single-caged under S2 conditions, afterwards they were transferred to the new cages and subjected to S1 level regulations.

2.11 Behavioral analysis

Two-bottle nicotine consumption: free-choice paradigm

Two-bottle drinking test was used to measure the consumption to nicotine relative to water, as described in[161]. Naïve to nicotine, stereotactically injected male adult mice were single housed and tested in their home cages. Mice were first presented with 2 bottles of water for 3 days to control the drinking side preference. Bottle with nicotine was in all cases presented on the less preferred side. As a next step, one of the bottles was removed and exchanged with a new one containing water supplemented with nicotine (12,5 µg/ml). The volume drank from each bottle was measured on the third day. Then following the same paradigm 3 different increasing concentrations were tested consecutively (25, 50 and 100 µg/ml). Percent of nicotine consumption was expressed as a ratio of the volume of nicotine solution consumed divided by the total fluid intake (ml nicotine x 100% / ml total).

Thermal nociception (Heargreaves' test)

Thermal withdrawal latency was determined using the Plantar Test (Ugo Basile, Milan, Italy), first described by Hargreaves et al., 1988). Animals were placed in the plexiglas chambers on the heated (30°C) glass surface for 30 min prior to the experiment. Subsequently, high intensity light beam was directed form below at the plantar surface of the hindpaw. The latency of the paw withdrawal has been measured and displayed on the digital unit of the system. Each hindpaw has

been assayed five times per experiment. Mean values were used for statistical analysis.

Mechanical nociception (aesthesiometer assay)

Mechanical sensitivity of the injected mice has been measured using a dynamic plantar aesthesiometer (Ugo Basile, Milan, Italy). Before the experiment, animals were acclimatized to the testing apparatus for 30 min by placing them in the plexiglas chambers on the metal grid of the setup. To assay the mechanical nociception of the mice, a metal rod, moving with an increasing mechanical force (1 g x s^{-1}) was applied to the plantar surface of the mouse hindpaw. After the mice withdrew the paw, the rod was retracted, stopping the counter. The paw withdrawal latency was measured by the digital unit of the system. Each paw was measured five times, averaged per mice and used for statistical analysis.

Partial Sciatic Nerve Ligation (PSCNL)

Mice were anesthetized with 3% isofluran and kept under isofluran anesthesia for the entire period of the surgery. First, incision below the pelvis was made and the muscles were cut along the fibers with a sterile scalpel in order to expose the sciatic nerve at the mid-thigh level. The nerve was then separated using curved forceps and very gently stretched on a distance of 5mm. The sciatic nerve was then tightly ligated by placing 3 nods over the nerve stretch with 5/0 silk threads (Catgut, Germany). Animals were allowed to recover for at least 1 to 2 weeks before testing for spontaneous pain and mechanical allodynia. The success of the surgery has been determined by overall motor coordination of the mice and lack of paw dragging.

Perfusion of mice

Mice were anesthetized by i.p. injection of the mixture of ketamine and xylazine (260 mg/kg and 20 mg/kg, respectively) and the stage of a deep anesthesia has been confirmed by the absence of paw reflex. The intercardiac perfusion has been performed by opening the thoracic cage along its length to the level of sternum and insertion of the 27 gauge injection needle into the left ventricle of

the heart, followed by a small incision in the right ventricle. Over the course of perfusion mice received 5 ml ice-cold 1 x PBS, followed by 10 ml 4 % PFA by the Reglo Digital tubing pump (Ismatec, Germany) with a flow rate of 1.3 ml/min. Subsequently the brains were removed, post-fixed for 4 h in 4 % PFA and transferred to 20 % sucrose in 1 x PBS o/n. Once the brains sunk to the bottom of the 20% sucrose solution, they were considered cryoprotected and prepared for cryosectioning.

Cryosections of perfused mouse brains

Following the perfusion and sucrose embedding, brains of the stereotactically injected mice were taken out from the 20% sucrose solution and span frozen with O.C.T.™ Tissue Tek compound (Sakura Finetek, Netherlands) to the horizontal base of SM2000R sliding microtome (Leica Microsystems GmbH, Germany) filled with dry ice. The brains were then cut into40 µm thick coronal sections and collected in the 24-well plate filled with cryosection buffer(0.1 M phosphate buffer with 25% glycerol and 25 % ethylene glycol, pH 7.4). From each brain, 5 brain sections containing medial habenula were selected and used for immunostaining; those were directly placed on the mesh in the 12-well cell-culture plate with 1xPBS. The remaining brain slices were stored at -20°C.

Immunostaining of brain sections

In order to determine the accuracy of the stereotactic injections brain sections containing medial habenula were stained for EGFP expression. Brain slices containing the medial habenula were blocked for 1h in the Blocking Solution (10 % goat serum and 0.3 % Triton X-100 in 1 x PBS) for 1h at RT. This step was performed to reduce unspecific antibody binding, as the serum originated from the same species in which the secondary antibody was raised. The Blocking Solution was supplemented with TritonX-100, a non-ionic surfactant, to reduce the surface tension and therefore allowing for better penetration of the antibody into the section. Next, the sections were transferred into the solution containing 1 % goat serum and 0.1 % Triton X-100, supplemented with 1/500 dilution of anti-EGFP antibody (rabbit polyclonal; A11122, Molecular Probes/Invitrogen, Germany)and incubated o/n at 4°C. The next day sections were washed three

times in 1 x PBS for 10 min each and subsequently incubated with 1/500 dilution of Alexa® Fluor 488 conjugated secondary antibody (goat anti-rabbit; A11034, Molecular Probes/Invitrogen, Germany) and 1/2000 DAPI in PBS containing 1 % goat serum and 0.1 % Triton X-100 for 2 h at RT. Brain sections were then washed three times for 15 min each in 1 x PBS. During washing wells were never used twice, as the antibodies tend to adhere to the rough walls of the cell-culture plates and that could lead to the increased background signal. Stained floating slices were then fixed on the glass slides using ImmuMount™ (Thermo Scientific, USA) tissue mounting glue. Images were acquired using a Leica SP5 confocal microscope with Leica application suite (LAS) software and processed with Adobe Photoshop CS3. Stained sections were kept at 4°C in the dark conditions.

3. Results

3.1 β4 subunit is rate limiting for α3β4 and α3β4α5 receptor function

Overexpression of β4 nAChR subunit leads to elevated nicotine response in *X.laevis* oocytes

These studies are prompted by our finding that transgenic Tabac mice (containing a BAC transgene of the α3β4α5 cluster) overexpress the β4 subunit in endogenous sites of expression of α3β4α5 nAChRs and that this leads to a functional upregulation of this receptor combination[46]. In order to exclude the possibility that this functional upregulation could be caused by other mechanisms independent of nAChRs, we wanted to first replicate this situation *in vitro*. To do this, *Xenopus laevis* oocytes were injected with equal and increasing (1:1, 1:2, 1:3, 1:4, 1:5, 1:10 and 10:1) amounts of cDNA transcripts of the mouse α3 and β4 subunits, as well as α3 and β2 in 1:1 and 1:10 ratios. Next, I performed two-electrode voltage clamp electrophysiological analysis, and recorded the nicotine-induced macroscopic currents in these oocytes.

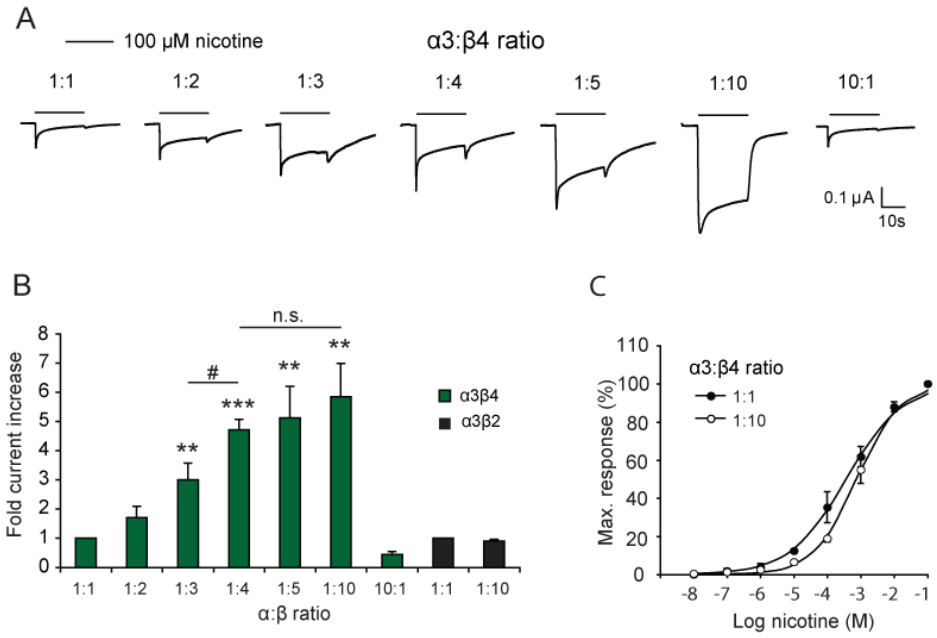

Figure 4. Nicotine-evoked currents recorded in *X.laevis* oocytes injected with α3 and β4 nAChR subunits

(**A**) Representative traces of two-electrode voltage clamp recordings (**B**) Quantification of inward current amplitudes obtained with the indicated α:β ratios of α3β4 (green) and α3β2 (black)

combinations relative to the amplitude of nicotine-evoked currents obtained at 1:1 ratio. Current amplitudes from 1:3 to 1:10 α3β4 ratios are significantly increased compared to 1:2 ratio ($p < 0.01$) with maximal currents at 1:4 ratio ($p < 0.05$). (**C**) Dose response curves expressed as percent of maximal current amplitudes in response to nicotine in oocytes injected with 1:1 and 1:10 ratios of α3:β4.

As shown in **Fig. 4B**, increasing the ratio of β4, but not of the α3 or β2 subunits produced an enhanced response to nicotine in a dose response manner with respect to the amount of β4 transcripts. Moreover, the effect of β4 nAChR subunit on the current amplitude did not alter the nicotine dose response curves, as presented on **Fig. 4C**. This result stays in line with the dose response curves recorded in the MHb neurons of Tabac mice[46]. This result indicated that the amount of β4, but not β2 is rate-limiting for receptor function.

The potentiating effect of β4 is independent on the species and of the type of α subunit

To determine, whether the potentiating effect of β4 is limited to the most commonly co-expressed α3 subunit and to the clones of mouse origin, I performed additional experiment injecting the mouse and chicken α4 subunits with β4 and β2 subunits in the ratios indicated on **Fig. 5B** into *Xenopus laevis* oocytes.

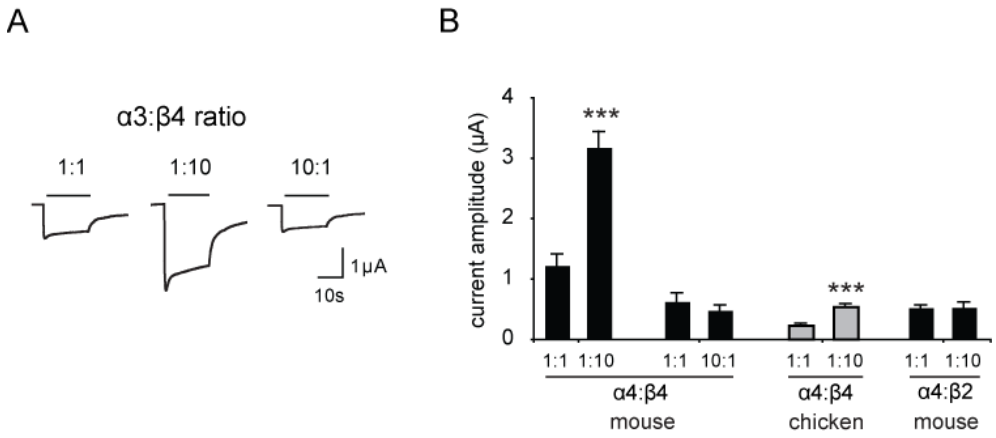

Figure 5. Electrophysiological recordings of α4β4 nAChR subunit combination in *X.laevis* oocytes

(**A**) Representative traces of nicotine-elicited current in oocytes co-injected with α4β4 combination of nicotinic acetylcholine subunits (**B**) Quantification of currents recorded in *X.laevis* oocytes injected with indicated subunits expressed as fold change.

As shown in **Fig. 5B** current potentiation was observed when β4, either of mouse or chicken origin, but not when β2 were expressed in combination with α4 subunits (P < 0,001). This result further confirmed, that despite their high sequence similarity, an unknown motif present in the β4 subunit, yet absent in the β2 plays a role in regulating the surface expression and nicotine-elicited currents.

3.2 Identification of the residue that is responsible for the potentiation

Generation of chimeric β4/β2 constructs

In order to determine, which part of the β4 subunit is responsible for its potentiating effect, several chimeric constructs have been generated. Since the long cytoplasmic loop is the most divergent domain between nAChR subunits and has been implicated in cell-surface expression and trafficking of α2 subunits[162-163], this domain, or short motifs and single residues within it, of β4 receptor was exchanged into the β2 nAChR backbone. Replacement of the cytoplasmic loop of the β2 subunit with the corresponding sequences present in β4 (β2/β4 322-496) led to strong potentiation of nicotinic currents (**Fig.6**). Next, to further delineate the elements within the cytoplasmic loop that could mediate this potentiation, two unique motifs present in β4 (a serine/tyrosine rich motif (β2/+β4 382-391) and gephyrin-like-binding motif (β2/+β4 401-419) were introduced into the β2 loop and no influence on current amplitudes was noticed **(Fig.6).**

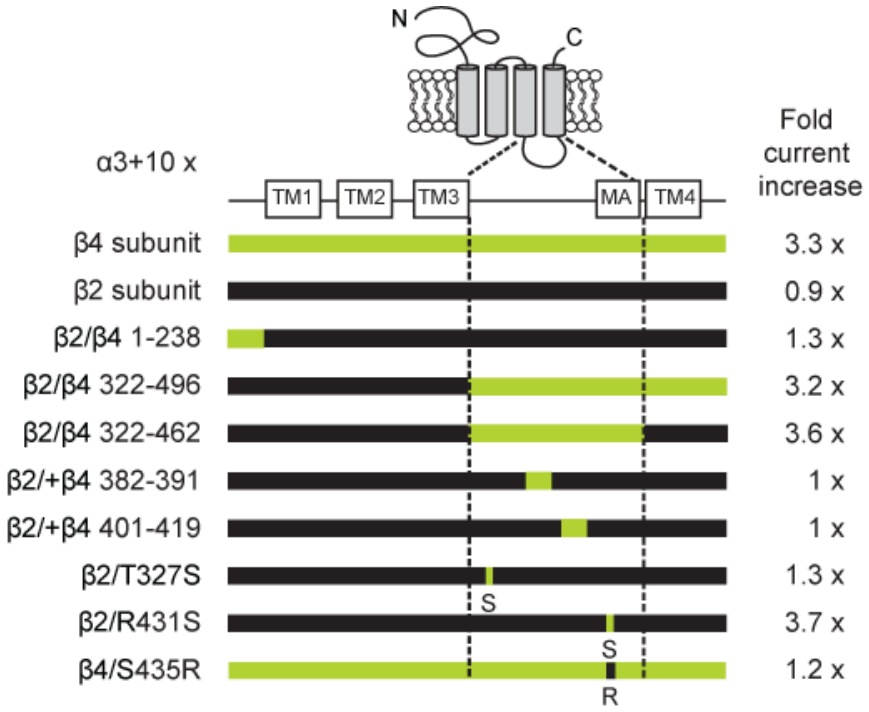

Figure 6. Mapping the unique site in β4 underlying its potentiation ability

Schematic representation of β2/β4 chimeras indicating the domains, motifs or residues exchanged between β4 (in green) and β2 (in black) subunits and corresponding amino acid number and substitutions (left). Fold current increase indicates the relative current amplitude of nicotine-evoked currents (1mM) for each β2/β4 chimera expressed with the α3 subunit at 1:10 relative to 1:1. All values are expressed as a fold change *n* = 5 per ratio in all experiments.

To further specify the unique sequence in the β4 subunit, a comparative bioinformatics analysis of CHRNB4, CHRNB4 and CHRNA5 protein sequences has been performed to identify differences in amino acids within their conserved motifs. Using this analysis as a starting point, eight potential candidates (indicated as T-1 to T-8), indicated on **Fig.7)** were selected. Residues T-2, T-3, T-6 and T-7 differ between mouse and chicken β4 subunits which are equally potent in enhancing nicotine-evoked currents, therefore they have been excluded from further analysis. Residue T-4 lies within the already tested motif in the β2/+β4 382-391 chimera and T-8 does not change the amino acid charge between subunits, therefore these residues were not further considered. The remaining 2 candidates T- 1 (S324 in β4 and T327 in β2) and T-7 (S435 in β4 and R431 in β2) **(Fig.7)** were selected for further analysis.

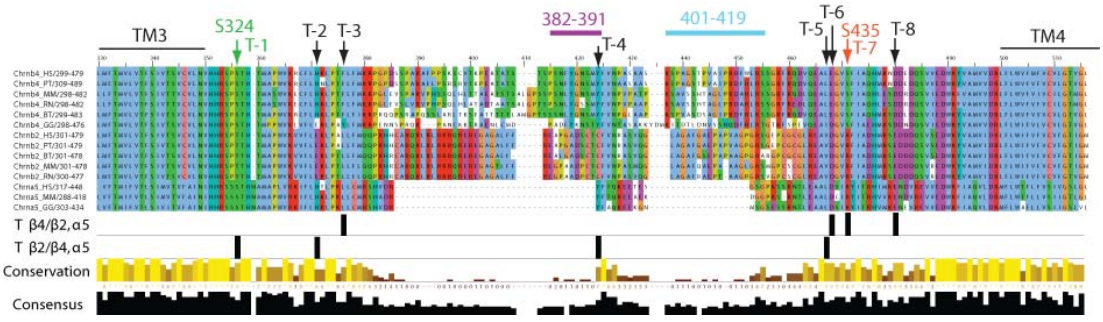
TM3
S324
T-1
T-2
T-3
382-391
T-4
401-419
T-6
T-5
S435
T-7
T-8
TM4
T β4/β2,α5
T β2/β4,α5
Conservation
Consensus

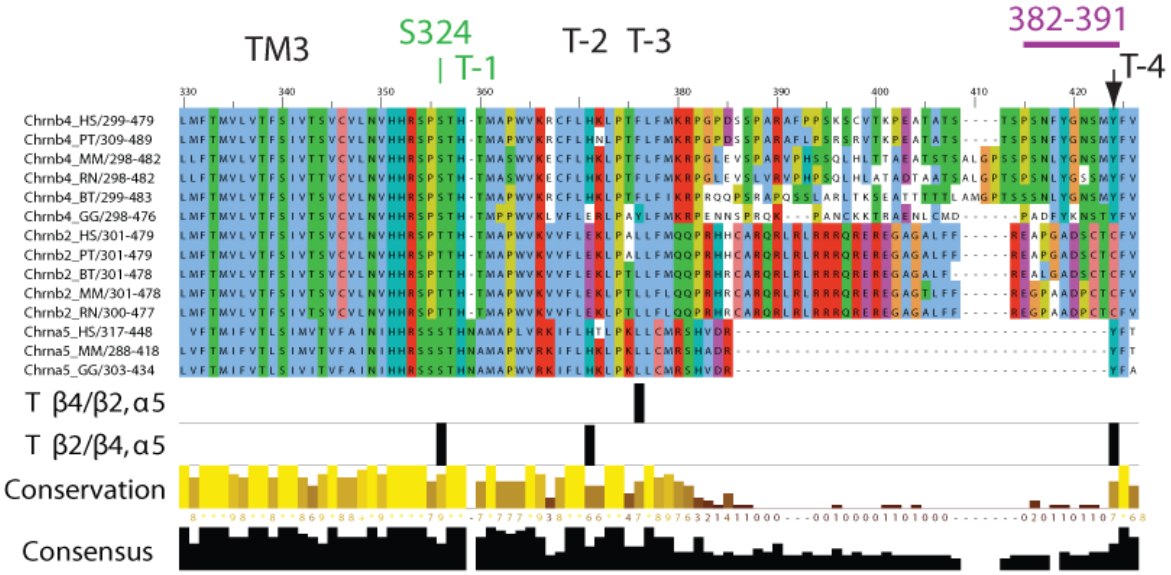
TM3
S324
T-1
T-2
T-3
382-391
T-4
Chrnb4_HS/299-479
Chrnb4_PT/309-489
Chrnb4_MM/298-482
Chrnb4_RN/298-482
Chrnb4_BT/299-483
Chrnb4_GG/298-476
Chrnb2_HS/301-479
Chrnb2_PT/301-479
Chrnb2_BT/301-478
Chrnb2_MM/301-478
Chrnb2_RN/300-477
Chrna5_HS/317-448
Chrna5_MM/288-418
Chrna5_GG/303-434
T β4/β2,α5
T β2/β4,α5
Conservation
Consensus

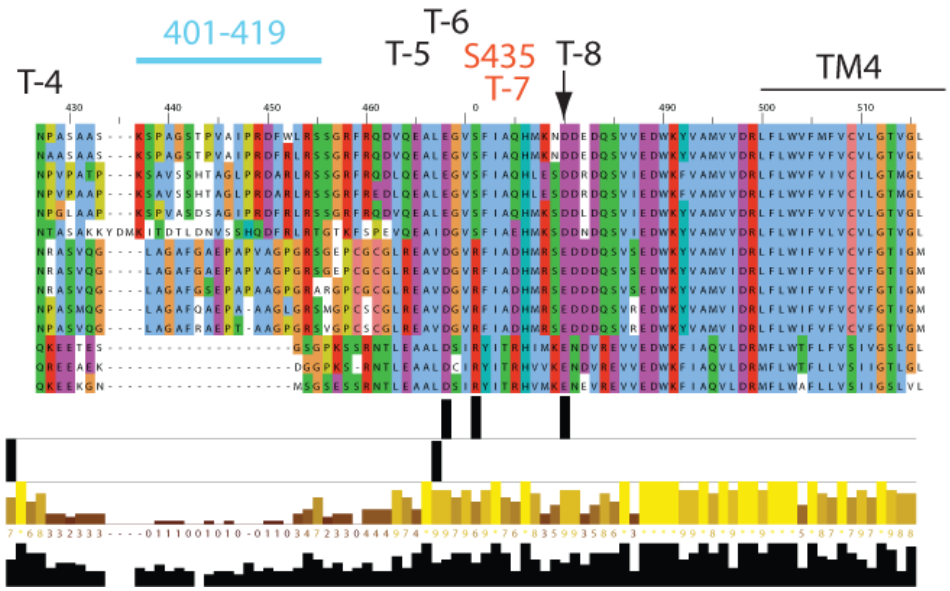
401-419
T-6
T-5
S435
T-7
T-8
T-4
TM4

Figure 7. Alignment over Chrnb4, Chrnb2 and Chrna5 protein sequences (J.-F. Fontaine)

Alignment of Chrnb4, Chrnb2 and Chrna5 protein sequences from different species reveals single differential amino acids within highly conserved regions. A custom track T β4/β2,α5 shows the differential conservation scores of β4 sequences compared to β2 and α5 (the resulting differential residues were designated T-3 and T-6-8). T β2/β4,α5 shows the differential conservation scores of β2 sequences compared to β4 and α5 (the resulting differential residues were designated T-1-2 and T-4- 5). The tracks below show the global conservation and the consensus residues. Two residues of β4 (S324 and S435, green and red arrows) showing differential conservation score were selected for generation of β2-β4 chimeras shown in figure 3. Abbreviations: Homo sapiens (HS), Pan troglodytes (PT), Mus musculus (MM), Rattus norvegicus (RN), Bos taurus (BT), Gallus gallus (GG), transmembrane domain (TM).

Potentiation of currents by β4 overexpression maps to a unique residue (S435) in the β4 nAChR

To determine, whether one of the candidate residues is capable to restore the potentiation of nicotinic currents, observed in β4, they were introduced by site-directed mutagenesis into the β2 nAChR subunit and injected into *X. laevis* oocytes. Macroscopic currents recorded in TEVC system revealed, that the β2 T327S point mutant did not potentiate currents, whereas replacement of β2 R431 with serine resulted in current potentiation equivalent to the native β4 subunit **(Fig.6)**.Furthermore, point mutation of the native S435 in the β4 subunit to the arginine residue present in β2 (β4 S435R) abolished the β4 specific activity. These results show that the unique ability of β4 to potentiate currents when overexpressed maps to a single residue S435 in β4 that confers this property to β2 upon substitution.

3.3 S435 in CHRNB4 maps to the intracellular vestibule in close proximity to several single nucleotide polymorphisms (SNPs)

S435 in β4nAChR subunit maps to the membrane associated-stretch (MA)

Mapping of the S435 in the β4 nAChR protein sequence revealed, that this residue maps to the membrane-associated stretch (MA), domain that precedes TM4[164] **(Fig. 8)**. Recent computational approaches, supported by experiential data, implicated this extracellular α-helical domain as an important determinant of ion permeation and selection[165-166]. This stretch is well conserved in the αβγδ

nAChR subunits from *Torpedo* and refined atomic-scale model of the *Torpedo* nAChR has been obtained [167]. The net charge over the MA stretch of the majority subunits of cation-selective ligand-gated ion channels is negative[167]. This high concentration of charged residues is illustrated in the sequence alignment and colour code of mouse human and torpedo subunits over this MA-stretch **(Fig. 8)**. This comparative analysis revealed that replacement of the polar serine residue in β4 by the positively charged arginine residue present in β2, may cause electrostatic alternations and therefore influence the channel function. Moreover, these analyses indicate that S435, polar residue with uncharged side chains, may cause electrostatic repulsion with the two positively charged lysine residues K443 present in the α3 subunits at the same position (**Fig. 8**) and less efficient assembly of subunits. This conclusion is supported by recent study of Peters [166] , reporting that point mutations within the MA stretch in the α4 and β2 nAChR that changed the amino acid charge significantly changed the resulting channel conductance.

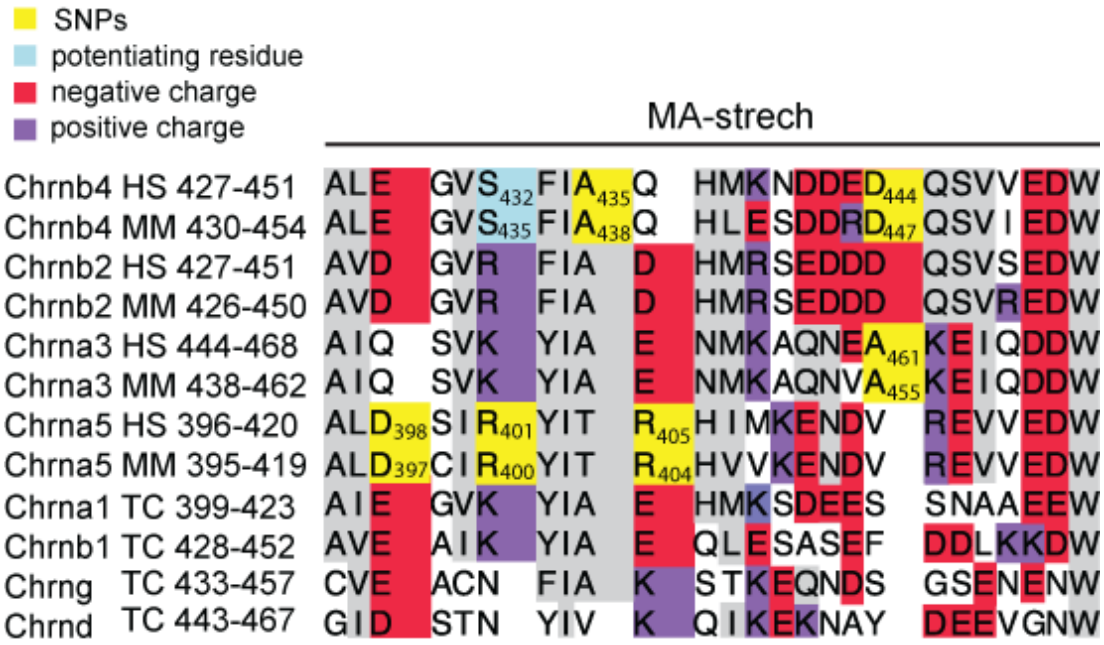

Figure 8. Alignment of human (HS), mouse (MM) and torpedo (TC) sequences spanning the MA-stretch of the indicated nAChR subunits.
Human SNPs and homologous mouse residues are indicated in yellow.

S435 in CHRNB4 is located in close proximity to 6 single nucleotide polymorphisms (SNPs) within the MA stretch

To investigate whether the critical residue S435 identified in β4 could associate with risk allele variants identified in the human population, SNP database of the CHRNB4-CHRNA3-CHRNA5 gene cluster (www.ncbi.nlm.nih.gov/projects/SNP) and were screened. These analyses indicated that six SNPs identified in Caucasians and African Americans are located within the intracellular vestibule of the receptor in close proximity to S435 in β4 **(Fig.8)**. Importantly, rs16969968 (corresponding to D398N in CHRNA5), which is one of the most common and significant SNPs associated with tobacco usage[115,133] lies at 3 amino acids distance from the position occupied by S435 in β4. The fact that four out of the six SNPs as well as the S435R substitution in β4, correspond to changes in charged amino acids **(Fig.8)**, indicate that the electrostatic balance of this vestibule is critical for nAChR function. To test this possibility the electrophysiological assays in oocytes injected with α3, β4 and α5 mouse transcripts containing the point mutations corresponding to the six SNP variants **(Fig. 9A-D)**.

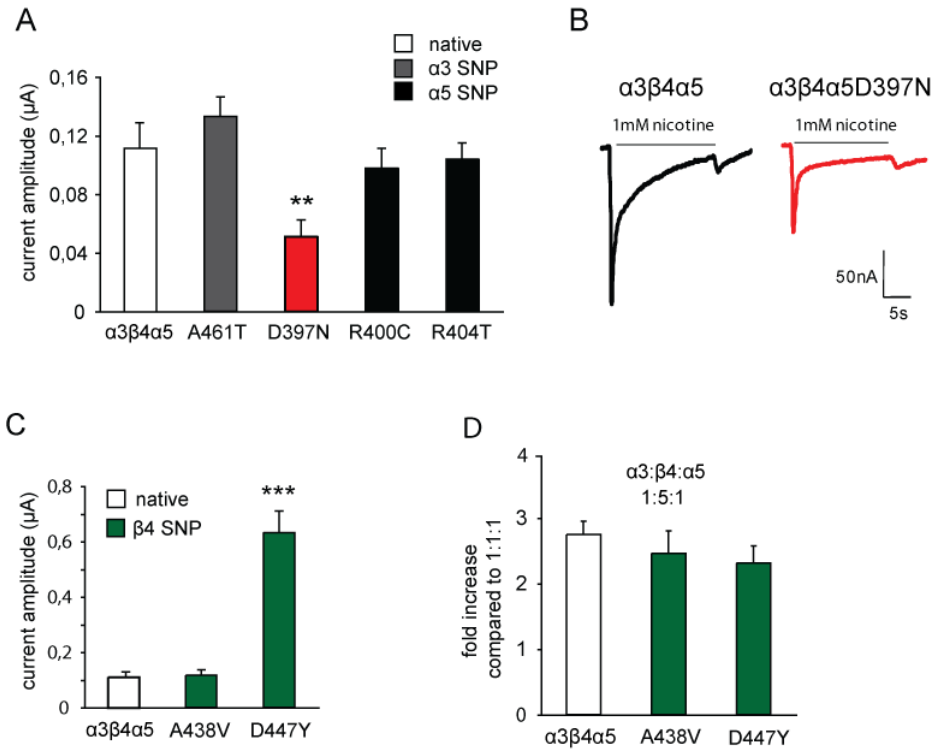

Figure 9. Nicotine-evoked current amplitudes (1mM, 20s) recorded in Xenopus oocytes injected with native α3β4α5 mouse subunits and the indicated point mutants corresponding to the SNPs shown in Fig 8.

(**A**) Peak current amplitudes of α3:β4:α5 nAChRs expressed at 1:1:1 and currents obtained substituting the corresponding subunit with the indicated point mutant of α3 (orange) and with the point mutant D397N of α5 (red) and with the other point mutants of α5 (black) ($P < 0.01$ for α5D397N). (**B**) Representative traces of nicotine-evoked currents in oocytes injected with native α3β4α5 and with α3β4α5D397N at 1:1:1 ratio. (**C**) Peak current amplitudes of α3:β4:α5 nAChRs expressed at 1:1:1 and currents obtained substituting native β4 with the indicated point mutants of β4 (green) ($P < 0.001$ for β4D447Y). (**D**) Relative fold increase of current amplitudes of α3:β4:α5 nAChRs expressed at 1:5:1 relative to 1:1:1 and currents obtained substituting β4 with the indicated point mutants of β4 (green). (n=10 oocytes for each combination).

These analyses showed that the α5 mutant D397N significantly decreased nicotine-evoked currents, while all other point mutants corresponding to α3 and α5 SNPs variants had no effect on current amplitudes **(Fig. 9A)**. Given that elevated levels of β4 potentiate currents in combination with α3 **(Fig.4B),** we tested native β4 and β4 variants with equal ratios (1:1:1) of transcripts encoding α5 and α3 **(Fig. 9B)** or in 5-fold excess of β4 **(Fig. 9C)**. These experiments showed that the β4 variant D447Y significantly increases nicotine-evoked currents at 1:1:1 ratios but leads to the same fold increase in current potentiation mediated by β4 overexpression (**Fig. 9D**). Taken together, our results support the hypothesis that changes in subunit stoichiometry and specific residues that alter the electrostatic charge of the receptor vestibule can strongly influence nicotine-evoked currents and behavioral responses to nicotine.

The relative levels of α5 and β4 subunits strongly affect α3β4α5 nAChR currents.

It has been shown that α5 competes with β4 for association with α4, and that this competition does not occur if β4 is substituted for by β2 [168]. Furthermore, it has been shown that CHRNA5-A3-B4 gene cluster regulates the co-expression of α5, β4 and α3 subunits, and that SNPs in the cluster regulatory regions as well as non-synonymous variants such as rs16969968 (corresponding to D398N in CHRNA5) are associated with nicotine dependence[115,134]. Therefore the next step was to elucidate whether variation of the proportion of α3, β4 and α5 (WT and D398N) subunits influences nicotine evoked currents. To measure this, electrophysiological recordings in oocytes injected with the different cRNA transcripts of the mouse subunits were made. In these experiments the concentrations of α3 and β4 at 1:10 were held constant whereas the cRNA

concentration of α5 wt and α5 D397N variant (corresponding to the human α5 variant D398N) was increased to ratios of 1:10:1, 1:10:5 and 1:10:10 (**Fig.10**).

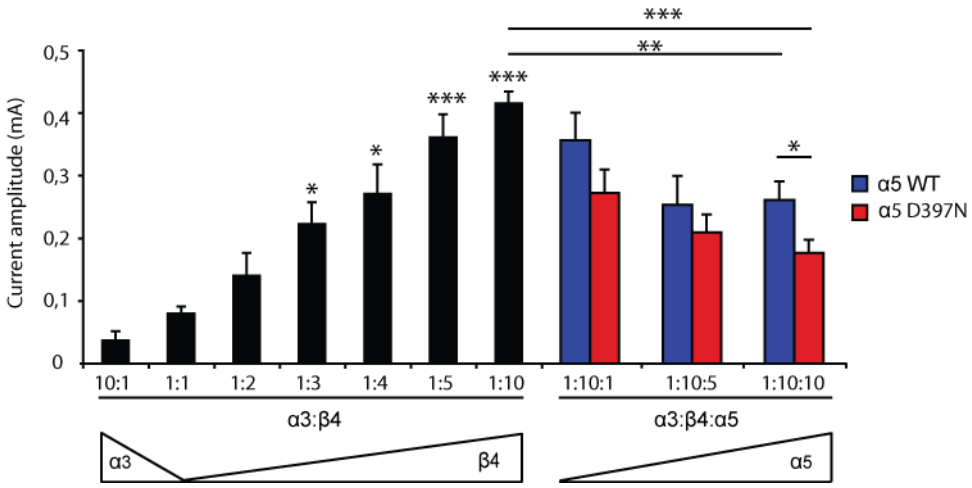

Figure 10. Quantification of nicotine-evoked currents (1mM, 20 s) recorded in *Xenopus* oocytes injected with mouse α3:β4:α5 cRNAs at the indicated ratios.

Addition of α 5 to the α3β4 complex leads to significant decrease of current amplitudes when equal amounts of β4 and α5 are injected (***P* < 0.01 for WT α5 and ****P* < 0.001 for α5 D397N). The D397N variant shows significantly stronger competition with β4 compared to WT α5 (**P* < 0.05).Triangle indicates increasing relative amount of the α5 subunit.

A significant decrease of current amplitudes was detected at higher concentrations of α5 and this effect was significantly more pronounced with α5 D397N. This result is consistent with the human association studies reported by[115], and indicates that α5 and β4 may compete for binding to α3 nAChR and that their balance influences nAChR activity.

3.4 Functional analyses of rare missense SNP variants in β4 nAChR

nAChR β4 overexpression potentiates currents *in vitro* and *in vivo* ([46] and this thesis] and this potentiation depends on a single residue S435. This suggests that β4 is rate-limiting for nAChR assembly. This residue is localized in close proximity to several SNPs, including rs56258098 (D447Y) in CHRNB4 and rs16969968 (D397N) in CHRN5, associated with nicotine addiction. Moreover, competition between the insertion of β4 and α5 subunits, more pronounced when α5 carries the D397N mutation, could be a potential mechanism regulating

nicotine-evoked currents and nicotine consumption. Additionally, two missense variants, rs12914008 (T91I) and rs61737499 (T375I) in CHRNB4, have been reported to be linked to decreased risk for nicotine dependence in humans, and shown to have increased nicotine currents *in vitro* [153]. Therefore I wanted to examine these two characterized SNPs and further determine, whether other SNPs in CHRNB4 may influence its function and alter the response to nicotine. A CHRNB4 SNP database search was performed to select other β4 nAChR SNPs for further analysis.

Selection of missense SNPs in CHRNB4 for functional analysis

CHNB4 SNP database (http://www.ncbi.nlm.nih.gov/snp/) reports 67 missense polymorphisms in the β4 coding region, although they exhibit very low allele frequency. From these 67 we selected 16 missense variants with a reported heterozygocity above p>0.001 were selected (**Fig.11**).

Gene	rs number	amino acid position (HS)	Allele frequency ±S.E.M.	amino acid position(MM)
CHRNB4	71653605	R22C	0.039±0.13	R21C
CHRNB4	72648898	R39C	0.004±0.04	R38C
CHRNB4	75495090	N41S	0.012±0.08	N40S
CHRNB4	149017618	I66F	0.001±0.03	I65F
CHRNB4	12914008	T91I	0.062±N.D	A90I
CHRNB4	149832833	R109H	0.001±0.02	R108H
CHRNB4	56095004	R136Q	0.012±0.08	R135Q
CHRNB4	143402850	V311I	0.001±0.03	V310I
CHRNB4	79914661	R322S	0.02±0.03	R321S
CHRNB4	56235003	R349C	0.014±0.08	R348C
CHRNB4	61737499	T375I	0.016±0.09	T374I
CHRNB4	133537787	T377A	0.5±0.0	S380A
CHRNB4	75124790	N391T	N.D.	N394T
CHRNB4	56317523	A435V	0.004±0.04	A348V
CHRNB4	56258098	D444Y	0.005±0.05	D447Y
CHRNB4	79647370	F462Y	0.002±0.03	F465Y

Figure 11. Selected CHRNB4 single nucleotide polymorphisms

16 single nucleotide polymorphisms were selected from dbSNP. Only the SNPs in the coding region and those leading to missense mutations with allele frequency >0,001 have been selected.

Generation and analyses of β4 mouse variants corresponding to the selected 16 human SNPs

Next, site-directed mutations corresponding to the selected SNPs were introduced in the cDNA of mouse β4 nAChR subunit using the Quikchange mutagenesis kit (Ambion, Austin, USA). RNA transcripts were prepared for mouse nAChR receptor clones in vitro using the mMessenger mMachine Kit. *Xenopus laevis* oocytes were injected with fixed ratio 1:1 of α3 and β4 subunit (or its point variant) and assayed for their response to nicotine in TEVC.

Moreover, a surface expression assay was performed in order to determine, whether the polymorphisms had an influence on the trafficking of the receptor. To allow protein detection, *X.laevis* oocytes were injected with a higher amount of transcripts (90ng of the β4 transcript) and quantified after 24h. Exposed β4 epitopes on the surface of intact oocytes were labeled with a monoclonal antibody to β4, then with a horseradish peroxidase–(HRP) conjugated secondary antibody. Antibody bound to the cell surface of intact oocytes was quantitated by luminometer[160].

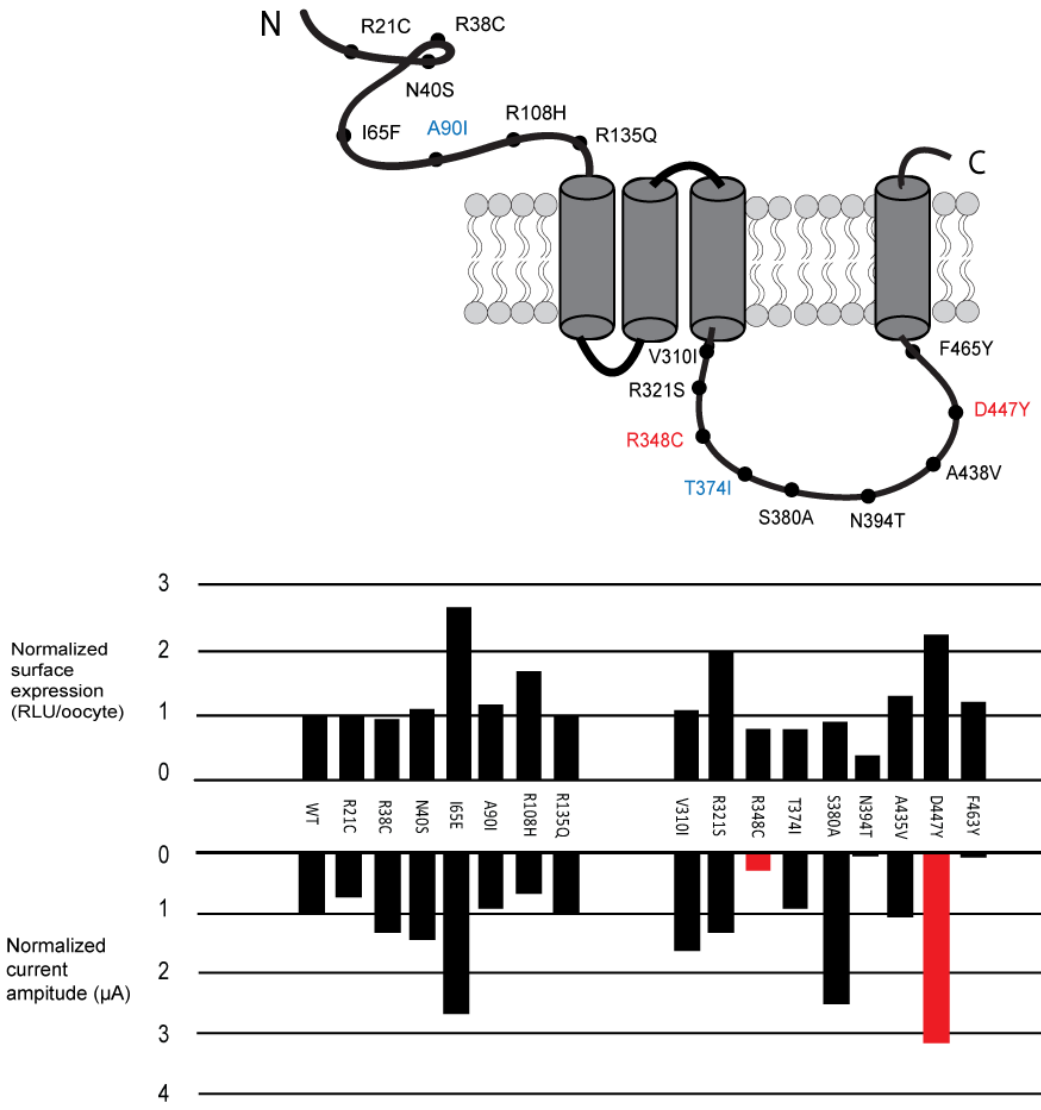

Figure 12. Effect of the rare β4 SNP variants on α3β4 nAChR currents and surface expression in *Xenopus* oocytes.

Electrophysiological macroscopic recordings of *Xenopus* oocytes co-injected with cRNA of α3 and β4 nAChR subunit and surface expression assayed with anti-β4 rabbit monoclonal antibody was aligned with a graphic representation of the β4 nAChR subunit indicating the location of the analyzed SNPs within the subunit's sequence.

Results shown in **Fig.12** revealed, that out of the 16 analyzed SNPs, four (I65E, R321S, R108H and D447Y) exhibited elevated currents when assayed with 1mM nicotine, while only one variant R348C show significantly lower nicotine currents. In contrast with the studies by Haller[153], T91I and 374I did not displayed increased nicotine-elicited currents. However those assays were performed in HEK293 cells instead of oocytes, which may give some expression differences, Surface expression analysis indicated, that in most cases the trafficking of the

receptor was unaffected by the carried mutation. Interestingly, the N394T β4 SNP was not detected on the oocyte surface. This finding suggests that this point mutation might be retained in the ER. In contrast, the D447Y variant, a rare single nucleotide polymorphism reported by Weiss and colleagues[139] in addition to elevated nicotinic currents showed increased number of receptors on the membrane. This result may have a double significance – not only the α3β4D447Y channel properties are altered in comparison to wild-type α3β4, but also the receptor trafficking to the cell surface seems to be more efficient. From these results we conclude that D447Y and R348C are the β4 variants that present stronger functional differences with respect to the native β4 subunit.

3.5 Functional analysis of the nAChR β4 subunit SNPs using lentivirus-mediated gene delivery *in vitro* and *in vivo*

Based on the functional and surface expression experiments in oocytes and the previous analyses of two SNPs present the human population, we selected the variants A90I, R348C, T374I and D447Y of the β4 subunit for further analysis in neuronal cultures and *in vivo*. For this purpose, we generated lentiviral vectors.

Lentiviral vectors, with the most commonly used HIV-1 virus, are considered as the most efficient tool for gene transfer into non-dividing target cells. They offer several advantages over other vectors, including stable integration into the host cell genome, lack of transfer of viral genes, and a relatively large capacity for foreign genes. A number of studies have demonstrated the ability of lentiviral vectors to achieve efficient and sustained transgene expression[169]. As HIV-1 virus' tropism is directed towards immune cells, recombinant HIV-1 vectors were pseudotyped, i.e., HIV-1 envelope proteins, which naturally recognize CD4 receptors on their target cells, were substituted by proteins from other viruses to alter the tropism of the virions [170] to broaden the potential uses of lentiviruses. This allows the targeting of a wider spectrum of specific cell types (e.g. neuronal cells) with high efficiencies. The infection rate of non-dividing cells has been described to be as high as 98%, whereas the lipofectamine-based methods when used to transfect postmitotic neurons, tend to give poorer results (typically 1–5%), although maximum values of up to 30% have been reported for primary

neurons. Recent developments have also reduced the risk posed by replication-competent lentiviruses as follows: (1) viral packaging elements are provided on individual plasmids that need to be co-transfected into packaging cells to produce virions; and (2) six of HIV-1's nine genes encoding important virulence factors have been eliminated without affecting its gene-transfer ability[171].

Already several early studies[172-174] have demonstrated the ability of lentiviral vectors based on HIV-1 are capable of infecting mature neurons in the adult rat brain. Nowadays the lentiviral gene delivery in vitro and in vivo is widely used in neuroscience and it has a substantial contribution to the nicotinic receptors research (reviewed in [175]).

Generation of lentiviral constructs for targeted expression of nAChRs *in vitro* and *in vivo*

HIV-1 based lentiviral particles were used to deliver the β4 subunit and its missense variants to neuronal cells. The constructs were designed to co-express the wild-type mouse β4 subunit (or its SNP variant) or α3 followed by bicistronic expression site (IRES) and EGFP or mCherry, respectively, as a reporter gene to monitor the level of infection (**Fig. 13A and 13B**). The generated lentiviral vectors were named pFU-β4-IRES-EGFP and pFU-α3-IRES-mCherry. The point mutations, corresponding to the single nucleotide polymorphisms, were introduced into the pFU-β4-IRES-EGFP using the site-directed mutagenesis kit [Stratagene, USA]. The advantage of this strategy over generating the fusion protein is the bicistronic expression without potential problems with trafficking or assembly. As a control, the lentivirus plasmid encoding for the transmembrane domain of PDGF receptor fused with EGFP (PE, **Fig. 13C**) was used.

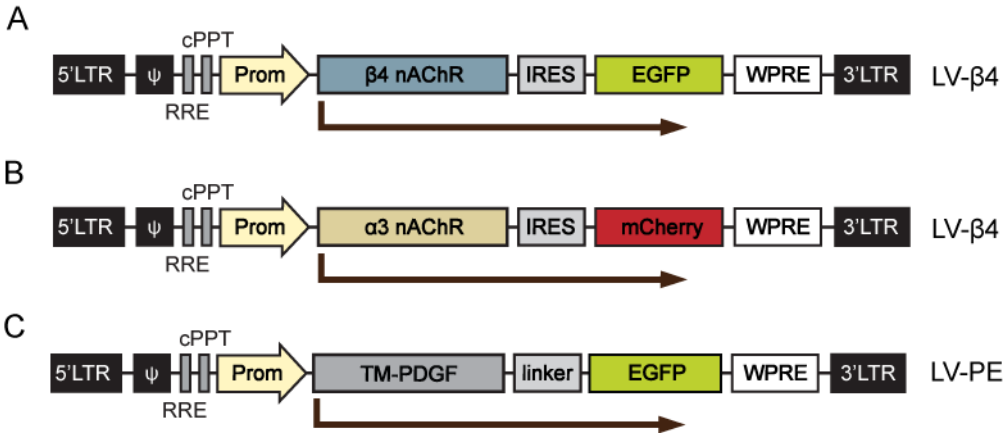

Figure 13. Schematic representation of the viral constructs used in this work

Graphic representation of the (**A**) β4 nAChR and (B) PE constructs used to generate lentiviral particles.*β4 nAChR*, mouse WT β4 nicotinic acetylcholine receptor subunit cDNA; *IRES*, internal ribosome entry site sequence; *EGFP*, enhanced green fluorescent protein; *Prom*, human ubiquitin 2 promoter; *WPRE*, woodchuck hepatitis B virus posttranscriptional regulatory element; *cPPT*, central polypurine tract; *RRE* rev-responsive element; *Ψ* packaging sequence

Expression analysis of the generated lentiviral constructs

Prior to functional assays the infection capabilities and reporter gene expression of the generated lentiviral particles was tested *in vitro*. Rat hippocampal neurons obtained from embryonic day 19 rats were cultured for 9 days in B27-supplemented neurobasal medium on glass coverslips. Mix of both β4 and α3-containg lentiviral particles (MOI=10) were added to the cultured neurons for 4h, then the cell culture medium was exchanged. EGFP and mCherry expression was first observed 24 h after infection. Four days after infection cells were fixed with a freshly prepared 4% paraformaldehyde, washed with 1xPBS and mounted on microscope slides for immunofluorescence analysis. Direct fluorescence analysis revealed in both cases bright fluorescence in the soma of the neurons (**Fig. 14**).

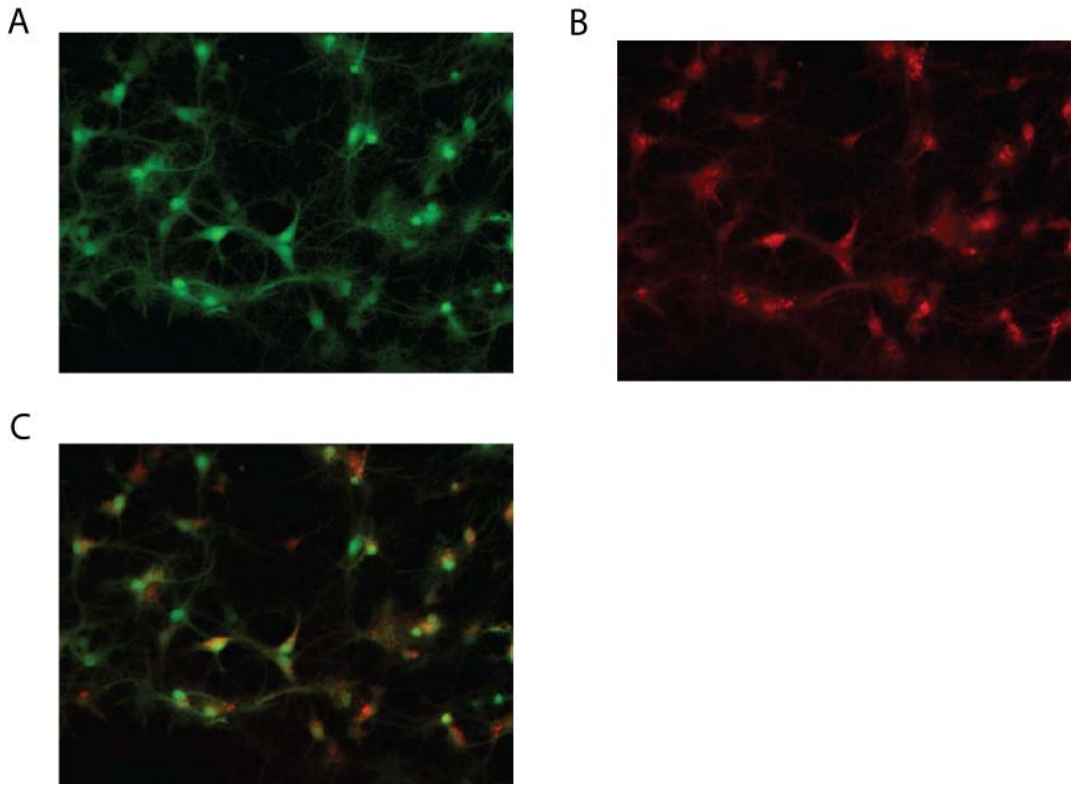

Figure 14. Expression analyses of the generated lentiviruses in rat hippocampal neurons.

Direct fluorescence of (A) β4-IRES- EGFP, (B) α3-IRES-mCherry and (C) merged image in lentivirally transduced neurons of dissociated rat hippocampus culture.

Electrophysiological recordings of β4 nAChR polymorphisms in rat hippocampal neurons

To evaluate further the modulatory effect of point mutations in β4 nAChR subunit on the response to nicotine, patch clamp analyses were performed in lentivirally transduced cultured rat hippocampal neurons. It has been reported that α3 and β4 subunits are expressed endogenously in less than 10% hippocampal neurons[176]. Rat hippocampal neurons obtained from embryonic day 19 rats were cultured for 9 days in B27-supplemented neurobasal medium on glass coverslips. Mix of both β4 and α3-containg lentiviral particles (MOI=10) were added to the cultured neurons for 4h, followed by complete medium removal. The cells were then transferred to the new well containing fresh medium. Dissociated neurons were allowed 4 days for expression of the lentivirally-delivered nicotinic receptor subunits and were subsequently assayed for their response to nicotine with patch-clamp whole cell recordings.

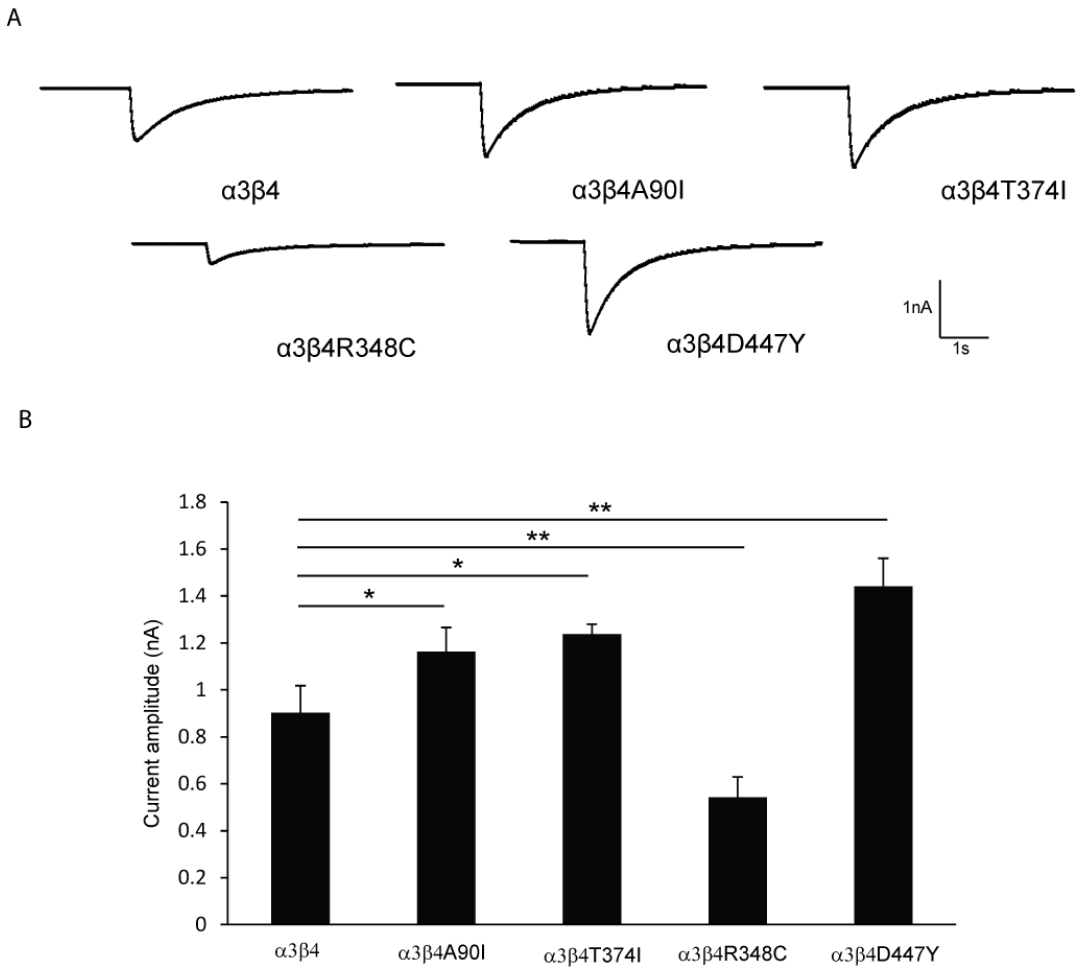

Figure 15. Electrophysiological analyses of β4 subunits and its SNP variants in rat hippocampal neurons

Cultured rat hippocampal neurons were infected with the lentivirus carrying the indicated variants of the β4 subunit (**A**) Representative traces of nicotine elicited currents (**B**) Quantification of nicotine-evoked currents show increased response when neurons were transduced with A90I($p<0,05$), T374I($p<0,05$) and D447Y ($p<0,01$) β4 SNP variants (when compared to control). In contrast, point mutation at R349C position resulted in significant ($p<0.01$) decrease in response to nicotine.

Current amplitudes in response to 30μM nicotine pressure application of A90I, T374I, R348C and D447Y polymorphisms were compared to the WT β4 nACh receptor. Analysis revealed that, in agreement with the results obtained by Haller[153] in HEK cells, point mutants β4A90I and T374I exhibited elevated responses to nicotine. Moreover, consistent with our oocytes studies (**Fig.12**) the SNP variant R348C showed reduced current amplitude, whereas D447Y β4 variant increases nicotine-elicited response when compared to the WT.

For further analysis, we selected the SNPs R349C T374I and D447Y, as they represent three diverse types of responses to nicotine; R349C decreases currents while T374I increases nicotine-elicited currents. These two were

compared for nicotine consumption studies. D447Y, which shows the highest currents was analyzed for pain behavior.

Stereotactic injection of β4 nAChR variants lentiviruses in the medial habenula of mice

To assess the functional influence of the missense variants of β4 nicotinic acetylcholine receptor subunit on nicotine-related behavior *in vivo* we employed the lentiviral-mediated transduction to express the WT, β4T374I and β4R394C in the MHb neurons of wild-type mice. Mice were bilaterally injected either with the control lentivirus (PE), wild-type β4 lentivirus or with a virus containing β4 subunit carrying the indicated point mutation. Mice were allowed to fully recover after the surgery for 2 weeks before the start of the experimental procedures. All injected animals were used for behavioral experiments, and excluded or not later depending on the accuracy of the lentiviral injections.
Animals used for pain assays (expressing lentivirally delivered into MHb control (PE), wild-type β4 and β4D447Y subunits) were obtained in separate injection set.

Immunohistochemistry

Several weeks after the surgery brain coronal sections from stereotactically injected mice were prepared to evaluate the infection efficiency and the accuracy of the stereotactic injection (**Fig.12**).The lentiviral constructs used for this experiment co-express the mouse β4 subunit and the EGFP reporter gene, separated by IRES (Internal Ribosomal Entry Site). This strategy has been selected to reduce the risk of compromised fusion protein function potentially due to improper protein folding or trafficking. However, it has been shown, that the expression of the gene downstream the IRES sequence can be reduced to 60% of the upstream gene[177]. Therefore, for better visualization of the infection area the sections were additionally stained with anti-EGFP antibody. Only the animals that received accurate injections to the medial habenula and showed robust EGFP fluorescence were considered in the analysis of the behavioral experiments.

Coronal sections of each animal are shown on **Fig. 16 A-D.** Animals considered for experimental procedures are underlined.

A

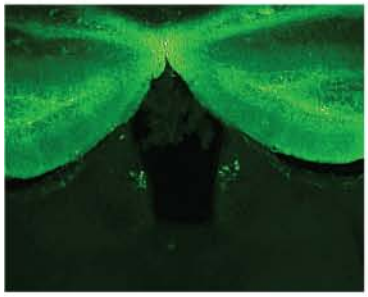

ATF-X0864

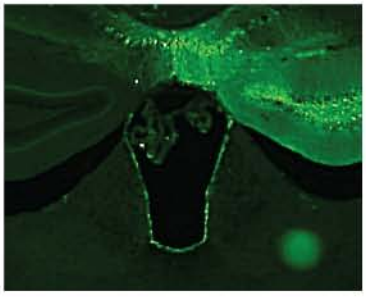

ATF-X0865

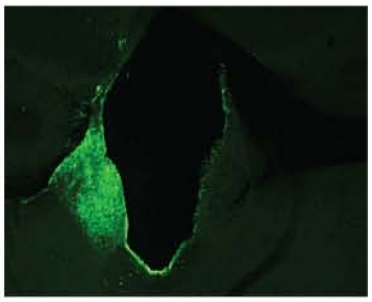

ATF-X0866

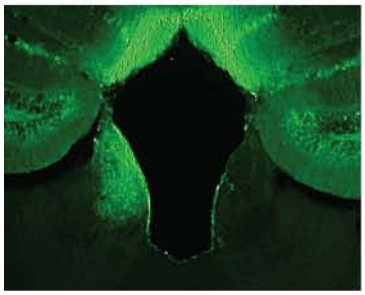

ATF-X0867

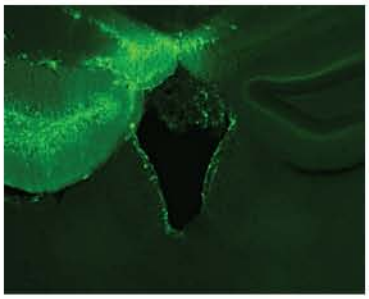

ATF-X0874

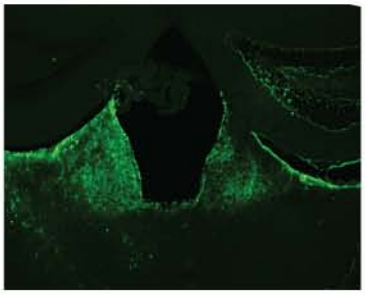

ATF-X0875

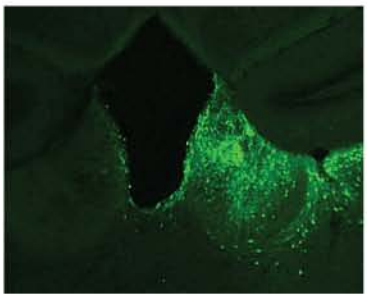

ATF-X0882

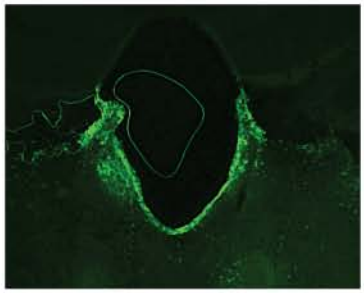

ATF-X0885

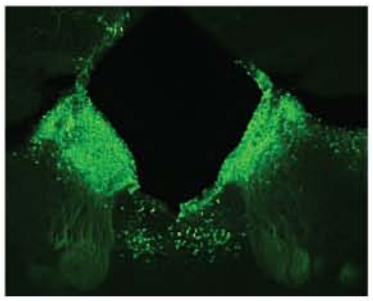

ATF-X0889

Animal ID	LV	Injection
AFQ-X0864	FU-PE-IE	no hit
AFQ-X0865	FU-PE-IE	no hit
AFQ-X0866	FU-PE-IE	one side
AFQ-X0867	FU-PE-IE	one side
AFQ-X0874	FU-PE-IE	no hit
AFQ-X0875	FU-PE-IE	both
AFQ-X0882	FU-PE-IE	one side
AFQ-X0885	FU-PE-IE	both
AFQ-X0889	FU-PE-IE	both

B

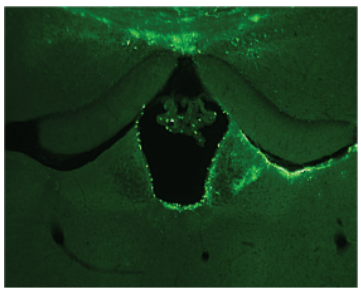

ATF-X0868

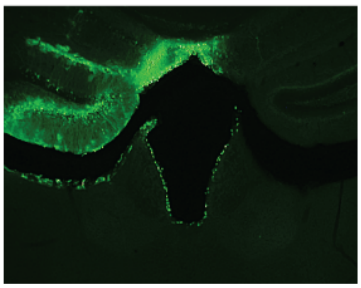

ATF-X0869

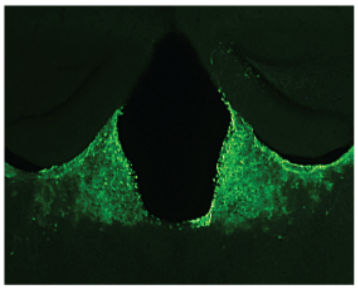

ATF-X0870

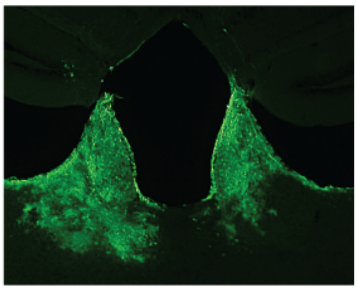

ATF-X0871

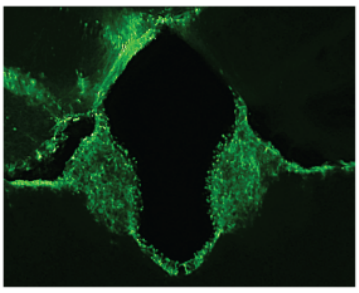

ATF-X0896

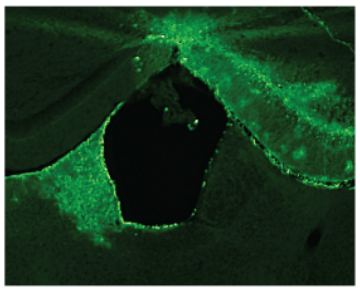

ATF-X0897

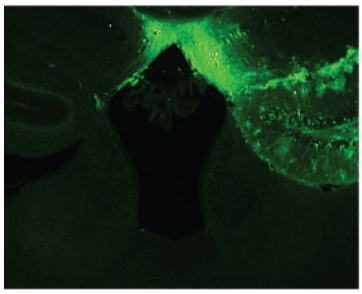

ATF-X0890

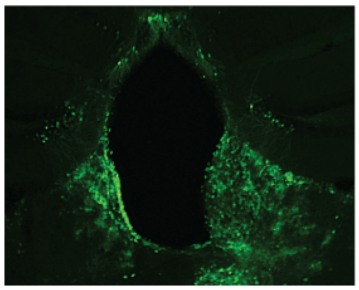

ATF-X0895

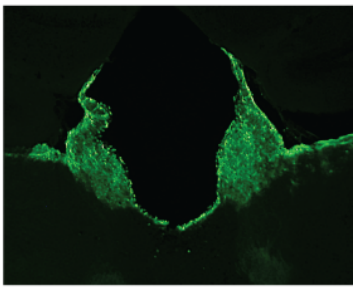

ATF-X0900

Animal ID	LV	Injection
AFQ-X0868	FU-β4-IE	one side
AFQ-X0869	FU-β4-IE	no hit
AFQ-X0870	FU-β4-IE	both
AFQ-X0871	FU-β4-IE	both
AFQ-X0896	FU-β4-IE	both
AFQ-X0897	FU-β4-IE	one side
AFQ-X0890	FU-β4-IE	no hit
AFQ-X0895	FU-β4-IE	both
AFQ-X0900	FU-β4-IE	both

C

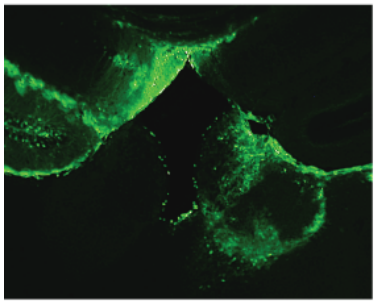

ATF-X0880

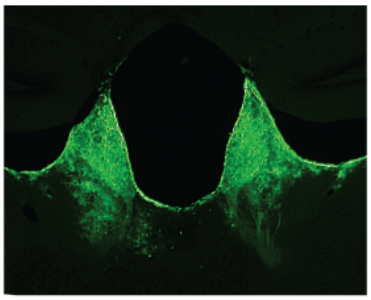

ATF-X0881

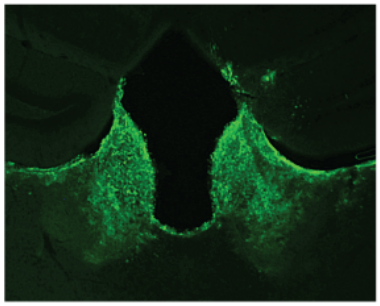

ATF-X0886

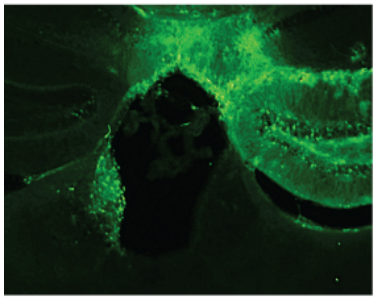

ATF-X0887

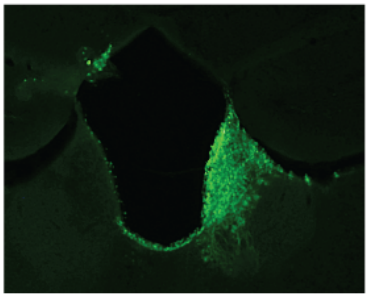

ATF-X0893

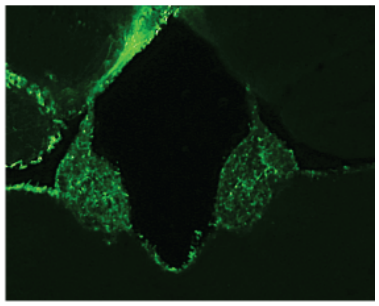

ATF-X0894

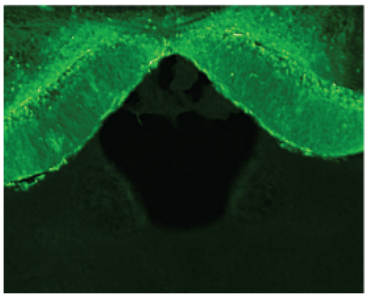

ATF-X0898

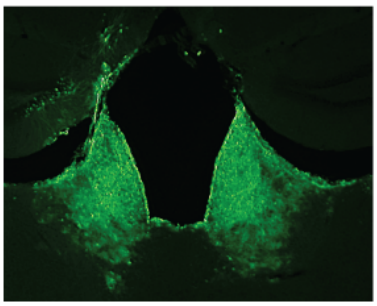

ATF-X0899

Animal ID	LV	Injection
AFQ-X0880	FU-β4R348C-IE	one side
AFQ-X0881	FU-β4R348C-IE	both
AFQ-X0886	FU-β4R348C-IE	both
AFQ-X0887	FU-β4R348C-IE	one side
AFQ-X0893	FU-β4R348C-IE	one side
AFQ-X0894	FU-β4R348C-IE	both
AFQ-X0898	FU-β4R348C-IE	no hit
AFQ-X0899	FU-β4R348C-IE	both

D

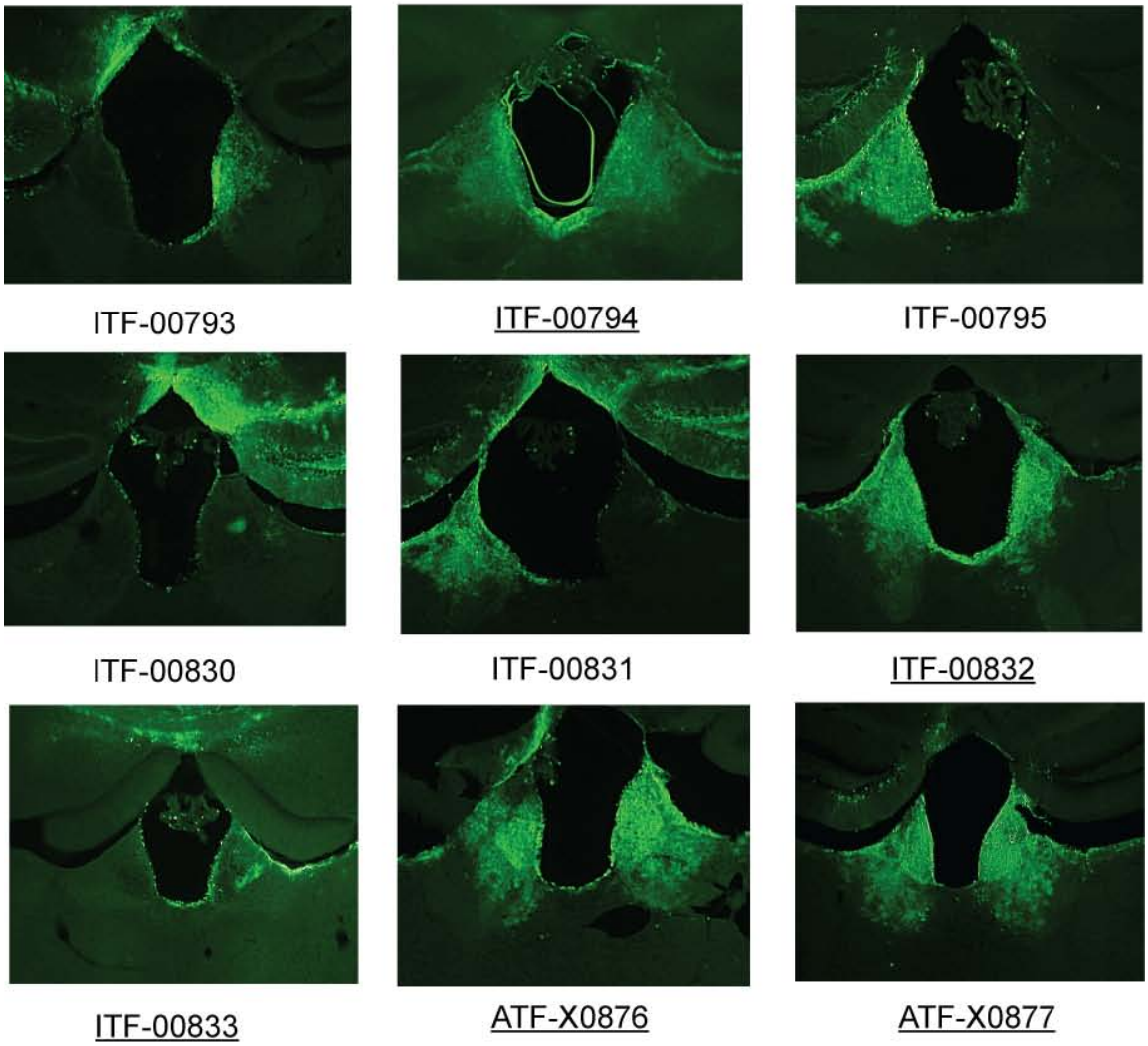

Animal ID	LV	Injection
ITF-00793	FU-β4T374I-IE	one side
ITF-00794	FU-β4T374I-IE	both
ITF-00795	FU-β4T374I-IE	one side
ITF-00830	FU-β4T374I-IE	no hit
ITF-00831	FU-β4T374I-IE	one side
ITF-00832	FU-β4T374I-IE	both
ITF-00833	FU-β4T374I-IE	both
AFQ-X0876	FU-β4T374I-IE	both
AFQ-X0877	FU-β4T374I-IE	both

Figure 16. Analysis of lentivirus expression in stereotactically injected mice

Immunostainings of coronal brain sections showing the site of the (A) PE (B) β4 (C) β4R349C (D) β4T374I lentivirus injection in MHb. EGFP fluorescence indicates the virally transduced area.

Nicotine-related behavior in stereotactically injected mice

Behavior tests were carried out with age and sex-matched littermates. Mice were indistinguishable in their body weight, spontaneous behavior and appearance.

Lentiviral-mediated expression of the polymorphic variants of nAChR β4 in the medial habenula alters nicotine consumption in wild-type mice

Genetic factors play an important role in regulating the oral intake of nicotine[178]. Extensive genome-wide studies have linked Single Nucleotide Polymorphisms (SNPs) in β4 nAChR to alternations in nicotine consumption. Moreover, the habenulo-interpeduncular pathway has been identified as a key neurocircuit controlling nicotine intake[46-47]. To test whether overexpression of R498C and T374I polymorphic β4 variants in the medial habenula of wild-type mice will influence their nicotine intake, animals were assayed for nicotine consumption by the free choice two-bottle nicotine drinking test[161,178-180]. In this paradigm, mice are allowed to choose between regular water and water supplemented with different concentrations of nicotine. First, animals are presented with two bottles of water to control for the side preference and the volume of water intake. Next, the bottle on the less-preferred side is filled with a nicotine (12,5µg/ml) solution made in tap water. The nicotine concentration was then increased every 3 days. After 3 days with the 12,5µg/ml solution, the nicotine solution is changed to 50 µg/ml and finally to 100 µg/ml. The amounts of each solution consumed per day were averaged over the periods that the mice were exposed to them (3 days). Preference was expressed as a percentage of the amount of drug solution consumed divided by the amount of total fluid (drug solution plus tap water) consumed.

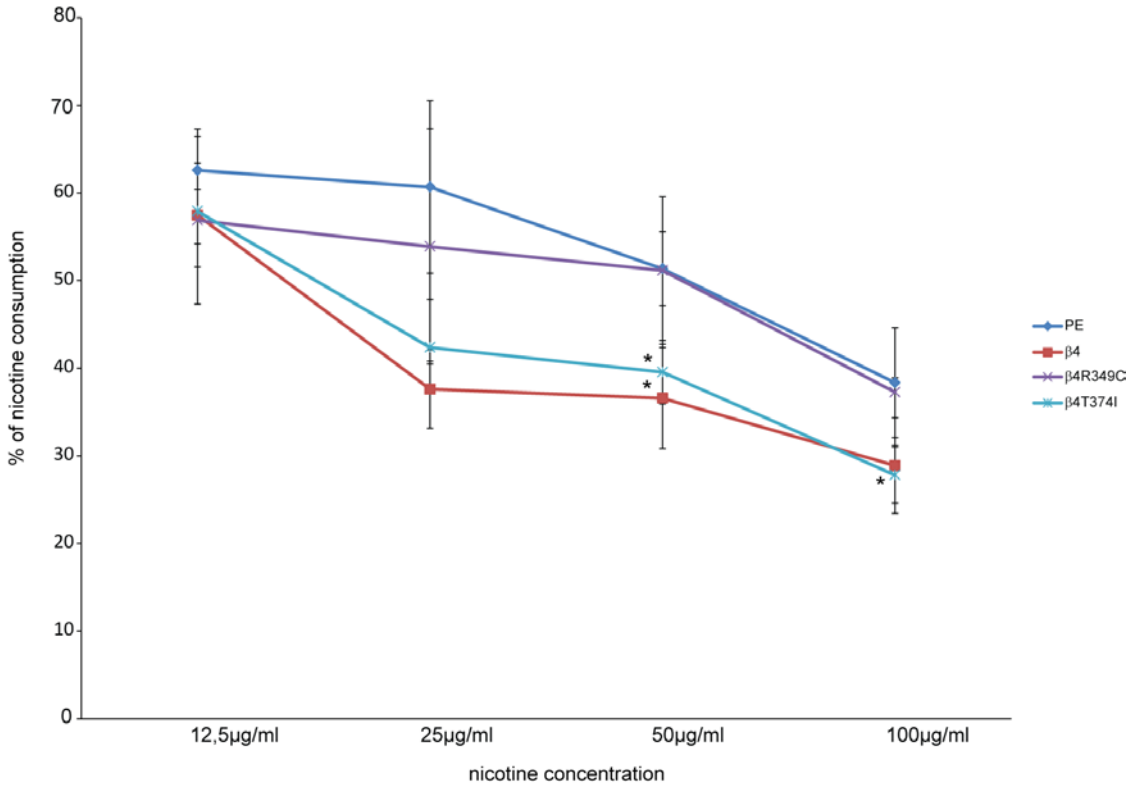

Figure 17. Two-bottle choice nicotine consumption in Tabac mice after stereotactic bilateral injection of control (PE), wild-type β4 and β4 containing the R348C and T374I mutations lentiviral constructs in the MHb.

Percent of nicotine consumption was expressed as a ratio of the volume of nicotine solution consumed divided by the total fluid intake (ml nicotine x 100% / ml total).

Analysis of the nicotine volume consumed relative to the total fluid intake revealed that mice expressing β4R349C showed no alteration in nicotine consumption with respect to the mice injected with the no-β4 control virus (PE). In contrast, animals injected with wild-type β4 subunit and β4D447Y exhibited significant reduction in nicotine consumption ($p<0,05$) at 50 µg/ml. This result stays in line with the observations made by[46], where authors report that Tabac mice with increased levels of β4 in the habenula have strong aversion to nicotine in the drinking water. Interestingly, animals that received injections to MHb with LV β4T374I also showed reduced nicotine intake with respect to PE-injected animals. Thus our studies support a protective nature of this SNP in the animal model, in agreement with the fact, that genome-wide studies linked this missense SNP T375I in CHRNB4 to decreased risk for nicotine addiction in humans[153].

MHb β4D447Y-injected mice show decreased responses to acute heat and mechanical stimuli

Both anatomical and biochemical studies have linked the medial habenula to pain modulation[30]. The role of nicotinic receptors in pain is not yet fully elucidated. Nonetheless, nicotine has been reported to produce analgesia in rats[181]. In order to evaluate whether increasing α3β4 nAChR currents in the MHb could influence pain perception, mice were stereotactically injected with β4 and with the highest current increasing β4 D447Y SNP. Mice then were tested for their responses to painful stimulation with a battery of nociception assays. First, the response to nociceptive thermal stimulus was tested using Hargreaves' model. This method uses mild focal radiant heat to measure thermal nociception. The latency of paw withdrawal characterizes the pain response measurement[182-183]. Next, mice were subjected to the mechanical sensitivity test. In this experimental setup, a constantly increasing (1g/s) force is applied by a blunt metal bar to the skin of the hindpaw of the test animal. Latency of paw withdrawal was taken as a measure of the tactile sensitivity of the animal.

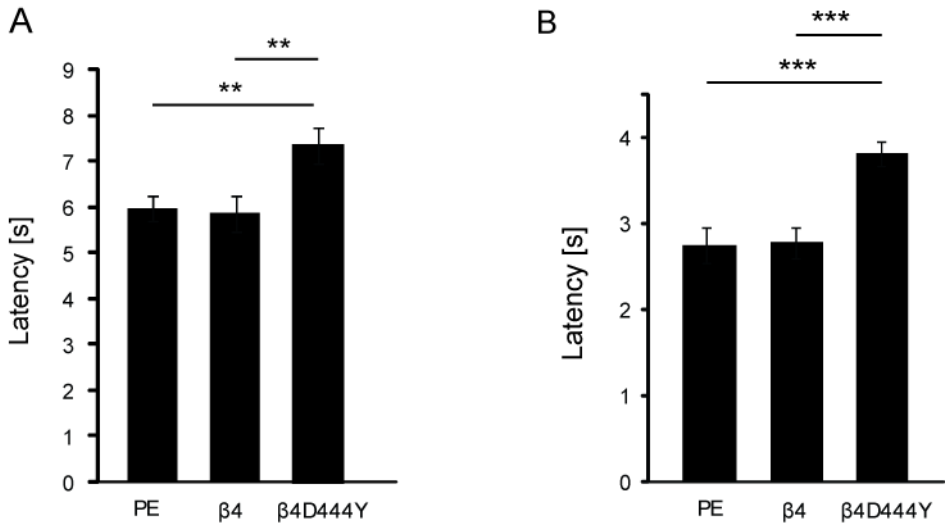

Figure 18. Acute mechanical and thermal nociception is decreased in mice injected into habenula with D444Y variant of the β4 nAChR subunit

(A) Mechanical pain stimuli were applied using a plantar dynamic aesthesiometer and measured as the force applied to the hindpaw of the mouse until paw withdrawal. Mice injected with D447Y polymorphic β4 subunit displayed delayed response to noxious heat ($p<0.001$; t-test) in comparison to the mice injected with either PE of wild-type β4 subunit (n=6 mice per group). **(B)** Responses to noxious thermal stimuli were measured using the Hargreaves apparatus. Bar graphs show the mean latency of paw withdrawal upon exposure to radiant heat. Mice injected with D447Y polymorphic β4 subunit displayed delayed response to noxious heat ($p<0.01$; t-test) in comparison to the mice injected with either PE of wild-type β4 subunit. Each bar graph represents the mean ± S.E.M for 6 animals per group.

Mice expressing β4D447Y nAChR subunit in the neurons of medial habenula when assayed for mechanical (**Fig.18A**) and thermal (**Fig.18B**) nociception, presented significantly ($p<0,01$ for aesthesiometer and $p<0,001$ for Hargreaves) longer latencies in response to these two noxious stimuli, in comparison to the control-injected animals. This data also show, that overexpression of wild-type β4 nAChR subunit in MHb did not influence the pain responses when compared with control. This finding is in line with the experiments performed on Tabac mice, in which the thermal and mechanical nociception was as well unchanged (unpublished data).

Acute inflammatory pain responses are reduced in β4D447Y-injected mice in the formalin test

Several studies have implicated the habenula in pain and analgesia. It has been shown that electrical stimulation of habenula produces analgesia in the formalin test[184]. Habenula may also play a role in mediating analgesia through direct effects on neurotransmitter system of this structure[30]. It has been reported that epibatadine, a nAChR agonist, reduces inflammatory responses in a mouse model of arthritis[185]. Thus, to test, whether modulation of the nAChR levels in the MHb have influence on inflammatory pain processing, injected mice were assayed in the formalin test. The noxious stimulus in this model is an injection of 5% formalin (diluted in saline) under the skin of the dorsal surface of the hindpaw. Formalin injection produces a localized inflammatory pain expressed in biphasic behavioral response. The first phase begins 0-5 min after injection due to direct activation of nociceptive neurons. The second phase initiates 15-30 min after formalin injection and is thought to represent inflammation-induced afferent activity[186]. Paw elevation, licking or flinching were considered as nociceptive responses and the number and duration of these events were quantified.

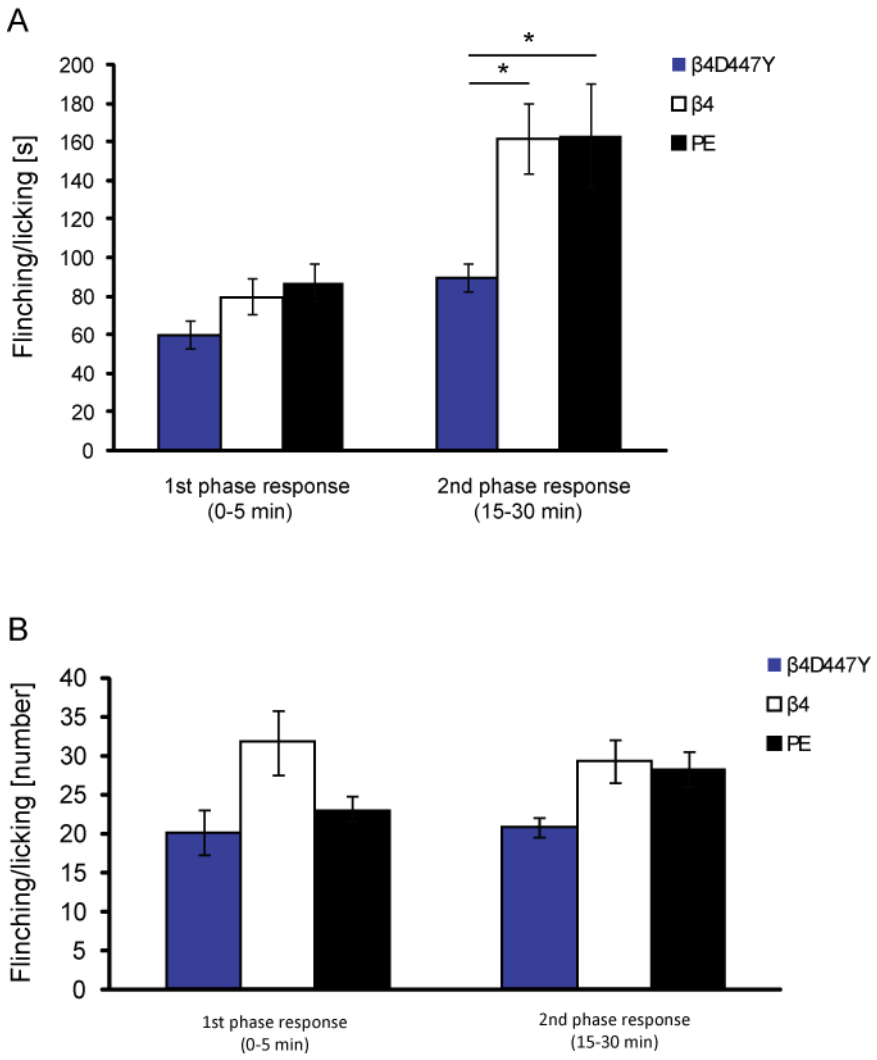

Figure 19.The flinching/licking behaviors after the injection of formalin into the plantar surface of the right hind paw of MHb injected animals

(A) Duration and (B) number of flicking/licking events in MHb injected mice. Each bar graph represents the mean ± SEM from 6 animals per group.

Subcutaneous injection of 5% formalin into the hindpaw of mice expressing β4D447Y nAChR subunit in MHb evoked similar number and duration of behavioral inflammatory responses in the first phase, where the C-fibers in the skin are directly activated. More importantly, in the second phase of the response to formalin, D447Y-injected mice exhibited lower number of body movements and significantly ($p<0,05$) faster recovery from the inflammation (**Fig.19**) in comparison to both β4- and PE injected mice. There was no difference observed between the acute inflammatory response between the WT β4-overexpressing mice and the control-injected animals in any of the considered parameters.

Neuropathic pain behavior may be influenced by lentivirally delivered β4D447Y subunit into the medial habenula

Neuropathic pain is a maladaptative type of pain; in contrast to acute pain it has no biological advantage. This type of pain usually results from damage to the peripheral nervous system – the peripheral nerve, the dorsal root or dorsal root ganglion, or the central nervous system. Whereas acute pain can be attenuated with non-steroidal anti-inflammatory drugs (NSAID) or with opiates, individuals suffering from neuropathic pain do not respond to this treatment. Nerve injury causes two classes of pain: persistent and in response to various environmental stimuli. Stimulus-independent neuropathic pain manifests itself as burning or coldness, "pins and needles" sensations, numbness and itching. Stimulus-evoked pain, second component of peripheral nerve injury, has two key features: hyperalgesia and allodynia. Hyperalgesia can be defined as an increased pain response to supra-threshold noxious stimuli, whereas allodynia is a sensation of pain caused by normally non-noxious stimuli[187].

Nerve injury-associated pain can be modeled in laboratory animals by chronic constriction injury (CCI). This procedure includes placing several loose ligatures around the sciatic nerve, but tight enough to stimulate the clinical conditions of chronic a nerve compression, similar to neuropathy[188].

In a chronic model of pain (neuropathic pain) the habenula was reported to have transiently expressed c-fos activity[189]. In the animal model of diabetes-induced pain in rats, habenula activation was decreased in response to pain stimuli[190]. These findings point to a modulatory role of habenula activation in chronic pain[30]. Although the role of neuronal nicotinic receptor in mediating the neuropathic pain is not clear, it has been reported that in a mouse model of neuropathic pain, intrathecal (i.t.) administration of nicotine and epibatidine is antiallodynic, whereas nicotine i.t. administration in sham operated mice is without effect[190].

In the present study, we show that the D447Y SNP variant of β4 nAChR when overexpressed in medial habenula causes analgesia in acute mechanical and thermal pain studies. In order to investigate, whether this mutation influences the neuropathic pain perception, mice expressing this mutation, as well as the LV β4 and control injected mice, underwent the constriction nerve injury (CCI). Upon

recovery, animals were assayed on aesthesiometer to measure the mechanical hyperalgesia caused by the CCI.

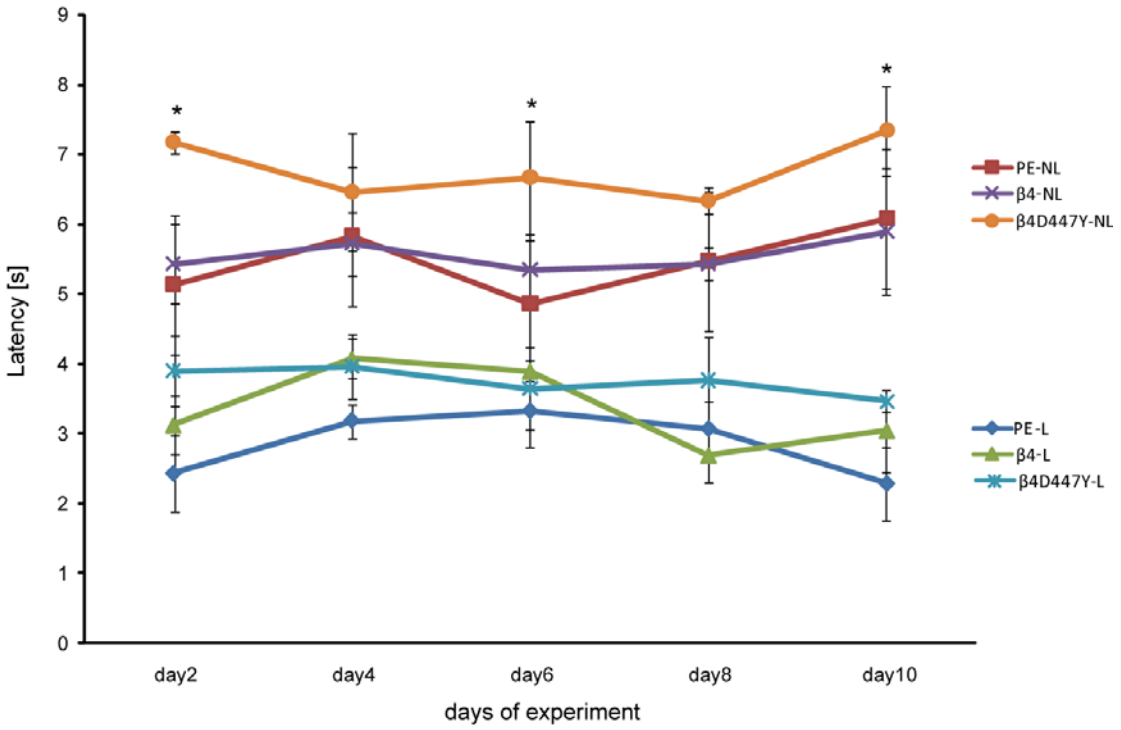

Figure 20. Mechanical hyperalgesia inβ4D447Y injected animals with chronic constriction injury

Mice, which were injected with D447Y variant of β4 nAChR and underwent chronic constriction injury, displayed delayed responses when assayed with aesthesiometer in comparison to PE- and β4-injected mice. Bar graphs are shown as mean ± S.E.M for 4 mice per group. *NL* non-ligated paw *L* ligated paw

Data collected from these experiments, presented in **Fig. 20** indicate that LV β4D447Y injected mice have significantly higher mechanical pain threshold ($p<0,05$) on day 2, day 6 and day 10, in the non-ligated paw consistent with the previously obtained results on basal perception of pain (**Fig. 13B**). Analysis of the withdrawal latency of the paw with CCI did not revealed significant changes between groups, but displayed a strong tendency ($p<0,06$) on day 2 and ($p<0,08$) at day 6 towards decreased hyperalgesia in the mice expressing D447Y variant of β4 nAChR in medial habenula neurons.

4. Discussion

These studies establish that the β4 nicotinic receptor subunit regulates nicotine intake and nociception in mice and identify the residues in this molecule that control α3β4 nAChR channel activity. One of these residues is native and unique in β4 and confers its ability to potentiate currents to the highly homologous and most abundant beta nAChR subunit, β2. The other four residues correspond to SNP variants found in humans, two of which have been linked to reduced risk of nicotine dependence.

Based on the discovery, that Tabac mice, overexpressing the β4 nAChR subunit in MHb neurons, display strong aversion to nicotine[46], the studies presented here provide *in vitro* evidence that increasing levels of β4 nAChR gradually elevate nicotine-elicited currents of α3β4 nAChR subunit combination. Further, analyses of β2/β4 chimeric nAChR subunits revealed, that the ability of β4 to enhance nicotine-evoked currents depends on a single critical residue (S435) located within the membrane-associated stretch in the intracellular vestibule of the receptor. Interestingly, sequence alignments revealed that 6 SNPs map to this region, one of them being the most common SNP associated with tobacco usage, D398N in the α5 subunit[115]. Functional analyses of these and other SNPs mapping to the intracellular vestibule in *Xenopus laevis* oocytes demonstrated that single mutations in this domain can result in profound effects on nicotine-evoked currents. For example, the D444Y variant in β4 (D447Y in mouse) caused a major increase in nicotine-evoked currents, whereas the D398N α5 variant (D397N in mouse) strongly depresses nicotine-evoked currents. Next, this study aimed to determine the influence of D447Y variant and other single nucleotide polymorphisms in the coding region of β4 nAChR subunit to channel function in response to nicotine, as well as how this translated into nicotine-mediated behavior. Upon assaying them for response to nicotine in oocytes as well as in dissociated rat hippocampal neurons, three additional β4SNPs with altered responses to nicotine were selected for further studies. Medial habenula is one of a few discrete expression sites of α3β4 nAChR combination and has been linked to both nicotine consumption and pain modulation[29]. Therefore lentiviruses carrying the wild-type β4 subunit as well as

the functionally distinct β4 rare missense variants were injected using stereotactic coordinated into medial habenula. Behavioral analysis showed, that mice overexpressing the β4T374I polymorphism in the MHb display strong aversion to nicotine in free-choice nicotine drinking test, whereas lentiviral delivery of β4D447Y subunit into MHb resulted in decreased sensitivity to mechanical and thermal nociceptive stimuli, as well as decreased response to acute inflammatory pain and reduced peripheral nerve injury-induced hyperalgesia.

Altogether, these studies are consistent with our previous results in Tabac mice showing that that increased α3β4 nAChR currents in the medial habenula result in nicotine aversion. Likewise the β4T374I variant, which increases currents, results in nicotine aversion while the R348C variant, which decreases currents, results in preference for nicotine in medial habenula injected mice. In addition, these studies provide, for the first time, molecular evidence that increased α3β4 - mediated currents in the medial habenula produce significant analgesia, thus indicating a relevant role of habenular cholinergic neurons in central pain processing.

4.1 β4 nAChR is rate limiting for β4* receptor function

Patch clamp recordings in Tabac mice revealed 16 fold increase in the nicotine-elicited current amplitude in MHb neurons, while the nicotine dose response recorded in these neurons did not differ from the one obtained from WT mice indicating no differences in ligand affinity. Moreover, radioligand binding studies demonstrated elevated levels of surface receptors in β4 endogenous expression sites in Tabac mice. These data lead to the conclusion that the enhanced nicotine-evoked currents in Tabac mice result from β4 mediated recruitment of additional functional α3β4* nAChR complexes on the cell surface[46]. In this work, the influence of the β4 nAChR availability on the nicotine-elicited currents was analyzed in *X.laevis* oocytes. Obtained results demonstrated that the more β4 nAChR subunit was available in the pool, the stronger was the nicotine-evoked response. This phenomenon depends on a single residue in the β4 subunit (S435) that is essential for the potentiation of currents observed in this study upon overexpression of the β4 subunit. Furthermore, R341S substitution can confer the potentiating property to the β2 nAChR subunit. Taken together, these

results suggest that the β4 subunit is rate limiting for the formation of α3β4 nAChRs. Although the precise role of S435 is not yet clear, it may be involved in stabilization of nAChR complexes, export of the receptors from the ER due to interactions with trafficking proteins, or alterations in its turnover from the cell surface. For example, rapsyn binding to the α-helical domains corresponding to the inner vestibule of α1β1γδ nAChR is required for surface expression of this receptor[191], and binding of UBXD4 to the cytoplasmic loop of α3 can interfere with its ubiquitination and, consequently, the number of α3 containing receptors at the cell surface[192]. Moreover, it has been shown that single residue substitution in GluN2 subunits controls NMDA receptor channel properties through the intrasubunit interaction[193]. Additional studies will be necessary to fully elucidate the role of this substitution. These would include computer modeling of both WT and S435R variants of β4 subunit in context of the assembled receptor to evaluate any conformational changes that this substitution could introduce. Additionally, analysis of the subunit trafficking, for example by tagging the WT and S435R β4 receptors with a 13-aa α-bungarotoxin (BTX)-binding site (BBS)[194] may be of importance to investigate the functional changes that this mutation introduces in the β4* receptors.

4.2 Single nucleotide polymorphisms in the CHRNB4-CHRNA3-CHRNA5 cluster influence the response to nicotine of β4* and α5* receptors *in vitro*

This work provides an important insight into the role of the intracellular vestibule of the α3β4α5 receptor in nicotine-evoked currents. Comparative analysis of the mouse β4 protein sequence versus sequences of closely related α and β nAChR subunits of different species and the sequence of Torpedo subunit revealed, that the S435 residue maps to the membrane-associated stretch domain of the receptor. This helical structure contains high concentration of charges, which is conserved in the superfamily of Cys-loop receptors[167,195]. The net charge over the MA stretch of the majority of subunits of cation-selective ligand-gated ion channels is negative[167]. Therefore it is probable that changes in the amino acid charge may strongly influence the net charge and therefore are critical for the receptor function. The MA stretch contains, in close proximity to S435 in β4, six

single nucleotide polymorphisms in α3, β4 and α5 subunits. Because of the fact, that genome wide association studies have shown that SNPs in both regulatory and coding regions of the CHRNB4- CHRNA3-CHRNA5 gene cluster are associated with nicotine dependence[134,144,196], the identified SNPs were generated and assayed for nicotine response in *X.laevis* oocytes in the α3β4α5 subunit combination. Changes in the current amplitude response to nicotine were not observed in the majority of the analyzed polymorphisms, except for substitutions of two negative residues (D447Y and D397N) which produced significant changes in current amplitude. Mutation of aspartic acid (D) to tyrosine (Y) at the position 447 in mouse sequence of β4 lead to strongly increased currents, in contrast to D397N substitution in α5, which reduced the currents of approximately 50%. This observation provides an additional proof that alterations of the negative electrostatic charge of the vestibule are critical for receptor function. This is consistent with studies of the inner vestibule in other Cys-loop receptor channels. For example, in 5HT3A receptors substitution of arginine positive residues (one of them at the position of D444) increases channel conductance, whereas introduction of basic residues in this domain of α1 glycine receptors decreases glycine evoked currents[195]. Taken together, these observations support the hypothesis that substitution of these charged residues modifies the vestibule electrostatic charge but not the number of receptors incorporated into the plasma membrane.

4.3 Competition of β4 and α5 nAChR for incorporation into the α3β4α5 receptor influences the response to nicotine

It has been shown that incorporation of the D398N α5 variant into α4β2-containing receptors in transfected cells results in a two-fold reduction in epibatidine evoked calcium currents without a change in surface expression[115]. The present work showed that incorporation of α5D397N subunit decreased the response of nicotine of α3β4α5 channel, when subunits were represented in equal ratios. Recent findings showed, that α5 competes with α4 for association with β4[168]. This work provides new evidence for the occurring competition between α5 and β4 at the saturating ratios of the subunits in α3β4α5 channel, leading to decrease of the current amplitude. Moreover, D397N variant of α5

competes more effectively with β4 leading to stronger reduction in nicotine-evoked current amplitudes reported here upon incorporation of this variant into α3β4α5 containing nAChRs. Although α5 D398N polymorphism has been linked by numerous studies to smoking quantity[115,134,146], its contribution to the activity of α3β4α5 receptors have not been addressed previously. This finding stays in line with human studies as reduced nicotine-elicited currents could lead to decreased initial aversion to nicotine and higher nicotine consumption in order to reach the saturating levels. Moreover, mice with a deletion of α5 nAChR subunit display markedly increased nicotine intake in comparison to their wild type littermates, which further supports this hypothesis[47].

4.4 Rare missense variants in CHRNB4 influence *in vitro* nicotine-elicited currents and expression on the surface

Rare variants in nicotinic acetylcholine receptor genes have been associated with nicotine dependence [147,153]. The α3β4 combination is the most common nAChR subtype containing β4. In this work 16 rare missense variants in the β4 subunit were co-expressed with the α3 subunit and assayed for their response to nicotine in *X.laevis* oocytes. In contrast to the numerous studies on CHRNA5 SNPs, very few studies have addressed the influence of CHRNB4 polymorphisms on channel function and nicotine dependence. For instance, Liang and colleagues[50], investigated four SNP variants of β4 nAChR in combination with the α4 subunit, which they assayed for the response to acetylcholine. They reported two SNPs exhibiting functional differences, one of which, T91I, this study confirmed. In addition, Haller and colleagues[153] analyzed two rare polymorphic variants in CHRNB4, rs12914008 (T91I) and rs61737499 (T375I) and showed that they increased the response to nicotine in HEK239 cells, when co-expressed with α3 subunit. Importantly, these SNPs have been associated in genome-wide studies with decreased risk of developing nicotine dependence in African Americans and European Americans and decrease the number of cigarettes consumed per day by smokers[153]. Additionally, βT91I has been shown to play a role in response to smoking cessation therapy[154]. In this context, it would be interesting to investigate whether the SNP variant rs56258098 (D444Y in β4), and the other identified functionally distinct variant

R348C influence nicotine consumption in humans as predicted by the functional data presented here. Therefore, our studies indicate that these two additional SNP variants may result in some subtle changes in related cholinergic functions in the nervous system. Additionally, single channel recordings would be necessary to determine, whether introduction of the SNPs leads to potential changes in channel gating or kinetics.

4.5 SNPs in CHRNB4 influence nicotine consumption

Analysis of human SNPs in mice is critical to clarify inconsistencies associated with *in vitro* data, to provide more precise information on the specificity of the SNP and to explore novel phenotypes. In addition mouse studies allow for the determination of molecular mechanisms that mediate the behavioral consequences of these SNPs, and as such contribute to a better understanding of their significance in human disease[197]. In this context, the studies presented here showed that mice stereotactically injected with the β4 subunit, leading to its overexpression in medial habenula, display decreased intake of nicotine in the two-bottle nicotine drinking test. This is consistent with the finding that the BAC-driven overexpression of the β4 subunit in medial habenula leads to nicotine aversion in Tabac transgenic mice[46]. As this aversion was shown to be successfully reversed with lentivirus-mediated delivery of the α5D397N variant, this work aimed to address whether lentiviral-based expression of β4R349C and β4T374I missense variants of the β4 subunit in medial habenula of wild-type mice would have an influence on nicotine consumption in mice. Medial habenula injection of the β4T374I variant produced similar aversion as observed in β4-overexpressing mice. The β4T374I missense variant was shown to elevate nicotine-elicited currents in the *in vitro* experiments conducted in this work, as well as in the work of [153]. Moreover, this CHRNB4 SNP was linked in human studies to reduced risk for nicotine addiction[153], which is consistent with our results in mice. On the other hand, the β4R349C variant that corresponds to the rs56235003 variant in humans, displayed reduced response to nicotine in both *X.laevis* oocytes and rat hippocampal neurons. Mice injected with the β4R349C lentivirus showed similar preference for nicotine as mice injected with no β4 subunit. Given that *per se* lentiviral-mediated overexpression of β4 (containing its native S435 residue) leads to aversion of nicotine, we expect that injection of

β4R349C without the native potentiating residue S345R will give a much stronger preference for nicotine. Surprisingly, this SNP was not analyzed in the study by Haller [153] and although this polymorphism has a low occurrence in the human population it might be associated to nicotine dependence and lung cancer: http://www.freepatentsonline.com/y2011/0091880.html. In addition, the R348C amino acid substitution is scored as malignant in the SIFT (Sorting Intolerant From Tolerant) program, while The β4T374I and T91I are tolerated. Thus, our studies indicate that this variant needs to be further analyzed in humans. Altogether our studies provide further mechanical insight into the finding, that SNPs in coding regions of the CHRNB4- CHRNA3-CHRNA5 gene cluster are associated with nicotine dependence[134,144,196] and with the fact, that medial habenula mediates nicotine consumption[46-47].

4.6 rs56258098 (D447Y) CHRNB4 variant decreases nociceptive responses in the MHb-injected animals

Reward and analgesia are mediated by overlapping brain circuits, and the analgesic effect of nicotine and tobacco smoke represents an important factor in dependence. It has been reported that individuals with chronic pain problems are at an increased risk for certain types of substance abuse and dependence[198-199]. Nonetheless, the links between cigarette smoking and chronic pain are not well described[200]. Chronic exposure to nicotine causes analgesia in rats[201]. The antinociceptive effect of nicotine is reversed by systemic administration of mecamylamine and not by hexamethonium, suggesting that nicotine produces antinociception by acting on central nicotinic acetylcholine receptors[4,202-203]. Neuroimaging data revealed activation of habenula during experimental thermal pain in human subjects[31]. Therefore in this work a plausible hypothesis has been to test whether the β4SNPs that affect nicotine mediated currents play a role in pain-related behavior. We focused our studies in the mice injected with the rs56258098 variant of CHRNB4 (D447Y), because this variant produced the strongest current increase in *in vitro* experiments. Our analyses showed that these mice exhibited reduced behavioral responses to acute mechanical and thermal nociceptive stimuli, as well as decreased symptoms of acute inflammatory pain in formalin test. Furthermore, these animals show a tendency

towards reduced allodynia in the chronic constriction injury model of neuropathic pain. Given that the medial habenula is enriched in substance P and opioid receptors, it is possible that nicotine produces analgesia by modulating the central release of endorphins (endogenous opiates). For instance, it has been shown that nicotine-induced antinociception is reduced in μ opioid receptor knockout mice[204]. Therefore the potential cross-talk between these receptors needs to be further considered. The medial habenula is a source of substance P (SP) fibers projecting via the fasciculus retroflexus to the IPN and from there to the ventral tegmental area (VTA)[205]. Additionally, the lateral habenula receives substance P projections from the MHb and further sends cholinergic outputs to the IPN[206]. The habenula efferent projections to dopaminergic (VTA, SNpc) and serotonergic (dorsal and medial raphe nuclei) contribute to pain modulation[43-45]. Substance P (SP) is known to inhibit nicotinic acetylcholine receptors and this inhibition is β subunit dependent. It has been shown that β4* subunit combination exhibited approximately 20-30 fold higher affinity to SP that those containing β2. Moreover, it has been speculated that β4 subunit may at least partially contribute to the SP binding site[207]. Thus from these reports and our data, it could be hypothesized that the D447Y mutation in the β4 subunit alters the cholinergic-SP balance, changing the response to acetylcholine (or nicotine) and thus affecting the downstream pain processing. Despite presented assumptions, the role of the D447Y variant remains unclear. To dissect further the contribution of this rare β4 variant to pain regulation cre-dependent β4D447Y lentivirus are about to be generated for expression of this subunit only in substance P-expressing neurons in the medial habenula using Cre-Tac1 mice or in cholinergic neurons of the MHb using Cre-CHAT mice. Furthermore, β4D447Y D447Y knockin mice are being generated to expand the studies on this mutation on its influence on nicotine consumption, anxiety, cognition and pain. It is important to note that substitution of aspartic acid (D) to tyrosine (Y) in the β4 sequence introduces a conserved motif YQSV (consensus YXXQ). This motif has been shown to be responsible for the rapid internalization of endocytic receptors from the plasma membrane, as well as for protein targeting to various endosomal compartments, lysosomes and the basolateral surface of polarized epithelial cells[208]. This motif (YIGF) is endogenously present in the α7 nAChR, where it has been shown to direct the subunits to the dendrites[209]. Further

investigation of the influence on this motif on the subunit turnover, as well as search for binding partners and modulators (e.g. by TRAP methodology in D447Y knock-in mice) known to be involved in pain responses may be considered.

4.7 MHb as an important relay station regulating nicotine consumption and pain perception

The work presented here demonstrates that the MHb has a major influence in the regulation of nicotine consumption, extending previous studies of the role of the habenula in nicotine withdrawal, drug addiction and nicotine self-administration[47,97-98,101,210]. Furthermore, this work brings an important novel insight into the role of the medial habenula in pain modulation, altogether establishing that pain and addiction might intersect in this small midbrain nucleus. While multiple interconnected brain regions, including the prefrontal cortex, thalamus, striatum and amygdala are affected by chronic use of nicotine, the habenular system is emerging as an important station in pathways regulating the behavioral effects of nicotine[64,96,211]. At the level of the circuit, MHb sends efferent projections to the IPN, which has been shown to regulate nicotine intake in rats[47]. Moreover, the MHb is directly connected to the LHb, which exerts a strong inhibition on midbrain dopamine neurons in the VTA. Midbrain dopamine (DA) neurons that originate from the ventral tegmental area (VTA) are important for motivated behaviors toward natural and pharmacological rewards[212]. Interestingly, VTA dopaminergic neurons project back to the MHb completing a reciprocal loop that is thought to have important functions in reward circuitry[213-214]. There is no available data linking SNPs in CHRNB4-CHRNA3-CHRNA5 cluster to any aspect of pain and analgesia, but recently neuroimaging data in humans shows that the habenula is activated by painful stimuli[30]. This study provides an excellent behavioral model for exploration of the involvement of β4 and its SNPs in α3βα5 nAChR function in medial habenula and how the altered channel function influences nicotine consumption and pain perception.

5. Summary

These studies establish that the β4 nicotinic receptor subunit regulates nicotine intake and nociception in mice and identify the residues in this molecule that control α3β4 nAChR channel activity. One of these residues is native and unique in β4 and confers its ability to potentiate currents to the highly homologous and most abundant beta nAChR subunit, β2. The other four residues correspond to SNP variants found in humans, two of which have been linked to reduced risk of nicotine dependence. Prompted by the discovery, that Tabac mice, overexpressing the β4 nAChR subunit in MHb neurons, display strong aversion to nicotine[46], the studies presented here provide *in vitro* evidence that increasing levels of β4 nAChR gradually elevate nicotine-elicited currents of α3β4 nAChR subunit combination. Further, analyses of β2/β4 chimeric nAChR subunits revealed, that the ability of β4 to enhance nicotine-evoked currents depends on a single critical residue (S435) located within the membrane-associated stretch in the intracellular vestibule of the receptor. Interestingly, sequence alignments revealed that 6 SNPs map to this region, one of them being the most common SNP associated with tobacco usage, D398N in the α5 subunit [115]. Functional analyses of these and other SNPs mapping to the intracellular vestibule in *Xenopus laevis* oocytes demonstrated that single mutations in this domain can result in profound effects on nicotine-evoked currents. For example, the D444Y variant in β4 (D447Y in mouse) caused a major increase in nicotine-evoked currents, whereas the D398N α5 variant (D397N in mouse) strongly depresses nicotine-evoked currents. Next, this study aimed to determine the influence of D447Y variant and other single nucleotide polymorphisms in the coding region of β4 nAChR subunit to channel function in response to nicotine, as well as how this translated into nicotine-mediated behavior. Upon assaying them for response to nicotine in oocytes as well as in dissociated rat hippocampal neurons, three additional β4SNPs with altered responses to nicotine were selected for further studies. Medial habenula is one of a few discrete expression sites of α3β4 nAChR combination and has been linked to both nicotine consumption and pain modulation[29]. Therefore lentiviruses carrying the wild-type β4 subunit as well as the functionally distinct β4 rare missense variants

were injected using stereotactic coordinated into medial habenula. Behavioral analysis showed, that mice overexpressing the β4T374I polymorphism in the MHb display strong aversion to nicotine in free-choice nicotine drinking test, whereas lentiviral delivery of β4D447Y subunit into MHb resulted in decreased sensitivity to mechanical and thermal nociceptive stimuli, as well as decreased response to acute inflammatory pain and reduced peripheral nerve injury-induced hyperalgesia. Altogether, these studies are consistent with our previous results in Tabac mice showing that that increased α3β4 nAChR currents in the medial habenula result in nicotine aversion. Likewise the β4T374I variant, which increases currents, results in nicotine aversion while the R348C variant, which decreases currents, results in preference for nicotine in medial habenula injected mice. In addition, these studies provide, for the first time, molecular evidence that increased α3β4 - mediated currents in the medial habenula produce significant analgesia, thus indicating a relevant role of habenular cholinergic neurons in central pain processing.

6. Zusammenfassung

Nikotinerge Azetylcholin Rezeptoren spielen eine wesentliche Rolle im Tabak-Konsum und Nikotin-Abhängigkeitsverhalten. Vor 4 Jahren wurden bei Rauchern erstmals Variationen in Genen entdeckt, die für die Expression des azetylcholinergen Rezeptors verantwortlich sind. Dabei handelt es sich speziell um eine Gruppe von 3 benachbarten Genen, die für die Untereinheiten α3, α5 und β4 des Azetylcholinrezeptors kodieren. Zusammen bilden diese Untereinheiten eine von vielen möglichen Varianten des heteromeren Azetylcholinrezeptors, ein Ionenkanal der spezifisch und gehäuft in der medialen Habenula vorkommt. Einzelnukleotidpolymorphismen (SNPs) in diesen Genen können bei Rauchern direkt mit der Menge gerauchter Zigaretten pro Tag korreliert werden. Anlässlich der Entdeckung, dass eine Überexpression von β4 in der medialen Habenula von transgenen Mäusen (genannt Tabac-Mäuse) eine ausgeprägte Aversion gegen Nikotin erzeugt[46], wurde in der vorliegenden Arbeit *in vitro* gezeigt, wie eine Erhöhung der relativen Menge an β4-cRNA einen graduellen Anstieg der Anzahl von funktionellen α3β4 nAChR-Rezeptoren hervorruft. Mithilfe elektrophysiologischer Untersuchungen an *Xenopus laevis* Oozyten konnte eine einzelne Aminosäure (S435) in der intrazellulären Domäne der β4-Untereinheit identifiziert werden, die für diese Erhöhung der Azetylcholinrezeptor-Dichte und der damit verbundenen Potenzierung der Einwärts-gerichteten Ströme verantwortlich ist. Interessanterweise ergaben Sequenz-Abgleichungs-Analysen, dass 6 SNPs des heteromeren Azetylcholinrezeptors in demselben intrazellulären Abschnitt wie S435 vorkommen, von denen D398N in der α5-Untereinheit den häufigsten Polymorphismus im Zusammenhang mit Nikotin-Abhängigkeit darstellt. Funktionelle Analysen dieses und der 5 anderen SNPs ergaben, dass einzelne Mutationen in diesem Bereich erheblichen Einfluss auf Nikotin-evozierte Einwärts-Ströme haben. Zum Beispiel verursacht die D444Y Variante in β4 (D447Y in der Maus) eine Erhöhung der Einwärts-Ströme, wohingegen die D398N α5-Variante (D397N in der Maus) Nikotin-evozierte Ströme erheblich verkleinert.

Darauf aufbauend wurde im Mausmodell erforscht, wie sich verschiedene SNPs des β4-Gens (Chrnb4) auf die Rezeptor-Funktion bzw. auf das Verhalten

auswirken. Die mediale Habenula ist eine der wenigen Gehirnregionen, die die α3β4 Rezeptor-Kombination exprimieren, welche kürzlich mit Nikotin-Konsum- sowie Schmerz-Verhalten in Zusammenhang gebracht werden konnte. Daher wurden Lentiviren, die die Wildtyp-Variante der β4-Sequenz oder eine der seltenen β4 Missense Varianten kodieren, in die mediale Habenula von Mäusen stereotaktisch injiziert. In Verhaltenstests konnte gezeigt werden, dass Mäuse die den β4 T374I Polymorphismus in der medialen Habenula überexprimieren, eine ausgeprägte Aversion gegenüber Nikotin-haltigem Trinkwasser aufwiesen, während diejenigen Mäuse die die β4 D447Y-Variante trugen, eine verringerte Sensitivität gegenüber mechanischen und thermalen Stimuli, sowie geringere Reaktionen auf inflammatorischen Schmerz und reduzierte verletzungsbedingte Hyperalgesie zeigten. Insgesamt sind die vorgestellten Ergebnisse in Einklang mit unseren vorherigen Erkenntnissen aus Tabac Mäusen, bei denen erhöhte $\alpha 3\beta 4$-Ströme in der medialen Habenula mit einer ausgeprägten Nikotin-Aversion einhergehen. Dementsprechend verursacht die β4T374I Variante, welche erhöhte Ströme bewirkt, Nikotin-Aversion, während die R348C Variante, welche reduzierte Ströme bewirkt, in einer Präferenz für Nikotin resultiert. Ausserdem konnte in dieser Studie zum ersten Mal auf molekularer Ebene ein Zusammenhang zwischen erhöhten α3β4-Strömen in der medialen Habenula und Analgesie gezeigt werden, wodurch den cholinergen Neuronen in der Habenula eine relevante Bedeutung in der zentralen Schmerzverarbeitung zukommt.

7. Appendix

7.1 Abbreviations

5-HT_3	5-hydroxytryptamine receptor 3A
BAC	Bacterial Artificial Chromosome
BSA	Bovine serum albumin
cDNA	Complementary DNA
CNS	Central nervous system
CHRNA3	Human gene for the neuronal acetylcholine receptor subunit alpha 3
Chrna3	Mouse gene corresponding to CHRNA3
CHRNA5	Human gene for the neuronal acetylcholine receptor subunit alpha 5
Chrna5	Mouse gene corresponding to CHRNA5
CHRNB4	Human gene for the neuronal acetylcholine receptor subunit beta 4
Chrnb4	Mouse gene corresponding to CHRNB4
DIV	Days in vitro
DMEM	Dulbecco's modified Eagle medium
DMSO	Dimethyl sulfoxide
DNA	Deoxyribonucleic acid
dNTP	Deoxynucleotidetriphosphate
DRG	Dorsal Root Ganglia
DTT	Dithiothreitol
EDTA	Ethylenediaminetetraacetic acid
EGFP	Enhanced green fluorescent protein
FBS	Fetal bovine serum
GABA	γ-aminobutyric acid
GWAS	Genome-Wide Association Studies
HCl	Hydrochloric acid
i.p.	intraperitoneal
IPN	Interpenduncular nucleus
LV	Lentivirus
MHb	medial habenula
MOI	Multiplicity of infection (virus particles/cell)

MQ	Type-I ultrapure water (from Barnstead E-pure system)
mRNA	Messenger ribonucleic acid
NAcc	Nucleus accumbens
nAChR	Nicotinic acetylcholine receptor
NaCl	Sodium chloride
NaOH	Sodium hydroxide
ND	Nicotine Dependence
o/n	Over night
OD	Optical density
PAG	Periaqueductal grey
PBS	Phosphate-buffered saline
PCR	Polymerase chain reaction
PDGF-R-TM	Platelet-derived growth factor receptor transmembrane domain
PFA	Paraformaldehyde
pH	*Potentium* hydrogenii
PNS	Peripheral nervous system
RHC	Rat hippocampus culture
RNase	Ribonuclease
rpm	Revolutions per minute
RT	Room temperature
S.E.M	Standard error of the mean
SD	Standard deviation
SDS	Sodium dodecyl sulphate
SI	Stereotaxic injection
SNP	Single Nucleotide Polymorphism
SNpc	Substantia nigra pars compacta
TAE	Tris-acetate EDTA
TE	Tris-EDTA
TEVC	Two-Electrode Voltage Clamp
TM	Transmembrane domain
Tris	Tris-(hydroxymethyl-) aminoethane
TU	Transducing unit
VTA	Ventral tegmental area

Units

bp	base pairs
˚C	Degrees Celsius
d	Days
g	Gram
h	Hour
kb	Kilobase
l	Liter
M	Molar
mg	Milligram
min	Minute
ml	Milliliter
mM	Millimolar
nA	Nanoampere
ng	Nanogram
pA	Picoampere
µg	Microgram
s	Second
U	Unit (for enzyme activity)

7.2 Plasmid maps

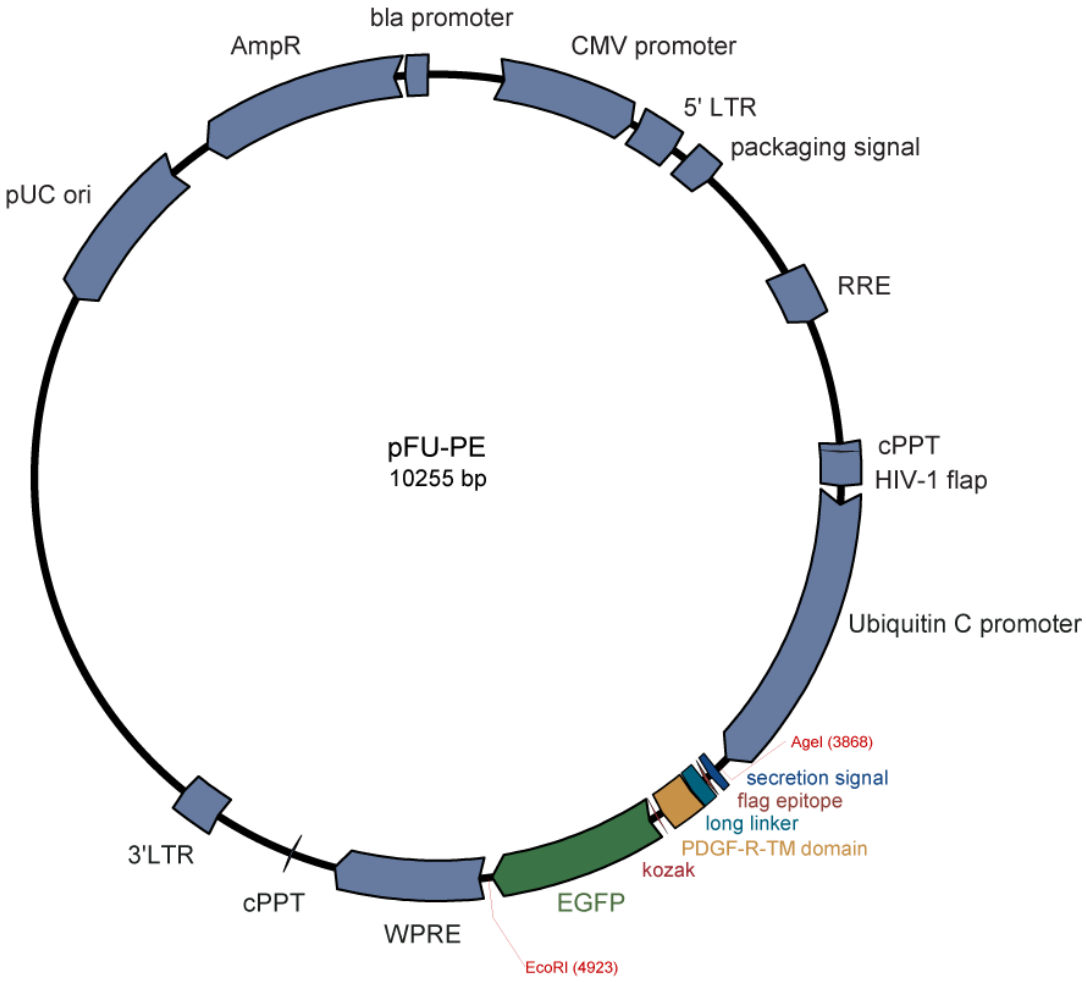

atgtctgcacttctgatcctagctcttgttggagctgcagttgctatcgattacaaagacgatgacgacaagcttgc
ggccgctggtaacggaaatggcaacgggaatggtaacggaaacggcaacggggatggtactcgagttgctg
tgggccaggacacgcaggaggtcatcgtggtgccacactccttgccctttaaggtggtggtgatctcagccatcc
tggccctggtggtgctcaccatcatctcccttatcatcctcatcatgctttggcagaagaaaccacgtaggatcca
ccggccggtcgccaccatggtgagcaagggcgaggagctgttcaccggggtggtgcccatcctggtcgagct
ggacggcgacgtaaacggccacaagttcagcgtgtccggcgagggcgagggcgatgccacctacggcaa
gctgaccctgaagttcatctgcaccaccggcaagctgcccgtgccctggcccaccctcgtgaccaccctgacct
acggcgtgcagtgcttcagccgctaccccgaccacatgaagcagcacgacttcttcaagtccgccatgcccga
aggctacgtccaggagcgcaccatcttcttcaaggacgacggcaactacaagacccgcgccgaggtgaagtt
cgagggcgacaccctggtgaaccgcatcgagctgaagggcatcgacttcaaggaggacggcaacatcctg
gggcacaagctggagtacaactacaacagccacaacgtctatatcatggccgacaagcagaagaacggca
tcaaggtgaacttcaagatccgccacaacatcgaggacggcagcgtgcagctcgccgaccactaccagcag
aacaccccatcggcgacggccccgtgctgctgcccgacaaccactacctgagcacccagtccgccctgag
caaagaccccaacgagaagcgcgatcacatggtcctgctggagttcgtgaccgccgccgggatcactctcgg
catggacgagctgtacaagtaa

Figure 21. Plasmid map and sequence of control construct PE in lentiviral vector pFU(from S. Auer)

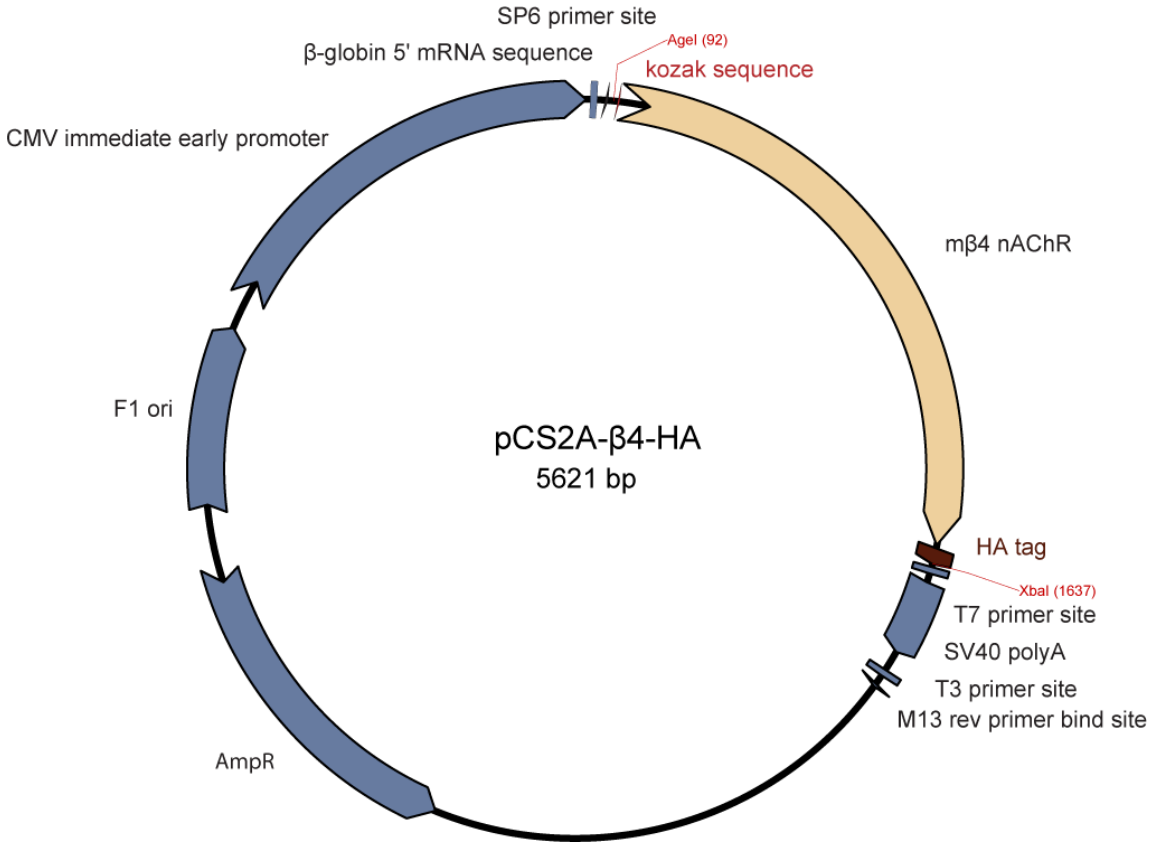

gccgccaccatgaggggtacgcccctgctcctcgtctctctgttcgctctgcttcagcctggggactgccgcctgg
ccaacgcagaggagaagctgatggatgatctcctgaacaaaacccgctacaacaacctgatccgcccagcc
accagctcctcccagctcatctccatccgcctggagctatcactgtcccagctcatcagtgtgaatgagcgagaa
cagatcatgaccaccagcatctggctgaaacaggaatggactgactaccgcctggcctggaacagctcctgct
atgaaggggtgaacattctgaggattcctgcaaagcgagtctggttgcctgacatcgtgttgtacaacaatgccg
atgggacctatgaggtgtctgtctacaccaacgtgatcgtgcgttccaacggcagcatccagtggctgcccctg
ccatctacaagagtgcctgcaagatagaggtgaagcactttcccttcgaccagcagaactgcaccctcaaattt
cgctcctggacctatgaccacacagagattgacatggttcttaaatcacccacagccatcatggatgactttacc
cccagcggtgaatgggacattgtggccctcccgggtcgaaggacagtgaacccacaggaccccagctatgtg
gacgtgacctatgacttcatcatcaagcgcaagccactcttctacaccatcaatctgatcatcccttgtgtgctcatc
acgtcgctggctatcctggtcttctacctgccctccgactgtggggagaagatgacgctctgcatctcagtgctgct
ggcactcacattcttcctgctgctcatctccaagatcgtgcctcccacctcccttgacattcccctcattggcaagta
cctcttgttcaccatggtgctggtcacctttttccatcgtcaccactgtgtgtgtcctcaatgtgcaccaccgttcaccc
agcactcacaccatggcatcctgggtcaaggagtgcttcctgcacaagctgcccaccttcctcttcatgaagcgc
cctggtctggaagtcagccccgccagggtccctcattccagccagctgcacttgaccacagctgaagctacgtc
cacctctgccttaggccccagcagcccatccaacctctatgggaattccatgtactttgtgaaccctgtccctgcc
actcctaagtctgcagtcagctcccacacggcaggcctccccagggatgcccggctgaggtcctctgggaggtt
ccggcaagatctacaggaagcattagagggcgtcagcttcatcgcacagcatttggagagtgatgatcgagat
cagagtgtcatcgaggactggaaattcgtcgcaatggtcgtcgaccgcctgttcctgtgggtgttcgtgattgtgtgt
attctgggcaccatggggctcttcctgccacccctcttccagatccacgcaccctccaagggcctctatccttatga
cgtgcctgactatgccagcctgggaggaccttag

Figure 22. Plasmid map and sequence of β4-HA in oocyte expression vector pCS2A.

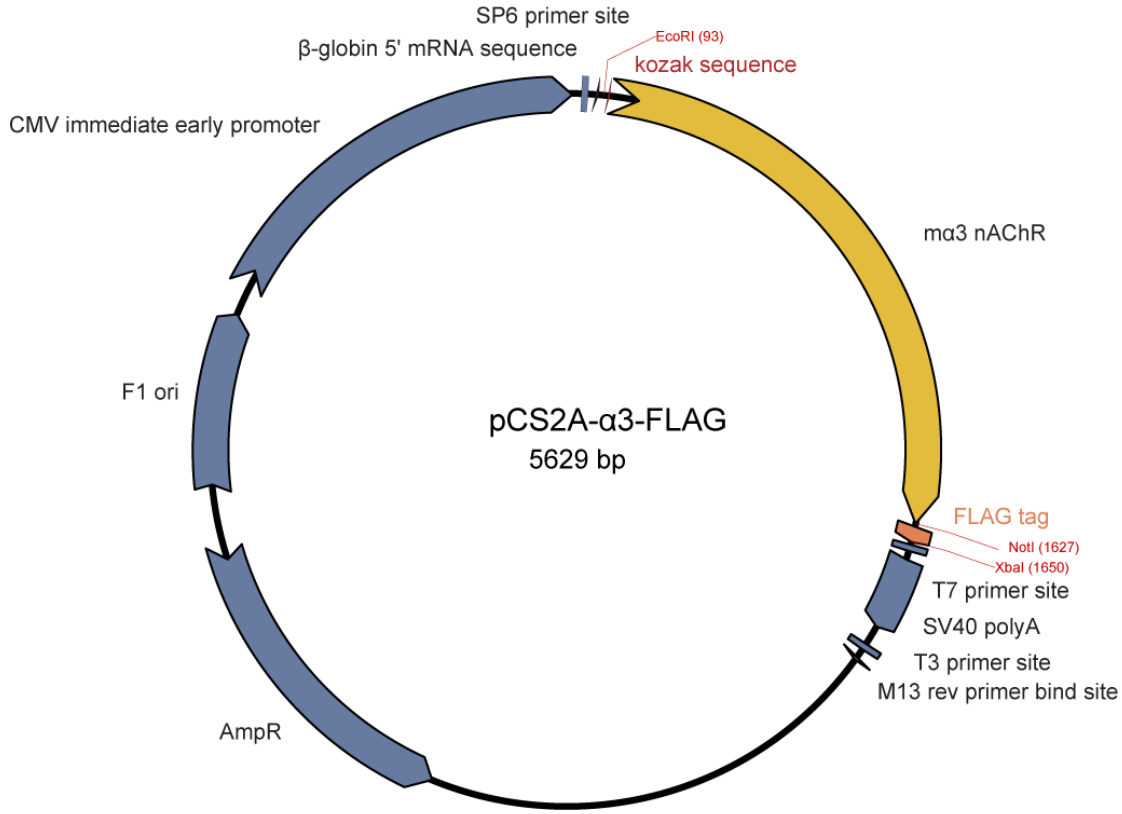

gtcgacgtcctgtccatgcggtcttcagacatgggtgttgtgctgcccccgccgccgctgtccatgctgatgctggt
gctgatgctgctgccagtggccagcgcctcggaagctgagcaccgcctgttccagtacctgtttgaagattacaa
cgagatcatccggccggtggctaacgtgtcccatcctgtcatcatccagtttgaggtgtctatgtctcagctggtga
aggtggatgaagtaaaccagatcatggaaaccaacctgtggctgaagcaaatctggaatgactacaagctga
aatggaaaccctctgactaccaaggggtggagttcatgcgagtccctgcagagaagatctggaaaccagaca
tcgtgctttacaacaacgccgatggggatttccaagtggatgacaaaaccaaagctctactcaagtacacagg
agaagtgacttggatccctccggccatctttaagagctcatgcaaaatcgatgtgacctacttcccgtttgactacc
aaaactgcaccatgaagttcggctcctggtcctacgacaaggcaaagatcgacctggtcctcattggctcctcc
atgaacctcaaggactattgggaaagtggcgagtgggccatcattaaagccccgggctacaaacatgaaatc
aagtacaactgctgtgaggagatctaccaagacatcacgtactcgctatacattcgccgcctgccgctgttctac
accatcaacctcatcattccgtgcctgctcatctccttcctcactgtgctcgtcttctacctgccctccgactgtgggg
agaaggtgacgctctgcatctccgtgctcctctccctgacggtctttctcctcgtgatcaccgagaccatcccttcc
acctcactggtcatcccctgatcggggagtacctcctcttcactatgatttttgtcaccttgtccatcgtcatcacagt
ctttgtgctcaacgtgcactacagaactccgaccacacacacgatgcccacttgggtcaaggctgtgtttttgaac
cttctccccagggtcatgtttatgactaggccaaccagcaccgaggaagacgccccaaagacgaggaacttct
acggtgctgagctctcaaacctgaactgcttcagccgtgcagactccaaaagctgcaaggaaggctacccctg
ccaagatgggacatgtggctattgccaccaccgtagggtaaaaatctcaaatttcagtgccaacctcacaaga
agctccagttctgagtctgttgatgctgtgttgtccctgtctgctctgtcaccagaaatcaaagaagccatccaaag
tgtgaagtatattgctgaaaatatgaaagcacagaatgtagccaaagagattcaagatgattggaagtatgttgc
catggtgattgatcgcatttttctctgggttttcatcctggtgtgcattttaggatctgcaggattatttctgcaacccttat
accagagttttttttctgcggccgcgactacaaggacgacgatgacaagtaa

Figure 23. Plasmid map and sequence of α3-FLAG in oocyte expression vector pCS2A

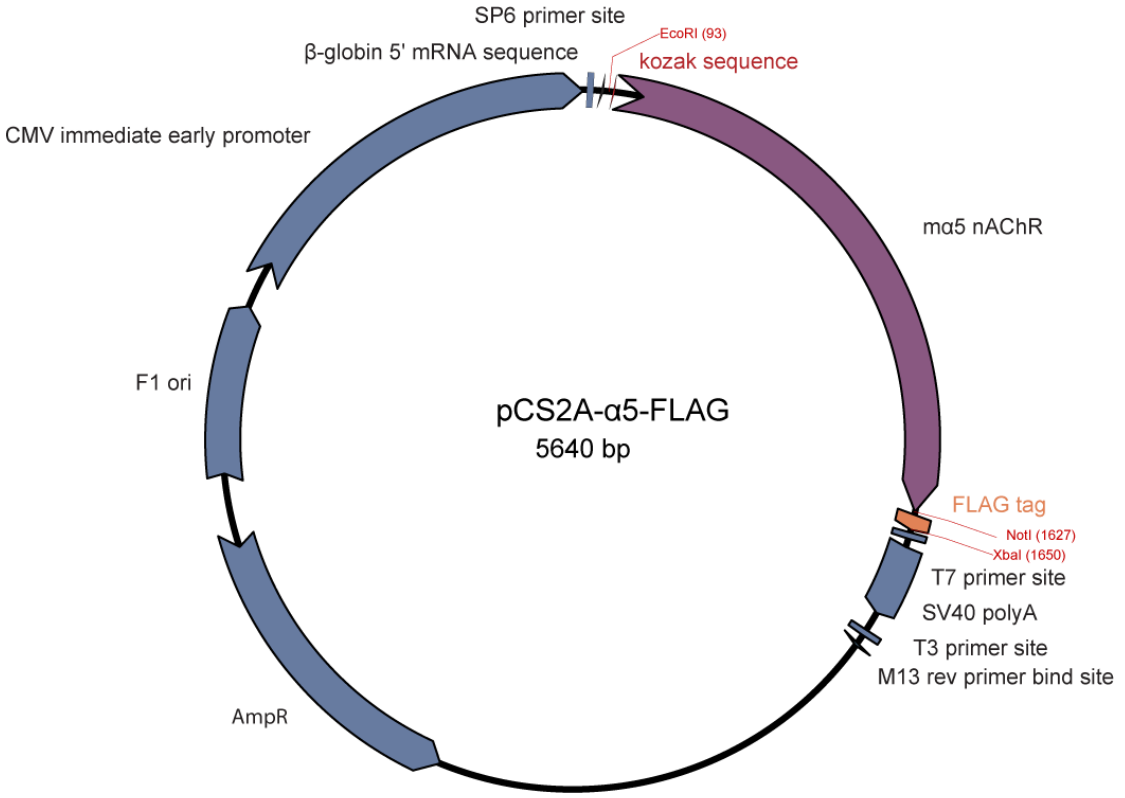

gccgccaccatgcagatctcgaatgcagggttgcctgagctatcctctgctgcaaaacatgaagacagtttgttt
agggatttatttgaagactatgaaaagtgggttcgtcctgtggaacacctgagtgacaagataaaaatcaagttt
ggccttgcaatatctcagttagtggacgtggatgagaaaaaccagctaatgaccaccaacgtctggttgaagca
ggaatggatagatgtaaagttaagatggaatcctgatgactatggtggaataaaaattatacgtgttccttcagac
tctctgtggatcccagacatcgttttgtttgataatgcagacggacgtttcgaaggggccagtacgaaaacagttg
tcaggtacaatggcactgtcacttggacgcagccagcaaactacaaaagttcttgcactatagatgtgacctttt
cccatttgatctccaaaattgctccatgaaattcggctcatggacgtatgatggatcccaggtcgatataatcctag
aggaccaagatgtcgacagaacagacttttttgacaatggagaatgggaaatcatgagcgcaatggggagca
aggggaaccggacggacagctgctgctggtacccctgcatcacctactccttcgtgatcaaacggctgcctctct
tctacaccctgtttcttatcataccctgcatcgggctctcgtttctgactgtggttgtcttctatctcccttcaaacgaag
gtgaaaagattagcctgtgcacttccgtgctggtctctctgactgtcttcctgctggtgattgaggaaattataccgtc
atcttccaaagtcatacctctgatcggggagtacttggtgttcaccatgatcttcgtgaccctatccattatggtgact
gtctttgccatcaacatccaccaccgctcttcttccacacacaatgctatggcgccgtgggttcgtaagatatttctc
cacaagcttcccaaactgctctgcatgagaagtcatgccgataggtacttcactcagagagaagaagccgag
aaagacggtggacctaaatctcggaatactttggaggccgcgctcgattgcattcgctacatcacgagacacgt
agtgaaagagaacgacgtccgcgaggttgttgaagattggaaattcatagcccaagttctcgatcggatgtttct
atggacgtttcttctggtttcaatcattgggacgctagggcttttgttcctgttatttataaatgggccaatataatagtc
ccagttcacattggaaacacaattaaggactacaaggacgacgatgacaagtaa

Figure 24. Plasmid map and sequence of α5-FLAG in oocyte expression vector pCS2A

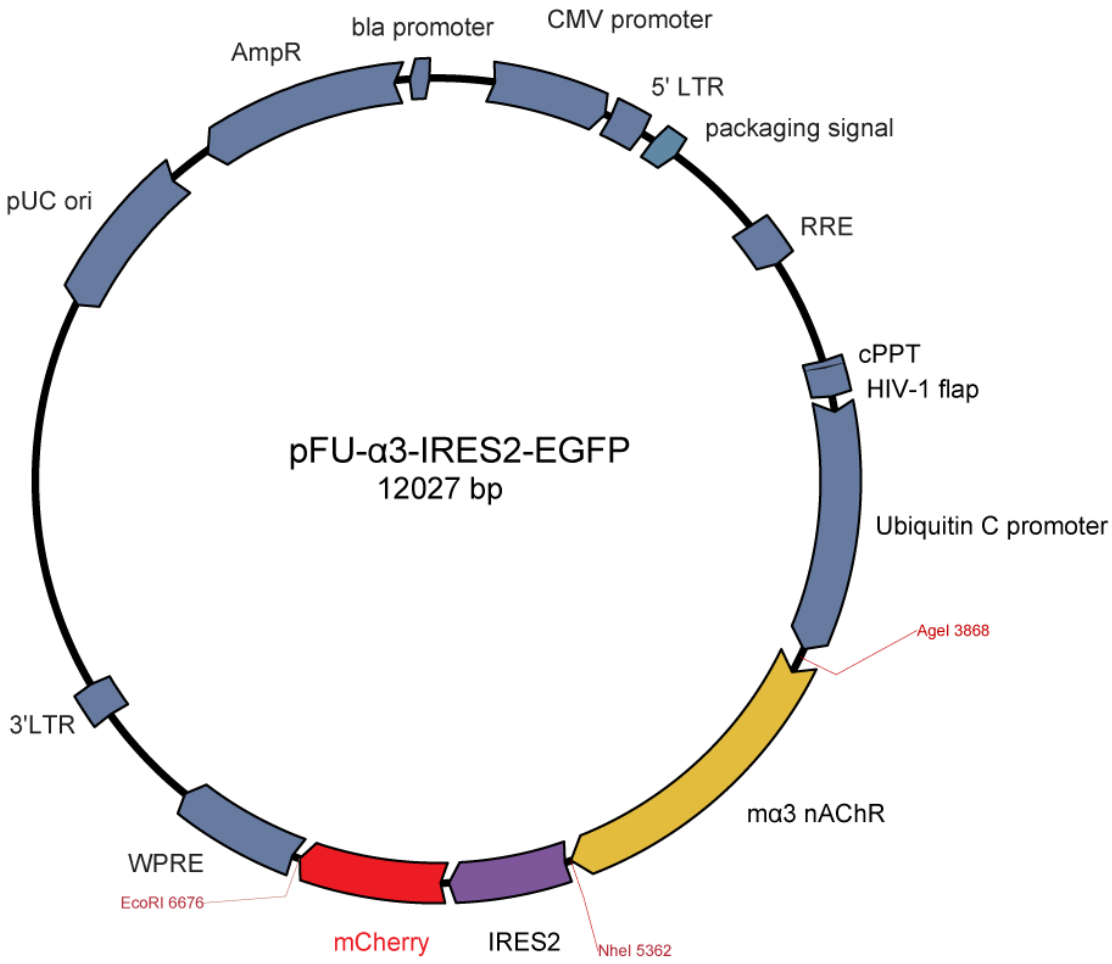

atgcggtcttcagacatgggtgttgtgctgcccccgccgccgctgtccatgctgatgctggtgctgatgctgctgcc
agtggccagcgcctcggaagctgagcaccgcctgttccagtacctgtttgaagattacaacgagatcatccggc
cggtggctaacgtgtcccatcctgtcatcatccagtttgaggtgtctatgtctcagctggtgaaggtggatgaagta
aaccagatcatggaaaccaacctgtggctgaagcaaatctggaatgactacaagctgaaatggaaaccctct
gactaccaaggggtggagttcatgcgagtccctgcagagaagatctggaaaccagacatcgtgctttacaaca
acgccgatggggatttccaagtggatgacaaaaccaaagctctactcaagtacacaggagaagtgacttgga
tccctccggccatctttaagagctcatgcaaaatcgatgtgacctacttcccgtttgactaccaaaactgcaccat
gaagttcggctcctggtcctacgacaaggcaaagatcgacctggtcctcattggctcctccatgaacctcaagg
actattgggaaagtggcgagtgggccatcattaaagccccgggctacaaacatgaaatcaagtacaactgctg
tgaggagatctaccaagacatcacgtactcgctatacattcgccgcctgccgctgttctacaccatcaacctcatc
attccgtgcctgctcatctccttcctcactgtgctcgtcttctacctgccctccgactgtggggagaaggtgacgctct
gcatctccgtgctcctctccctgacggtctttctcctcgtgatcaccgagaccatcccttccacctcactggtcatcc
ccttgatcggggagtacctcctcttcactatgatttttgtcaccttgtccatcgtcatcacagtctttgtgctcaacgtgc
actacagaactccgaccacacacacgatgcccacttgggtcaaggctgtgtttttgaaccttctccccagggtca
tgtttatgactaggccaaccagcaccgaggaagacgccccaaagacgaggaacttctacggtgctgagctctc
aaacctgaactgcttcagccgtgcagactccaaaagctgcaaggaaggctacccctgccaagatgggacatg
tggctattgccaccaccgtagggtaaaaatctcaaatttcagtgccaacctcacaagaagctccagttctgagtct
gttgatgctgtgttgtccctgtctgctctgtcaccagaaatcaaagaagccatccaaagtgtgaagtatattgctga
aaatatgaaagcacagaatgtagccaaagagattcaagatgattggaagtatgttgccatggtgattgatcgca
ttttttctctgggttttcatcctggtgtgcattttaggaactgcaggattatttctgcaacccttgatggccagagatgaca
cataagctagcgcccctctccctcccccccccctaacgttactggccgaagccgcttggaataaggccggtgtg
cgtttgtctatatgttattttccaccatattgccgtcttttggcaatgtgagggcccggaaacctggccctgtcttcttga
cgagcattcctaggggtctttcccctctcgccaaaggaatgcaaggtctgttgaatgtcgtgaaggaagcagttc
ctctggaagcttcttgaagacaaacaacgtctgtagcgacccttgcaggcagcggaacccccccacctggcga

caggtgcctctgcggccaaaagccacgtgtataagatacacctgcaaaggcggcacaaccccagtgccacg
ttgtgagttggatagttgtggaaagagtcaaatggctctcctcaagcgtattcaacaaggggctgaaggatgccc
agaaggtaccccattgtatgggatctgatctggggcctcggtgcacatgctttacatgtgtttagtcgaggttaaaa
aaacgtctaggccccccgaaccacggggacgtggttttcctttgaaaaacacgatgataatatggccacaacc
atggtgagcaagggcgaggaggataacatggccatcatcaaggagttcatgcgcttcaaggtgcacatggag
ggctccgtgaacggccacgagttcgagatcgagggcgagggcgagggccgcccctacgagggcacccag
accgccaagctgaaggtgaccaagggtggcccctgcccttcgcctgggacatcctgtcccctcagttcatgta
cggctccaaggcctacgtgaagcaccccgccgacatccccgactacttgaagctgtccttccccgagggcttc
aagtgggagcgcgtgatgaacttcgaggacggcggcgtggtgaccgtgacccaggactcctccctgcagga
cggcgagttcatctacaaggtgaagctgcgcggcaccaacttcccctcagacggccccgtaatgcagaagaa
gaccatgggctgggaggcctcctccgagcggatgtaccccgaggacggcgccctgaagggcgagatcaag
cagaggctgaagctgaaggacggcggccactacgacgctgaggtcaagaccacctacaaggccaagaag
cccgtgcagctgcccggcgcctacaacgtcaacatcaagttggacatcacctcccacaacgaggactacacc
atcgtggaacagtacgaacgcgccgagggccgccactccaccggcggcatggacgagctgtacaagtaa

Figure 25. Plasmid map and sequence of α3-IRES-mCherry in lentiviral vector pFU

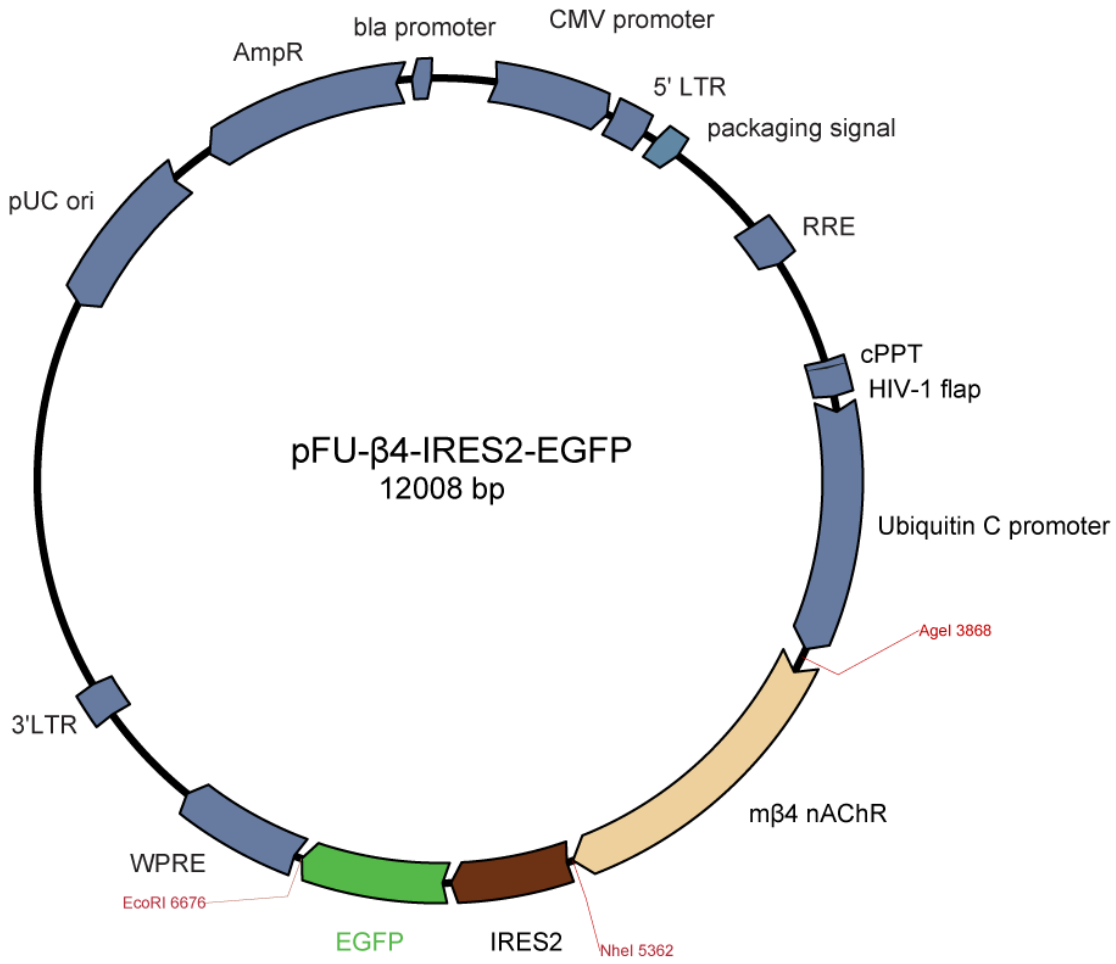

atgaggggtacgcccctgctcctcgtctctctgttcgctctgcttcagcctggggactgccgcctggccaacgcag
aggagaagctgatggatgatctcctgaacaaaacccgctacaacaacctgatccgcccagccaccagctcct
cccagctcatctccatccgcctggagctatcactgtcccagctcatcagtgtgaatgagcgagaacagatcatg
accaccagcatctggctgaaacaggaatggactgactaccgcctggcctggaacagctcctgctatgaaggg
gtgaacattctgaggattcctgcaaagcgagtctggttgcctgacatcgtgttgtacaacaatgccgatgggacct
atgaggtgtctgtctacaccaacgtgatcgtgcgttccaacggcagcatccagtggctgccccctgccatctaca
agagtgcctgcaagatagaggtgaagcactttcccttcgaccagcagaactgcaccctcaaatttcgctcctgg
acctatgaccacacagagattgacatggttcttaaatcacccacagccatcatggatgactttacccccagcggt
gaatgggacattgtggccctcccgggtcgaaggacagtgaacccacaggaccccagctatgtggacgtgacc
tatgacttcatcatcaagcgcaagccactcttctacaccatcaatctgatcatcccttgtgtgctcatcacgtcgctg
gctatcctggtcttctacctgccctccgactgtggggagaagatgacgctctgcatctcagtgctgctggcactca
cattcttcctgctgctcatctccaagatcgtgcctcccacctcccttgacattcccctcattggcaagtacctcttgttc
accatggtgctggtcacctttccatcgtcaccactgtgtgtgtcctcaatgtgcaccaccgttcacccagcactca
caccatggcatcctgggtcaaggagtgcttcctgcacaagctgcccaccttcctcttcatgaagcgccctggtctg
gaagtcagccccgccagggtccctcattccagccagctgcacttgaccacagctgaagctacgtccacctctg
ccttaggccccagcagcccatccaacctctatgggaattccatgtactttgtgaaccctgtccctgccactcctaa
gtctgcagtcagctcccacacggcaggcctccccagggatgcccggctgaggtcctctgggaggttccggcaa
gatctacaggaagcattagagggcgtcagcttcatcgcacagcatttggagagtgatgatcgagatcagagtgt
catcgaggactggaaattcgtcgcaatggtcgtcgaccgcctgttcctgtgggtgttcgtgattgtgtgtattctggg
caccatggggctcttcctgccacccctcttccagatccacgcaccctccaagggcctctaggctagcgcccctct
ccctcccccccccctaacgttactggccgaagccgcttggaataaggccggtgtgcgtttgtctatatgttatttttcc
accatattgccgtcttttggcaatgtgagggcccggaaacctggccctgtcttcttgacgagcattcctaggggtctt
tcccctctcgccaaaggaatgcaaggtctgttgaatgtcgtgaaggaagcagttcctctggaagcttcttgaaga

caaacaacgtctgtagcgacccttgcaggcagcggaacccccacctggcgacaggtgcctctgcggccaa
aagccacgtgtataagatacacctgcaaaggcggcacaaccccagtgccacgttgtgagttggatagttgtgg
aaagagtcaaatggctctcctcaagcgtattcaacaaggggctgaaggatgcccagaaggtaccccattgtat
gggatctgatctggggcctcggtgcacatgctttacatgtgtttagtcgaggttaaaaaaacgtctaggcccccg
aaccacggggacgtggttttcctttgaaaaacacgatgataatatggccacaaccatggtgagcaagggcga
ggagctgttcaccggggtggtgcccatcctggtcgagctggacggcgacgtaaacggccacaagttcagcgt
gtccggcgagggcgagggcgatgccacctacggcaagctgaccctgaagttcatctgcaccaccggcaagc
tgcccgtgccctggcccaccctcgtgaccaccctgacctacggcgtgcagtgcttcagccgctaccccgacca
catgaagcagcacgacttcttcaagtccgccatgcccgaaggctacgtccaggagcgcaccatcttcttcaag
gacgacggcaactacaagacccgcgccgaggtgaagttcgagggcgacaccctggtgaaccgcatcgagc
tgaagggcatcgacttcaaggaggacggcaacatcctggggcacaagctggagtacaactacaacagcca
caacgtctatatcatggccgacaagcagaagaacggcatcaaggtgaacttcaagatccgccacaacatcg
aggacggcagcgtgcagctcgccgaccactaccagcagaacaccccatcggcgacggccccgtgctgct
gcccgacaaccactacctgagcacccagtccgccctgagcaaagaccccaacgagaagcgcgatcacatg
gtcctgctggagttcgtgaccgccgccgggatcactctcggcatggacgagctgtacaagtaa

Figure26. Plasmid map and sequence of β4-IRES-EGFP in lentiviral vector pFU.

7.3 Index of figures

7.4 Index of tables

Erklärung

Hiermit versichere ich, Marta Anna Ślimak, dass ich die vorgelegte Dissertation mit dem Titel ‚Molecular determinants of the β4 nAChR subunit in channel function and nicotine mediated behavior' selbstständig, ohne unerlaubte Hilfe angefertigt habe.

Ort, Datum

Unterschrift

7.5 Publication and presentation list

Publication list

Santos-Torres J, **Ślimak MA**, Auer S, Ibañez-Tallon I. Cross-reactivity of acid-sensing ion channel and Na^+-H^+ exchanger antagonists with nicotinic acetylcholine receptors.J Physiol. 2011 Nov 1;589(Pt 21):5109-23. Epub 2011 Sep 12.

Frahm S, **Ślimak MA**, Ferrarese L, Santos-Torres J, Antolin-Fontes B, Auer S, Filkin S, Pons S, Fontaine JF, Tsetlin V, Maskos U, Ibañez-Tallon I.Aversion to nicotine is regulated by the balanced activity of β4 and α5 nicotinic receptor subunits in the medial habenula. Neuron 2011 May 12;70(3):522-35.

Oral presentations

"α3β4α5 nicotinic receptor : a critical role of the intracellular vestibule." MDC Neuro Retreat 2010.Split, Croatia, 16-1809.2010.

Poster presentations

Slimak MA., Antolin-Fontes B., Santos-Torres J, Ables J., Ferrarese L., Ibañez-Tallon I. "Functional analysis of the single nucleotide polymorphisms in the coding region of the β4 subunit of nAChR." SFB665: Developmental disturbances in the nervous system 2011. Seminaris SeeHotel Potsdam, Germany, 27-29.10.2011

Slimak MA., Antolin-Fontes B., Frahm S., Santos-Torres J., Ferrarese L., Sebastian Auer, Filkin S., Maskos U., Tsetlin V., Ibañez-Tallon I. "Genetic and molecular studies to dissect the contribution of nAChRs in the habenular circuit to brain function and behavior" Society for Neuroscience 2010 Meeting, San Diego, CA, USA,13-17.11.2010

Slimak MA., Frahm S., Ibañez-Tallon I "Nicotinic acetylcholine receptor β4 subunit is rate-limiting for nicotinic function *in vitro* and *in vivo*". Joint MDC-FMP PhD Retreat 2009, Hotel Sommerfeld, Kremmen, Germany, 3-5.09.2009

Slimak MA., Frahm S., Ibañez-Tallon I. "Nicotinic acetylcholine receptor β_4 subunit potentiates nicotinic currents in a gain-of-function transgenic mouse model"
Berlin Brain Days 2008. MDC, Berlin, Germany, 10-12.12. 2008.

Curriculum Vitae

For reasons of data protection,
the curriculum vitae is not included in the online version

8. References

1. Esch, T. & Stefano, G.B. The neurobiology of pleasure, reward processes, addiction and their health implications. *Neuro Endocrinol Lett* **25**, 235-251 (2004).
2. Koob, G.F. & Volkow, N.D. Neurocircuitry of addiction. *Neuropsychopharmacology* **35**, 217-238 (2010).
3. Dickenson, A.H. Mechanisms of the analgesic actions of opiates and opioids. *Br Med Bull* **47**, 690-702 (1991).
4. Tripathi, H.L., Martin, B.R. & Aceto, M.D. Nicotine-induced antinociception in rats and mice: correlation with nicotine brain levels. *J Pharmacol Exp Ther* **221**, 91-96 (1982).
5. Woodrow, K.M. & Eltherington, L.G. Feeling no pain: alcohol as an analgesic. *Pain* **32**, 159-163 (1988).
6. Leknes, S. & Tracey, I. A common neurobiology for pain and pleasure. *Nat Rev Neurosci* **9**, 314-320 (2008).
7. Jones, S. & Bonci, A. Synaptic plasticity and drug addiction. *Curr Opin Pharmacol* **5**, 20-25 (2005).
8. Kourrich, S., Rothwell, P.E., Klug, J.R. & Thomas, M.J. Cocaine experience controls bidirectional synaptic plasticity in the nucleus accumbens. *J Neurosci* **27**, 7921-7928 (2007).
9. Floresco, S.B. & Ghods-Sharifi, S. Amygdala-prefrontal cortical circuitry regulates effort-based decision making. *Cereb Cortex* **17**, 251-260 (2007).
10. Eisch, A.J. & Harburg, G.C. Opiates, psychostimulants, and adult hippocampal neurogenesis: Insights for addiction and stem cell biology. *Hippocampus* **16**, 271-286 (2006).
11. Kornetsky, C. & Esposito, R.U. Euphorigenic drugs: effects on the reward pathways of the brain. *Fed Proc* **38**, 2473-2476 (1979).
12. Koob, G.F. Neural mechanisms of drug reinforcement. *Ann N Y Acad Sci* **654**, 171-191 (1992).
13. Nestler, E.J. The neurobiology of cocaine addiction. *Sci Pract Perspect* **3**, 4-10 (2005).
14. Hnasko, T.S., Sotak, B.N. & Palmiter, R.D. Morphine reward in dopamine-deficient mice. *Nature* **438**, 854-857 (2005).
15. Corrigall, W.A., Franklin, K.B., Coen, K.M. & Clarke, P.B. The mesolimbic dopaminergic system is implicated in the reinforcing effects of nicotine. *Psychopharmacology (Berl)* **107**, 285-289 (1992).
16. Corrigall, W.A., Coen, K.M. & Adamson, K.L. Self-administered nicotine activates the mesolimbic dopamine system through the ventral tegmental area. *Brain Res* **653**, 278-284 (1994).
17. Malin, D.H.*, et al.* Subcutaneous injection of an analog of neuropeptide FF precipitates morphine abstinence syndrome. *Life Sci* **53**, PL261-266 (1993).
18. Pontieri, F.E.*, et al.* Effects of the intravenous administration of [Lys7]dermorphin on local cerebral glucose utilization in the rat. *Eur J Pharmacol* **544**, 17-20 (2006).
19. McGregor, A. & Roberts, D.C. Dopaminergic antagonism within the nucleus accumbens or the amygdala produces differential effects on intravenous cocaine self-administration under fixed and progressive ratio schedules of reinforcement. *Brain Res* **624**, 245-252 (1993).

20. Koob, G.F. & Le Moal, M. Drug addiction, dysregulation of reward, and allostasis. *Neuropsychopharmacology* **24**, 97-129 (2001).
21. Di Chiara, G. & Imperato, A. Drugs abused by humans preferentially increase synaptic dopamine concentrations in the mesolimbic system of freely moving rats. *Proc Natl Acad Sci U S A* **85**, 5274-5278 (1988).
22. Jensen, M.P., Karoly, P. & Huger, R. The development and preliminary validation of an instrument to assess patients' attitudes toward pain. *J Psychosom Res* **31**, 393-400 (1987).
23. Dill, R.E. & Costa, E. Behavioural dissociation of the enkephalinergic systems of nucleus accumbens and nucleus caudatus. *Neuropharmacology* **16**, 323-326 (1977).
24. Yu, L.C. & Han, J.S. Involvement of arcuate nucleus of hypothalamus in the descending pathway from nucleus accumbens to periaqueductal grey subserving an antinociceptive effect. *Int J Neurosci* **48**, 71-78 (1989).
25. Tseng, L.F. & Wang, Q. Forebrain sites differentially sensitive to beta-endorphin and morphine for analgesia and release of Met-enkephalin in the pentobarbital-anesthesized rat. *J Pharmacol Exp Ther* **261**, 1028-1036 (1992).
26. Daghero, A.M., Bradley, E.L., Jr. & Kissin, I. Midazolam antagonizes the analgesic effect of morphine in rats. *Anesth Analg* **66**, 944-947 (1987).
27. Gear, R.W. & Levine, J.D. Antinociception produced by an ascending spino-supraspinal pathway. *J Neurosci* **15**, 3154-3161 (1995).
28. Gear, R.W., Aley, K.O. & Levine, J.D. Pain-induced analgesia mediated by mesolimbic reward circuits. *J Neurosci* **19**, 7175-7181 (1999).
29. Hikosaka, O. The habenula: from stress evasion to value-based decision-making. *Nat Rev Neurosci* **11**, 503-513 (2010).
30. Shelton, L., Becerra, L. & Borsook, D. Unmasking the mysteries of the habenula in pain and analgesia. *Prog Neurobiol* **96**, 208-219 (2012).
31. Shelton, L.*, et al.* Mapping Pain Activation and Connectivity of the Human Habenula. *J Neurophysiol* (2012).
32. Bianco, I.H. & Wilson, S.W. The habenular nuclei: a conserved asymmetric relay station in the vertebrate brain. *Philos Trans R Soc Lond B Biol Sci* **364**, 1005-1020 (2009).
33. Kim, U. & Chang, S.Y. Dendritic morphology, local circuitry, and intrinsic electrophysiology of neurons in the rat medial and lateral habenular nuclei of the epithalamus. *J Comp Neurol* **483**, 236-250 (2005).
34. Craig, A.D. Distribution of trigeminothalamic and spinothalamic lamina I terminations in the cat. *Somatosens Mot Res* **20**, 209-222 (2003).
35. Dafny, N.*, et al.* Lateral hypothalamus: site involved in pain modulation. *Neuroscience* **70**, 449-460 (1996).
36. Burstein, R., Cliffer, K.D. & Giesler, G.J., Jr. Cells of origin of the spinohypothalamic tract in the rat. *J Comp Neurol* **291**, 329-344 (1990).
37. Casey, K.L. Forebrain mechanisms of nociception and pain: analysis through imaging. *Proc Natl Acad Sci U S A* **96**, 7668-7674 (1999).
38. Becerra, L. & Borsook, D. Signal valence in the nucleus accumbens to pain onset and offset. *Eur J Pain* **12**, 866-869 (2008).
39. Ma, Q.P. & Han, J.S. Neurochemical studies on the mesolimbic circuitry of antinociception. *Brain Res* **566**, 95-102 (1991).
40. Ma, Q.P., Shi, Y.S. & Han, J.S. Further studies on interactions between periaqueductal gray, nucleus accumbens and habenula in antinociception. *Brain Res* **583**, 292-295 (1992).

41. Behbehani, M.M. Functional characteristics of the midbrain periaqueductal gray. *Prog Neurobiol* **46**, 575-605 (1995).
42. Ren, K. & Dubner, R. Descending modulation in persistent pain: an update. *Pain* **100**, 1-6 (2002).
43. Bromberg-Martin, E.S., Matsumoto, M. & Hikosaka, O. Dopamine in motivational control: rewarding, aversive, and alerting. *Neuron* **68**, 815-834 (2010).
44. Ferraro, G., Montalbano, M.E., Sardo, P. & La Grutta, V. Lateral habenular influence on dorsal raphe neurons. *Brain Res Bull* **41**, 47-52 (1996).
45. Alenina, N., Bashammakh, S. & Bader, M. Specification and differentiation of serotonergic neurons. *Stem Cell Rev* **2**, 5-10 (2006).
46. Frahm, S.*, et al.* Aversion to nicotine is regulated by the balanced activity of beta4 and alpha5 nicotinic receptor subunits in the medial habenula. *Neuron* **70**, 522-535 (2011).
47. Fowler, C.D., Lu, Q., Johnson, P.M., Marks, M.J. & Kenny, P.J. Habenular alpha5 nicotinic receptor subunit signalling controls nicotine intake. *Nature* **471**, 597-601 (2011).
48. Changeux, J.P., Devillers-Thiery, A. & Chemouilli, P. Acetylcholine receptor: an allosteric protein. *Science* **225**, 1335-1345 (1984).
49. Lal, R. & Yu, L. Atomic force microscopy of cloned nicotinic acetylcholine receptor expressed in Xenopus oocytes. *Proc Natl Acad Sci U S A* **90**, 7280-7284 (1993).
50. Liang, Y.*, et al.* Functional polymorphisms in the human beta4 subunit of nicotinic acetylcholine receptors. *Neurogenetics* **6**, 37-44 (2005).
51. Palma, E., Maggi, L., Barabino, B., Eusebi, F. & Ballivet, M. Nicotinic acetylcholine receptors assembled from the alpha7 and beta3 subunits. *J Biol Chem* **274**, 18335-18340 (1999).
52. Khiroug, S.S.*, et al.* Rat nicotinic ACh receptor alpha7 and beta2 subunits co-assemble to form functional heteromeric nicotinic receptor channels. *J Physiol* **540**, 425-434 (2002).
53. Kuo, Y.P.*, et al.* Roles for nicotinic acetylcholine receptor subunit large cytoplasmic loop sequences in receptor expression and function. *J Pharmacol Exp Ther* **314**, 455-466 (2005).
54. Jones, S., Sudweeks, S. & Yakel, J.L. Nicotinic receptors in the brain: correlating physiology with function. *Trends Neurosci* **22**, 555-561 (1999).
55. McGehee, D.S. Molecular diversity of neuronal nicotinic acetylcholine receptors. *Ann N Y Acad Sci* **868**, 565-577 (1999).
56. Nordberg, A. Human nicotinic receptors--their role in aging and dementia. *Neurochem Int* **25**, 93-97 (1994).
57. Steinlein, O.K.*, et al.* A missense mutation in the neuronal nicotinic acetylcholine receptor alpha 4 subunit is associated with autosomal dominant nocturnal frontal lobe epilepsy. *Nat Genet* **11**, 201-203 (1995).
58. Freedman, R.*, et al.* Linkage of a neurophysiological deficit in schizophrenia to a chromosome 15 locus. *Proc Natl Acad Sci U S A* **94**, 587-592 (1997).
59. Paterson, D. & Nordberg, A. Neuronal nicotinic receptors in the human brain. *Prog Neurobiol* **61**, 75-111 (2000).
60. Court, J.*, et al.* Nicotinic receptor abnormalities in Alzheimer's disease. *Biol Psychiatry* **49**, 175-184 (2001).

61. Dani, J.A. Overview of nicotinic receptors and their roles in the central nervous system. *Biol Psychiatry* **49**, 166-174 (2001).
62. Stolerman, I.P. & Jarvis, M.J. The scientific case that nicotine is addictive. *Psychopharmacology (Berl)* **117**, 2-10; discussion 14-20 (1995).
63. Markou, A. Review. Neurobiology of nicotine dependence. *Philos Trans R Soc Lond B Biol Sci* **363**, 3159-3168 (2008).
64. Changeux, J.P. Nicotine addiction and nicotinic receptors: lessons from genetically modified mice. *Nat Rev Neurosci* **11**, 389-401 (2010).
65. Benowitz, N.L. Neurobiology of nicotine addiction: implications for smoking cessation treatment. *Am J Med* **121**, S3-10 (2008).
66. Benowitz, N.L. Clinical pharmacology of nicotine: implications for understanding, preventing, and treating tobacco addiction. *Clin Pharmacol Ther* **83**, 531-541 (2008).
67. Buchhalter, A.R., Fant, R.V. & Henningfield, J.E. Novel pharmacological approaches for treating tobacco dependence and withdrawal: current status. *Drugs* **68**, 1067-1088 (2008).
68. Carmody, T.P., Vieten, C. & Astin, J.A. Negative affect, emotional acceptance, and smoking cessation. *J Psychoactive Drugs* **39**, 499-508 (2007).
69. Kenny, P.J. & Markou, A. Neurobiology of the nicotine withdrawal syndrome. *Pharmacol Biochem Behav* **70**, 531-549 (2001).
70. Heintz, N. BAC to the future: the use of bac transgenic mice for neuroscience research. *Nat Rev Neurosci* **2**, 861-870 (2001).
71. Giraldo, P. & Montoliu, L. Size matters: use of YACs, BACs and PACs in transgenic animals. *Transgenic Res* **10**, 83-103 (2001).
72. Sauer, B. Functional expression of the cre-lox site-specific recombination system in the yeast Saccharomyces cerevisiae. *Mol Cell Biol* **7**, 2087-2096 (1987).
73. Stricklett, P.K., Nelson, R.D. & Kohan, D.E. The Cre/loxP system and gene targeting in the kidney. *Am J Physiol* **276**, F651-657 (1999).
74. Rajewsky, K.*, et al.* Conditional gene targeting. *J Clin Invest* **98**, 600-603 (1996).
75. Boyden, E.S., Zhang, F., Bamberg, E., Nagel, G. & Deisseroth, K. Millisecond-timescale, genetically targeted optical control of neural activity. *Nat Neurosci* **8**, 1263-1268 (2005).
76. Gradinaru, V., Mogri, M., Thompson, K.R., Henderson, J.M. & Deisseroth, K. Optical deconstruction of parkinsonian neural circuitry. *Science* **324**, 354-359 (2009).
77. Cardin, V. & Smith, A.T. Sensitivity of human visual and vestibular cortical regions to egomotion-compatible visual stimulation. *Cereb Cortex* **20**, 1964-1973 (2010).
78. Sohal, V.S., Zhang, F., Yizhar, O. & Deisseroth, K. Parvalbumin neurons and gamma rhythms enhance cortical circuit performance. *Nature* **459**, 698-702 (2009).
79. Tsai, H.C.*, et al.* Phasic firing in dopaminergic neurons is sufficient for behavioral conditioning. *Science* **324**, 1080-1084 (2009).
80. Witten, I.B.*, et al.* Cholinergic interneurons control local circuit activity and cocaine conditioning. *Science* **330**, 1677-1681 (2010).
81. Oztas, E. Neuronal tracing. *Neuroanatomy* **2**, 2-5 (2003).

82. Wickersham, I.R., Finke, S., Conzelmann, K.K. & Callaway, E.M. Retrograde neuronal tracing with a deletion-mutant rabies virus. *Nat Methods* **4**, 47-49 (2007).
83. Wickersham, I.R.*, et al.* Monosynaptic restriction of transsynaptic tracing from single, genetically targeted neurons. *Neuron* **53**, 639-647 (2007).
84. Ugolini, G. Use of rabies virus as a transneuronal tracer of neuronal connections: implications for the understanding of rabies pathogenesis. *[Research Support, Non-U.S. Gov't Review]. Dev Biol (Basel)* **131**, 496-506 (2008).
85. Hillary, F.G. & Biswal, B. The influence of neuropathology on the FMRI signal: a measurement of brain or vein? *Clin Neuropsychol* **21**, 58-72 (2007).
86. Hillary, F.G.*, et al.* Examining lactate in severe TBI using proton magnetic resonance spectroscopy. *Brain Inj* **21**, 981-991 (2007).
87. Mathieu-Kia, A.M., Kellogg, S.H., Butelman, E.R. & Kreek, M.J. Nicotine addiction: insights from recent animal studies. *Psychopharmacology (Berl)* **162**, 102-118 (2002).
88. Rogers, S.W. Mouse models and genetic of nicotine dependence. *Phenotypes and Endophenotypes*
Foundations for Genetic Studies of Nicotine Use and Dependence, 133-186 (2008).
89. Berrettini, W.H. & Lerman, C.E. Pharmacotherapy and pharmacogenetics of nicotine dependence. *Am J Psychiatry* **162**, 1441-1451 (2005).
90. Kellar, K.J., Davila-Garcia, M.I. & Xiao, Y. Pharmacology of neuronal nicotinic acetylcholine recceptors: effects of acute and chronic nicotine. *Nicotine Tob Res* **1 Suppl 2**, S117-120; discussion S139-140 (1999).
91. Whiting, P.J. & Lindstrom, J.M. Characterization of bovine and human neuronal nicotinic acetylcholine receptors using monoclonal antibodies. *J Neurosci* **8**, 3395-3404 (1988).
92. Maskos, U.*, et al.* Nicotine reinforcement and cognition restored by targeted expression of nicotinic receptors. *Nature* **436**, 103-107 (2005).
93. Picciotto, M.R.*, et al.* Acetylcholine receptors containing the beta2 subunit are involved in the reinforcing properties of nicotine. *Nature* **391**, 173-177 (1998).
94. Tapper, A.R.*, et al.* Nicotine activation of alpha4* receptors: sufficient for reward, tolerance, and sensitization. *Science* **306**, 1029-1032 (2004).
95. Zoli, M., Le Novere, N., Hill, J.A., Jr. & Changeux, J.P. Developmental regulation of nicotinic ACh receptor subunit mRNAs in the rat central and peripheral nervous systems. *J Neurosci* **15**, 1912-1939 (1995).
96. Rose, J.E. Multiple brain pathways and receptors underlying tobacco addiction. *Biochem Pharmacol* **74**, 1263-1270 (2007).
97. Jackson, K.J., Martin, B.R., Changeux, J.P. & Damaj, M.I. Differential role of nicotinic acetylcholine receptor subunits in physical and affective nicotine withdrawal signs. *J Pharmacol Exp Ther* **325**, 302-312 (2008).
98. Salas, R., Pieri, F. & De Biasi, M. Decreased signs of nicotine withdrawal in mice null for the beta4 nicotinic acetylcholine receptor subunit. *J Neurosci* **24**, 10035-10039 (2004).
99. Salas, R., Sturm, R., Boulter, J. & De Biasi, M. Nicotinic receptors in the habenulo-interpeduncular system are necessary for nicotine withdrawal in mice. *J Neurosci* **29**, 3014-3018 (2009).

100. Kedmi, M., Beaudet, A.L. & Orr-Urtreger, A. Mice lacking neuronal nicotinic acetylcholine receptor beta4-subunit and mice lacking both alpha5- and beta4-subunits are highly resistant to nicotine-induced seizures. *Physiol Genomics* **17**, 221-229 (2004).
101. Salas, R., Cook, K.D., Bassetto, L. & De Biasi, M. The alpha3 and beta4 nicotinic acetylcholine receptor subunits are necessary for nicotine-induced seizures and hypolocomotion in mice. *Neuropharmacology* **47**, 401-407 (2004).
102. Xu, W*., et al.* Megacystis, mydriasis, and ion channel defect in mice lacking the alpha3 neuronal nicotinic acetylcholine receptor. *Proc Natl Acad Sci U S A* **96**, 5746-5751 (1999).
103. Bigger, C.B., Melnikova, I.N. & Gardner, P.D. Sp1 and Sp3 regulate expression of the neuronal nicotinic acetylcholine receptor beta4 subunit gene. *J Biol Chem* **272**, 25976-25982 (1997).
104. Medel, Y.F. & Gardner, P.D. Transcriptional repression by a conserved intronic sequence in the nicotinic receptor alpha3 subunit gene. *J Biol Chem* **282**, 19062-19070 (2007).
105. Xu, X., Scott, M.M. & Deneris, E.S. Shared long-range regulatory elements coordinate expression of a gene cluster encoding nicotinic receptor heteromeric subtypes. *Mol Cell Biol* **26**, 5636-5649 (2006).
106. Scofield, M.D., Tapper, A.R. & Gardner, P.D. A transcriptional regulatory element critical for CHRNB4 promoter activity in vivo. *Neuroscience* **170**, 1056-1064 (2010).
107. Gong, S*., et al.* A gene expression atlas of the central nervous system based on bacterial artificial chromosomes. *Nature* **425**, 917-925 (2003).
108. Broms, U*., et al.* The Nicotine Dependence Syndrome Scale in Finnish smokers. *Drug Alcohol Depend* **89**, 42-51 (2007).
109. Li, M.D. The genetics of smoking related behavior: a brief review. *Am J Med Sci* **326**, 168-173 (2003).
110. Maes, H.H*., et al.* A twin study of genetic and environmental influences on tobacco initiation, regular tobacco use and nicotine dependence. *Psychol Med* **34**, 1251-1261 (2004).
111. Vink, J.M., Willemsen, G. & Boomsma, D.I. Heritability of smoking initiation and nicotine dependence. *Behav Genet* **35**, 397-406 (2005).
112. Lessov, C.N*., et al.* Defining nicotine dependence for genetic research: evidence from Australian twins. *Psychol Med* **34**, 865-879 (2004).
113. Baker, T.B*., et al.* Human neuronal acetylcholine receptor A5-A3-B4 haplotypes are associated with multiple nicotine dependence phenotypes. *Nicotine Tob Res* **11**, 785-796 (2009).
114. Bergen, A.W*., et al.* Dopamine genes and nicotine dependence in treatment-seeking and community smokers. *Neuropsychopharmacology* **34**, 2252-2264 (2009).
115. Bierut, L.J*., et al.* Variants in nicotinic receptors and risk for nicotine dependence. *Am J Psychiatry* **165**, 1163-1171 (2008).
116. Breitling, L.P*., et al.* Association of nicotinic acetylcholine receptor subunit alpha 4 polymorphisms with nicotine dependence in 5500 Germans. *Pharmacogenomics J* **9**, 219-224 (2009).
117. Chen, X*., et al.* Cannabinoid receptor 1 gene association with nicotine dependence. *Arch Gen Psychiatry* **65**, 816-824 (2008).

118. Chen, X.*, et al.* Variants in nicotinic acetylcholine receptors alpha5 and alpha3 increase risks to nicotine dependence. *Am J Med Genet B Neuropsychiatr Genet* **150B**, 926-933 (2009).
119. Chen, X., Cho, K., Singer, B.H. & Zhang, H. PKNOX2 gene is significantly associated with substance dependence in European-origin women. *Proc Natl Acad Sci U S A* (2009).
120. Etter, J.F.*, et al.* Association of genes coding for the alpha-4, alpha-5, beta-2 and beta-3 subunits of nicotinic receptors with cigarette smoking and nicotine dependence. *Addict Behav* **34**, 772-775 (2009).
121. Freathy, R.M.*, et al.* A common genetic variant in the 15q24 nicotinic acetylcholine receptor gene cluster (CHRNA5-CHRNA3-CHRNB4) is associated with a reduced ability of women to quit smoking in pregnancy. *Hum Mol Genet* **18**, 2922-2927 (2009).
122. Greenbaum, L.*, et al.* Why do young women smoke? I. Direct and interactive effects of environment, psychological characteristics and nicotinic cholinergic receptor genes. *Mol Psychiatry* **11**, 312-322, 223 (2006).
123. Hoft, N.R.*, et al.* Genetic association of the CHRNA6 and CHRNB3 genes with tobacco dependence in a nationally representative sample. *Neuropsychopharmacology* **34**, 698-706 (2009).
124. Keskitalo, K.*, et al.* Association of serum cotinine level with a cluster of three nicotinic acetylcholine receptor genes (CHRNA3/CHRNA5/CHRNB4) on chromosome 15. *Hum Mol Genet* **18**, 4007-4012 (2009).
125. Le Marchand, L.*, et al.* Smokers with the CHRNA lung cancer-associated variants are exposed to higher levels of nicotine equivalents and a carcinogenic tobacco-specific nitrosamine. *Cancer Res* **68**, 9137-9140 (2008).
126. Li, M.D. Identifying susceptibility loci for nicotine dependence: 2008 update based on recent genome-wide linkage analyses. *Hum Genet* **123**, 119-131 (2008).
127. Li, M.D.*, et al.* Association and interaction analyses of GABBR1 and GABBR2 with nicotine dependence in European- and African-American populations. *PLoS One* **4**, e7055 (2009).
128. Perkins, K.A.*, et al.* Gene and gene by sex associations with initial sensitivity to nicotine in nonsmokers. *Behav Pharmacol* **19**, 630-640 (2008).
129. Perkins, K.A.*, et al.* Dopamine and opioid gene variants are associated with increased smoking reward and reinforcement owing to negative mood. *Behav Pharmacol* **19**, 641-649 (2008).
130. Perkins, K.A., Lerman, C., Mercincavage, M., Fonte, C.A. & Briski, J.L. Nicotinic acetylcholine receptor beta2 subunit (CHRNB2) gene and short-term ability to quit smoking in response to nicotine patch. *Cancer Epidemiol Biomarkers Prev* **18**, 2608-2612 (2009).
131. Philibert, R.A.*, et al.* Role of GABRA2 on risk for alcohol, nicotine, and cannabis dependence in the Iowa Adoption Studies. *Psychiatr Genet* **19**, 91-98 (2009).
132. Rigbi, A.*, et al.* Why do young women smoke? V. Role of direct and interactive effects of nicotinic cholinergic receptor gene variation on neurocognitive function. *Genes Brain Behav* **7**, 164-172 (2008).

133. Saccone, N.L.*, et al.* Multiple distinct risk loci for nicotine dependence identified by dense coverage of the complete family of nicotinic receptor subunit (CHRN) genes. *Am J Med Genet B Neuropsychiatr Genet* **150B**, 453-466 (2009).
134. Saccone, N.L.*, et al.* The CHRNA5-CHRNA3-CHRNB4 nicotinic receptor subunit gene cluster affects risk for nicotine dependence in African-Americans and in European-Americans. *Cancer Res* **69**, 6848-6856 (2009).
135. Sherva, R.*, et al.* Association of a single nucleotide polymorphism in neuronal acetylcholine receptor subunit alpha 5 (CHRNA5) with smoking status and with 'pleasurable buzz' during early experimentation with smoking. *Addiction* **103**, 1544-1552 (2008).
136. Spitz, M.R., Amos, C.I., Dong, Q., Lin, J. & Wu, X. The CHRNA5-A3 region on chromosome 15q24-25.1 is a risk factor both for nicotine dependence and for lung cancer. *J Natl Cancer Inst* **100**, 1552-1556 (2008).
137. Stevens, V.L.*, et al.* Nicotinic receptor gene variants influence susceptibility to heavy smoking. *Cancer Epidemiol Biomarkers Prev* **17**, 3517-3525 (2008).
138. Wang, J.C.*, et al.* Genetic variation in the CHRNA5 gene affects mRNA levels and is associated with risk for alcohol dependence. *Mol Psychiatry* **14**, 501-510 (2009).
139. Weiss, R.B.*, et al.* A candidate gene approach identifies the CHRNA5-A3-B4 region as a risk factor for age-dependent nicotine addiction. *PLoS Genet* **4**, e1000125 (2008).
140. Drgon, T.*, et al.* Genome-wide association for smoking cessation success: participants in a trial with adjunctive denicotinized cigarettes. *Mol Med* **15**, 268-274 (2009).
141. Drgon, T.*, et al.* Genome-wide association for nicotine dependence and smoking cessation success in NIH research volunteers. *Mol Med* **15**, 21-27 (2009).
142. Liu, Y.*, et al.* Haplotype and cell proliferation analyses of candidate lung cancer susceptibility genes on chromosome 15q24-25.1. *Cancer Res* **69**, 7844-7850 (2009).
143. Liu, J.Z.*, et al.* Meta-analysis and imputation refines the association of 15q25 with smoking quantity. *Nat Genet* **42**, 436-440 (2010).
144. Thorgeirsson, T.E. & Stefansson, K. Genetics of smoking behavior and its consequences: the role of nicotinic acetylcholine receptors. *Biol Psychiatry* **64**, 919-921 (2008).
145. Amos, C.I.*, et al.* Nicotinic acetylcholine receptor region on chromosome 15q25 and lung cancer risk among African Americans: a case-control study. *J Natl Cancer Inst* **102**, 1199-1205 (2010).
146. Bierut, L.J. Convergence of genetic findings for nicotine dependence and smoking related diseases with chromosome 15q24-25. *Trends Pharmacol Sci* **31**, 46-51 (2010).
147. Saccone, S.F.*, et al.* Cholinergic nicotinic receptor genes implicated in a nicotine dependence association study targeting 348 candidate genes with 3713 SNPs. *Hum Mol Genet* **16**, 36-49 (2007).
148. Berrettini, W.*, et al.* Alpha-5/alpha-3 nicotinic receptor subunit alleles increase risk for heavy smoking. *Mol Psychiatry* **13**, 368-373 (2008).

149. Zoli, M.*, et al.* Identification of the nicotinic receptor subtypes expressed on dopaminergic terminals in the rat striatum. *J Neurosci* **22**, 8785-8789 (2002).
150. Salminen, O.*, et al.* Subunit composition and pharmacology of two classes of striatal presynaptic nicotinic acetylcholine receptors mediating dopamine release in mice. *Mol Pharmacol* **65**, 1526-1535 (2004).
151. Saccone, N.L.*, et al.* Multiple independent loci at chromosome 15q25.1 affect smoking quantity: a meta-analysis and comparison with lung cancer and COPD. *PLoS Genet* **6**(2010).
152. Lu, Y. & Wang, X. Genes associated with idiopathic epilepsies: a current overview. *Neurol Res* **31**, 135-143 (2009).
153. Haller, G.*, et al.* Rare missense variants in CHRNB4 are associated with reduced risk of nicotine dependence. *Hum Mol Genet* **21**, 647-655 (2012).
154. Sarginson, J.E.*, et al.* Markers in the 15q24 nicotinic receptor subunit gene cluster (CHRNA5-A3-B4) predict severity of nicotine addiction and response to smoking cessation therapy. *Am J Med Genet B Neuropsychiatr Genet* **156B**, 275-284 (2011).
155. Mullis, K.*, et al.* Specific enzymatic amplification of DNA in vitro: the polymerase chain reaction. *Cold Spring Harb Symp Quant Biol* **51 Pt 1**, 263-273 (1986).
156. Horton, R.M., Cai, Z.L., Ho, S.N. & Pease, L.R. Gene splicing by overlap extension: tailor-made genes using the polymerase chain reaction. *Biotechniques* **8**, 528-535 (1990).
157. Mandel, M. & Higa, A. Calcium-dependent bacteriophage DNA infection. *J Mol Biol* **53**, 159-162 (1970).
158. Delenda, C. Lentiviral vectors: optimization of packaging, transduction and gene expression. *J Gene Med* **6** S125-138 (2004).
159. Auer, S. Freie Universität Berlin (2010).
160. Zerangue, N., Schwappach, B., Jan, Y.N. & Jan, L.Y. A new ER trafficking signal regulates the subunit stoichiometry of plasma membrane K(ATP) channels. *Neuron* **22**, 537-548 (1999).
161. Butt, C.M., King, N.M., Hutton, S.R., Collins, A.C. & Stitzel, J.A. Modulation of nicotine but not ethanol preference by the mouse Chrna4 A529T polymorphism. *Behav Neurosci* **119**, 26-37 (2005).
162. Nashmi, R.*, et al.* Assembly of alpha4beta2 nicotinic acetylcholine receptors assessed with functional fluorescently labeled subunits: effects of localization, trafficking, and nicotine-induced upregulation in clonal mammalian cells and in cultured midbrain neurons. *J Neurosci* **23**, 11554-11567 (2003).
163. Ren, X.Q.*, et al.* Structural determinants of alpha4beta2 nicotinic acetylcholine receptor trafficking. *J Neurosci* **25**, 6676-6686 (2005).
164. Finer-Moore, J. & Stroud, R.M. Amphipathic analysis and possible formation of the ion channel in an acetylcholine receptor. *Proc Natl Acad Sci U S A* **81**, 155-159 (1984).
165. Peters, J.A.*, et al.* Novel structural determinants of single-channel conductance in nicotinic acetylcholine and 5-hydroxytryptamine type-3 receptors. *Biochem Soc Trans* **34**, 882-886 (2006).
166. Peters, J.A.*, et al.* Novel structural determinants of single channel conductance and ion selectivity in 5-hydroxytryptamine type 3 and nicotinic acetylcholine receptors. *J Physiol* **588**, 587-596 (2010).

167. Unwin, N. Refined structure of the nicotinic acetylcholine receptor at 4A resolution. *J Mol Biol* **346**, 967-989 (2005).
168. Gahring, L.C. & Rogers, S.W. Nicotinic receptor subunit alpha5 modifies assembly, up-regulation, and response to pro-inflammatory cytokines. *J Biol Chem* **285**, 26049-26057 (2010).
169. Wong, S.M., Koh, D.C. & Liu, D. Identification of plant virus IRES. *Methods Mol Biol* **451**, 125-133 (2008).
170. Cockrell, A.S. & Kafri, T. Gene delivery by lentivirus vectors. *Mol Biotechnol* **36**, 184-204 (2007).
171. Karra, D. & Dahm, R. Transfection techniques for neuronal cells. *J Neurosci* **30**, 6171-6177 (2010).
172. Naldini, L., Blomer, U., Gage, F.H., Trono, D. & Verma, I.M. Efficient transfer, integration, and sustained long-term expression of the transgene in adult rat brains injected with a lentiviral vector. *Proc Natl Acad Sci U S A* **93**, 11382-11388 (1996).
173. Naldini, L.*, et al.* In vivo gene delivery and stable transduction of nondividing cells by a lentiviral vector. *Science* **272**, 263-267 (1996).
174. Blomer, U.*, et al.* Highly efficient and sustained gene transfer in adult neurons with a lentivirus vector. *J Virol* **71**, 6641-6649 (1997).
175. Molles, B.E.*, et al.* Targeted in vivo expression of nicotinic acetylcholine receptors in mouse brain using lentiviral expression vectors. *J Mol Neurosci* **30**, 105-106 (2006).
176. Son, J.H. & Winzer-Serhan, U.H. Expression of neuronal nicotinic acetylcholine receptor subunit mRNAs in rat hippocampal GABAergic interneurons. *J Comp Neurol* **511**, 286-299 (2008).
177. Mizuguchi, H., Xu, Z., Ishii-Watabe, A., Uchida, E. & Hayakawa, T. IRES-dependent second gene expression is significantly lower than cap-dependent first gene expression in a bicistronic vector. *Mol Ther* **1**, 376-382 (2000).
178. Robinson, S.F., Marks, M.J. & Collins, A.C. Inbred mouse strains vary in oral self-selection of nicotine. *Psychopharmacology (Berl)* **124**, 332-339 (1996).
179. Glatt, A.R., Denton, K. & Boughter, J.D., Jr. Variation in nicotine consumption in inbred mice is not linked to orosensory ability. *Chem Senses* **34**, 27-35 (2009).
180. Meliska, C.J., Bartke, A., Vandergriff, J.L. & Jensen, R.A. Ethanol and nicotine consumption and preference in transgenic mice overexpressing the bovine growth hormone gene. *Pharmacol Biochem Behav* **50**, 563-570 (1995).
181. Cepeda-Benito, A., Reynoso, J. & Erath, S.A. Dose-response analyses of associative tolerance to nicotine analgesia in the rat: tail-flick and hot-plate tests. *Exp Clin Psychopharmacol* **8**, 112-116 (2000).
182. Hargreaves, K., Dubner, R., Brown, F., Flores, C. & Joris, J. A new and sensitive method for measuring thermal nociception in cutaneous hyperalgesia. *Pain* **32**, 77-88 (1988).
183. Yeomans, D.C. & Proudfit, H.K. Characterization of the foot withdrawal response to noxious radiant heat in the rat. *Pain* **59**, 85-94 (1994).
184. Cohen, S.R. & Melzack, R. The habenula and pain: repeated electrical stimulation produces prolonged analgesia but lesions have no effect on formalin pain or morphine analgesia. *Behav Brain Res* **54**, 171-178 (1993).

185. Lawand, N.B., Lu, Y. & Westlund, K.N. Nicotinic cholinergic receptors: potential targets for inflammatory pain relief. *Pain* **80**, 291-299 (1999).
186. Dubuisson, D. & Dennis, S.G. The formalin test: a quantitative study of the analgesic effects of morphine, meperidine, and brain stem stimulation in rats and cats. *Pain* **4**, 161-174 (1977).
187. Woolf, C.J. & Mannion, R.J. Neuropathic pain: aetiology, symptoms, mechanisms, and management. *Lancet* **353**, 1959-1964 (1999).
188. Zimmermann, M. Pathobiology of neuropathic pain. *Eur J Pharmacol* **429**, 23-37 (2001).
189. Sun, H.*, et al.* Dorsal horn-enriched genes identified by DNA microarray, in situ hybridization and immunohistochemistry. *BMC Neurosci* **3**, 11 (2002).
190. Paulson, P.E., Wiley, J.W. & Morrow, T.J. Concurrent activation of the somatosensory forebrain and deactivation of periaqueductal gray associated with diabetes-induced neuropathic pain. *Exp Neurol* **208**, 305-313 (2007).
191. Lee, Y., Rudell, J. & Ferns, M. Rapsyn interacts with the muscle acetylcholine receptor via alpha-helical domains in the alpha, beta, and epsilon subunit intracellular loops. *Neuroscience* **163**, 222-232 (2009).
192. Rezvani, K., Teng, Y. & De Biasi, M. The ubiquitin-proteasome system regulates the stability of neuronal nicotinic acetylcholine receptors. *J Mol Neurosci* **40**, 177-184 (2010).
193. Retchless, B.S., Gao, W. & Johnson, J.W. A single GluN2 subunit residue controls NMDA receptor channel properties via intersubunit interaction. *Nature Neuroscience* **15**, 406-413 (2012).
194. Sekine-Aizawa, Y. & Huganir, R.L. Imaging of receptor trafficking by using alpha-bungarotoxin-binding-site-tagged receptors. *Proc Natl Acad Sci U S A* **101**, 17114-17119 (2004).
195. Carland, J.E.*, et al.* Characterization of the effects of charged residues in the intracellular loop on ion permeation in alpha1 glycine receptor channels. *J Biol Chem* **284**, 2023-2030 (2009).
196. Levitin, F.*, et al.* PATE gene clusters code for multiple, secreted TFP/Ly-6/uPAR proteins that are expressed in reproductive and neuron-rich tissues and possess neuromodulatory activity. *J Biol Chem* **283**, 16928-16939 (2008).
197. Blendy, J.A. Modeling neuropsychiatric disease-relevant human SNPs in mice. *Neuropsychopharmacology* **36**, 364-365 (2011).
198. Denisco, R.A., Chandler, R.K. & Compton, W.M. Addressing the intersecting problems of opioid misuse and chronic pain treatment. *Exp Clin Psychopharmacol* **16**, 417-428 (2008).
199. Fishbain, D.A., Rosomoff, H.L. & Rosomoff, R.S. Drug abuse, dependence, and addiction in chronic pain patients. *Clin J Pain* **8**, 77-85 (1992).
200. Freedman, M.K., Saulino, M.F., Overton, E.A., Holding, M.Y. & Kornbluth, I.D. Interventions in chronic pain management. 5. Approaches to medication and lifestyle in chronic pain syndromes. *Arch Phys Med Rehabil* **89**, S56-60 (2008).
201. Anderson, K.L.*, et al.* Antinociception induced by chronic exposure of rats to cigarette smoke. *Neurosci Lett* **366**, 86-91 (2004).

202. Mattila, M.J., Ahtee, L. & Saarnivaara, L. The analgesic and sedative effects of nicotine in white mice, rabbits and golden hamsters. *Ann Med Exp Biol Fenn* **46**, 78-84 (1968).
203. Sahley, T.L. & Berntson, G.G. Antinociceptive effects of central and systemic administrations of nicotine in the rat. *Psychopharmacology (Berl)* **65**, 279-283 (1979).
204. Berrendero, F.*, et al.* Nicotine-induced antinociception, rewarding effects, and physical dependence are decreased in mice lacking the preproenkephalin gene. *J Neurosci* **25**, 1103-1112 (2005).
205. Cuello, A.C., Jessell, T.M., Kanazawa, I. & Iversen, L.L. Substance P: localization in synaptic vesicles in rat central nervous system. *J Neurochem* **29**, 747-751 (1977).
206. Cuello, A.C., Galfre, G. & Milstein, C. Detection of substance P in the central nervous system by a monoclonal antibody. *Proc Natl Acad Sci U S A* **76**, 3532-3536 (1979).
207. Stafford, G.A., Oswald, R.E. & Weiland, G.A. The beta subunit of neuronal nicotinic acetylcholine receptors is a determinant of the affinity for substance P inhibition. *Mol Pharmacol* **45**, 758-762 (1994).
208. Marks, M.S., Woodruff, L., Ohno, H. & Bonifacino, J.S. Protein targeting by tyrosine- and di-leucine-based signals: evidence for distinct saturable components. *J Cell Biol* **135**, 341-354 (1996).
209. Xu, J., Zhu, Y. & Heinemann, S.F. Identification of sequence motifs that target neuronal nicotinic receptors to dendrites and axons. *J Neurosci* **26**, 9780-9793 (2006).
210. Taraschenko, O.D., Rubbinaccio, H.Y., Shulan, J.M., Glick, S.D. & Maisonneuve, I.M. Morphine-induced changes in acetylcholine release in the interpeduncular nucleus and relationship to changes in motor behavior in rats. *Neuropharmacology* **53**, 18-26 (2007).
211. De Biasi, M. & Salas, R. Influence of neuronal nicotinic receptors over nicotine addiction and withdrawal. *Exp Biol Med (Maywood)* **233**, 917-929 (2008).
212. Caille, S., Guillem, K., Cador, M., Manzoni, O. & Georges, F. Voluntary nicotine consumption triggers in vivo potentiation of cortical excitatory drives to midbrain dopaminergic neurons. *J Neurosci* **29**, 10410-10415 (2009).
213. Kim, S.E. & Han, S.M. Nicotine- and methamphetamine-induced dopamine release evaluated with in-vivo binding of radiolabelled raclopride to dopamine D2 receptors: comparison with in-vivo microdialysis data. *Int J Neuropsychopharmacol* **12**, 833-841 (2009).
214. Phillipson, O.T. & Pycock, C.J. Dopamine neurones of the ventral tegmentum project to both medial and lateral habenula. Some implications for habenular function. *Exp Brain Res* **45**, 89-94 (1982).